JOURNAL OF GEOPHYSICAL RESEARCH, VOL. 98, NO. E6, PAGES 10,973–11,016, JUNE 25, 1993

A Model for the Hydrologic and Climatic Behavior of Water on Mars

STEPHEN M. CLIFFORD

Lunar and Planetary Institute, Houston, Texas

Past studies of the climatic behavior of water on Mars have universally assumed that the atmosphere is the sole pathway available for volatile exchange between the planet's crustal and polar reservoirs of H_2O. However, if the planetary inventory of outgassed H_2O exceeds the pore volume of the cryosphere by more than a few percent, then a subpermafrost groundwater system of global extent will necessarily result. The existence of such a system raises the possibility that subsurface transport may complement long-term atmospheric exchange. In this paper, the hydrologic response of a water-rich Mars to climate change and to the physical and thermal evolution of its crust is considered. The analysis assumes that the atmospheric leg of the planet's long-term hydrologic cycle is reasonably described by current models of insolation-driven exchange. Under the climatic conditions that have apparently prevailed throughout most of Martian geologic history, the thermal instability of ground ice at low- to mid-latitudes has led to a net atmospheric transport of H_2O from the "hot" equatorial region to the colder poles. Theoretical arguments and various lines of morphologic evidence suggest that this poleward flux of H_2O has been episodically augmented by additional releases of water resulting from impacts, catastrophic floods, and volcanism. Given an initially ice-saturated cryosphere, the deposition of material at the poles (or any other location on the planet's surface) will result in a situation where the local equilibrium depth to the melting isotherm has been exceeded, melting ice at the base of the cryosphere until thermodynamic equilibrium is once again established. The downward percolation of basal meltwater into the global aquifer will result in the rise of the local water table in the form of a groundwater mound. Given geologically reasonable values of large-scale crustal permeability (i.e., $\gtrsim 10^{-2}$ darcies), the gradient in hydraulic head created by the presence of the mound could then drive the equatorward flow of a significant volume of groundwater ($\gtrsim 10^8$ km^3) over the course of Martian geologic history. At temperate and equatorial latitudes, the presence of a geothermal gradient will then result in a net discharge of the system as water vapor is thermally pumped from the higher temperature (higher vapor pressure) depths to the colder (lower vapor pressure) near-surface crust. By this process, a gradient as small as 15 K km^{-1} could drive the vertical transport of 1 km of water to the freezing front at the base of the cryosphere every 10^6–10^7 years, or the equivalent of ~10^2–10^3 km of water over the course of Martian geologic history. In this manner, much of the H_2O that has been lost from the crust by the sublimation of equatorial ground ice, impacts, and catastrophic floods may ultimately be replenished. The validity of this analysis is supported by a detailed review of relevant spacecraft data, discussions of lunar and terrestrial analogs, and the use of well-established hydrologic models. Among the additional topics discussed are the thermal and hydrologic properties of the crust, the potential distribution of ground ice and groundwater, the thermal evolution of the early cryosphere, the recharge of the valley networks and outflow channels, the polar mass balance, and a review of several important processes that are likely to drive the large-scale vertical and horizontal transport of H_2O beneath the Martian surface. Given a geologically reasonable description of the crust, and an outgassed inventory of water that exceeds the pore volume of the cryosphere by just a few percent, basic physics suggests that the hydrologic model described here will naturally evolve. If so, subsurface transport has likely played an important role in the geomorphic evolution of the Martian surface and the long-term cycling of H_2O between the atmosphere, polar caps, and near-surface crust.

CONTENTS

Paper number 93JE00225.
0148-0227/93/93JE-00225$05.00

1. INTRODUCTION

Virtually all past studies of the climatic behavior of water on Mars have focused on the potential for insolation-driven exchange between the regolith, atmosphere, and polar caps [e.g., *Leighton and Murray*, 1966; *Toon et al.*, 1980; *Fanale et al.*, 1982, 1986]. Implicit in this work has been the assumption that the atmosphere is the sole pathway available for volatile exchange. However, if the planetary inventory of outgassed H_2O exceeds by more than a few percent the quantity required to saturate the pore volume of the cryosphere (that region of the crust where the temperature remains continuously below the freezing point of water), then a subpermafrost groundwater system of global extent will necessarily result. As discussed by *Clifford* [1981*b*, 1984], the existence of such a system may have played a critical role in the long-term climatic cycling of water on Mars.

This paper examines the potential hydrologic response of a water-rich Mars to both climate change and to the physical and thermal evolution of its crust. It is based on the ad hoc assumption that Mars possesses a global inventory of water sufficient to both saturate the pore volume of the cryosphere and create a groundwater system of global extent. Evidence for such a large inventory is provided by a long list of Martian landforms whose morphology has been attributed to the existence of subsurface volatiles [*Rossbacher and Judson*, 1981; *Carr*, 1986, 1987; *Squyres*, 1989]. In particular, it is supported by the existence of the outflow channels, whose distribution, size, and range of ages, suggests that a significant body of groundwater has been present on Mars throughout much of its geologic history [*Baker*, 1982; *Tanaka*, 1986; *Tanaka and Scott*, 1986; *Carr*, 1986, 1987; *Mouginis-Mark*, 1990; *Baker et al.*, 1992]. Based on a conservative estimate of the discharge required to erode the channels, and the likely extent of their original source region, *Carr* [1986, 1987] estimates that Mars may possess a crustal inventory of water equivalent to a global ocean 0.5–1 km deep.

Under the climatic conditions that have apparently prevailed on Mars throughout most of its geologic history, ground ice is unstable with respect to the water vapor content of the atmosphere at latitudes equatorward of ±40° [*Toon et al.*, 1980; *Clifford and Hillel*, 1983; *Fanale et al.*, 1986]. As a result, the inventory of equatorial ground ice is thought to have experienced a steady decline. Because the cold polar regions are the dominant thermodynamic sink for any H_2O released to the atmosphere, there is a preferential transfer of H_2O from the comparatively "hot" equatorial region to the colder poles. Theoretical arguments and various lines of morphologic evidence suggest that this poleward flux of H_2O has been augmented throughout the planet's history by additional releases of water resulting from impacts, catastrophic floods, and volcanism. The subsequent deposition of dust and H_2O at the poles will ultimately result in a situation where the thermal equilibrium depth to the melting isotherm has been exceeded. In response to this deposition, melting will begin and continue at the base of the polar cryosphere until thermal equilibrium is once again established. The downward percolation of meltwater beneath the polar caps will then result in the rise of the local water table in the form of a groundwater mound. Given geologically reasonable values of crustal permeability, the gradient in hydraulic head created by the presence of the mound will then drive the flow of groundwater away from the poles and towards the equator. At equatorial and temperate latitudes, the presence of a geothermal gradient will result in the local discharge of the system as water vapor is thermally pumped from the higher temperature (higher vapor pressure) depths to the colder (lower vapor pressure) near-surface crust. In this fashion, much of the ground ice and groundwater that has been removed from the crust by impacts, catastrophic floods, and long-term sublimation, may ultimately be replenished.

Various aspects of this model, including the inherent instability of equatorial ground ice [*Clifford and Hillel*, 1983], and polar basal melting [*Clifford*, 1987*b*], have been discussed in detail elsewhere. The focus of this paper will therefore be on those aspects of the hydrologic response of Mars to climate change that have so far received little or no attention, with particular emphasis on the potential role of subsurface transport. Among the topics discussed are the thermal and hydrologic properties of the crust, the potential distribution of ground ice and groundwater, the stability and replenishment of equatorial ground ice, basal melting and the polar mass balance, the thermal evolution of the early cryosphere, the recharge of the valley networks and outflow channels, and a review of several processes that are likely to drive the large-scale vertical and horizontal transport of H_2O within the crust. Throughout this discussion it is assumed that the atmospheric leg of the long-term hydrologic cycle is reasonably described by current models of insolation-driven exchange [*Toon et al.* 1980; *Fanale et al.* 1982, 1986]. Therefore, this paper will emphasize the geologic requirements and actual physics of subsurface flow.

Finally, it should be stressed again that this is a theoretical analysis, one whose scope is purposely restricted to consideration of the hydrologic evolution of a water-rich Mars. For this reason, no attempt has been made to conclusively demonstrate that Mars is indeed water-rich, or that it possesses an inventory of water sufficiently large to form a groundwater system of global extent. Rather, the volume of water required to satisfy this condition is estimated and its potential hydrologic consequences explored. The results of this analysis suggest that, given a geologically reasonable description of the physical properties of the planet's crust and an inventory of water that exceeds the pore volume of the cryosphere by as little as a few percent, the hydrologic model described here will naturally evolve. If so, subsurface transport has likely played an important role in the geomorphic evolution of the Martian surface and the long-term cycling of H_2O between the atmosphere, polar caps, and near-surface crust.

2. THE GEOPHYSICAL BASIS FOR A GLOBAL GROUNDWATER SYSTEM ON MARS

The existence of a global groundwater system on Mars is necessarily subject to certain geologic constraints; the most obvious of which is that there must exist a suitably porous and permeable layer in which the groundwater can reside. In this section the evidence supporting the existence of such a layer is summarized. In addition, several relevant parameters are discussed, including: the variation of porosity with depth, the thermal structure of the crust, and how these two factors interact to influence the state and distribution of water within the crust.

2.1. *Porosity Versus Depth*

Impact processes have played a major role in the structural evolution of the Martian crust [*Soderblom et al.*, 1974; *Gurnis*, 1981]. Field studies of terrestrial impact craters [*Shoemaker*, 1963; *Short*, 1970; *Dence et al.*, 1977] and theoretical models of the cratering process [*Melosh*, 1980, 1989; *O'Keefe and Ahrens*, 1981] have shown that impacts modify the structure of a planetary surface in at least two important ways: (1) by the production and dispersal of large quantities of ejecta, and (2) through the intense fracturing of the surrounding and underlying basement. *Fanale* [1976] has estimated that over the course of Martian geologic history, the volume of ejecta produced by impacts was sufficient to create a global blanket of debris up to 2 km thick. As noted by *Carr* [1979], it is likely that this ejecta layer is interbedded with volcanic flows, weathering products, and sedimentary deposits, all overlying an intensely fractured basement (Figure 1). This description of the Martian crust is essentially identical to that proposed by *Hartmann* [1973, 1980] for the near-surface of the Moon, where the early period of intense bombardment is believed to have resulted in the production of a blocky, porous "megaregolith" that extends to considerable depth, a view that is supported by the seismic propagation characteristics of the lunar crust [*Toksöz et al.*, 1972, 1974; *Toksöz*, 1979].

For the near-surface of the moon, *P* wave velocities increase with depth until they reach a local maximum at about 20–25 km [*Toksöz et al.*, 1972, 1974; *Simmons et al.*, 1973; *Toksöz*, 1979]. This behavior is consistent with a reduction in crustal porosity with increasing lithostatic pressure. The transition between fractured and coherent lunar basement is believed to coincide with the beginning of the constant velocity zone at a depth of ~20 km, where the lithostatic pressure is thought to be sufficient (>1 kbar = 10^8 Pa) to close virtually all impact-generated pore space [*Toksöz et al.*, 1972, 1974; *Toksöz*, 1979].

A closure pressure of 1 kbar is consistent with most laboratory studies of fractured igneous rock [*Birch*, 1961; *Siegfried et al.*, 1981], but pressures in excess of 5 kbar are sometimes required to ensure the closure of all fracture openings [*Gold et al.*, 1971; *Todd et al.*, 1973; *Siegfried et al.*, 1977]. Still greater pressures (>>10 kbar) are often necessary to eliminate primary porosity, such as vesicles in basalt or the intergranular pore space of sedimentary rock [*Birch*, 1961; *Gold et al.*, 1971; *Todd et al.*, 1973; *Siegfried et al.*, 1977]. Thus, any estimate of crustal porosity, based on the assumption of a 1 kbar closure pressure, is necessarily conservative.

Binder and Lange [1980] suggest that the seismic properties of the lunar crust are best described by an exponential decline in porosity with depth, a relationship that is consistent with that observed in many geologic environments on Earth [e.g., *Athy*, 1930; *Schmoker and Gautier*, 1988]. According to this model, the porosity at a depth z is given by

$$\Phi(z) = \Phi(0) \exp(-z/K) \quad (1)$$

where $\Phi(0)$ is the porosity at the surface and K is the porosity decay constant.

Assuming that the density of the Martian crust is comparable to its lunar counterpart, the inferred value of the lunar porosity decay constant (~6.5 km) can be gravitationally scaled to find the appropriate value for Mars, i.e.,

$$K_{Mars} = 6.5 \text{ km } (g_{Moon} / g_{Mars}) = 2.82 \text{ km.}$$

where g_{Moon} (=1.62 m s^{-2}) and g_{Mars} (=3.71 m s^{-2}) are the gravitational accelerations at the surface of the Moon and Mars, respectively.

Two potential porosity profiles of the Martian crust are illustrated in Figure 2. The first is based on a surface porosity of 20%, the same value assumed for the Moon by *Binder and Lange* [1980], and one that agrees reasonably well with the measured porosity of lunar breccias [*Warren and Rasmussen*, 1987]. This model yields a self-compaction depth (the depth at which crustal porosity falls below 1%) of approximately 8.5 km. By integrating the porosity of the crust down to this depth, the total pore volume is found to be sufficient to store a global layer of water approximately 540 m deep [*Clifford*, 1981*a*].

In the second profile, a surface porosity of 50% is assumed, a value consistent with estimates of the bulk porosity of Martian

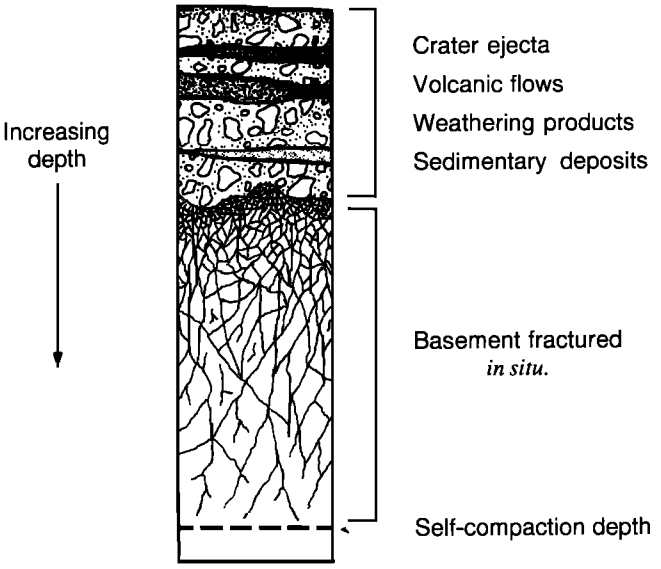

Fig. 1. An idealized stratigraphic column of the Martian crust *Clifford* [1981*a*, 1984].

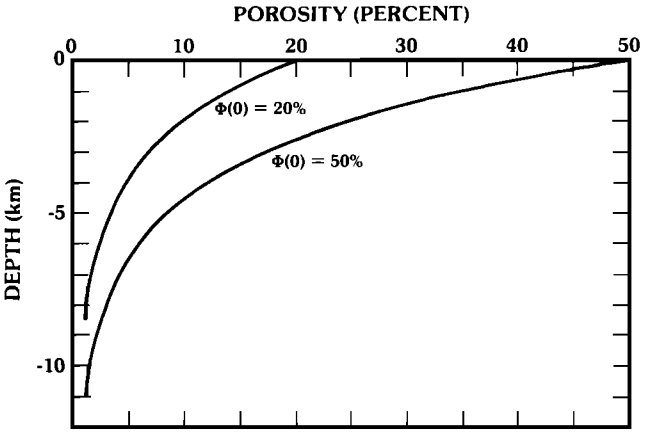

Fig. 2. Theoretical porosity profiles of the Martian crust based on the lunar model of *Binder and Lange* [1980]. The curve based on a surface porosity of 20% is simply the lunar model of *Binder and Lange* [1980] gravitationally scaled to Mars. The curve corresponding to a surface porosity of 50% is included to account for the possibility that various processes of physical and chemical weathering and large-scale ice segregation may have substantially increased the available pore space in the outer crust [*Clifford*, 1984, 1987*a*].

soil as analyzed by the Viking Landers [*Clark et al.*, 1976]. A surface porosity this large may be appropriate if the regolith has undergone a significant degree of weathering [e.g., *Malin*, 1974; *Huguenin*, 1976; *Gooding*, 1978] or if it contains large segregated bodies of ground ice. The self-compaction depth predicted by this model is roughly 11 km, while its total pore volume is equivalent to a global ocean some 1.4 km deep [*Clifford*, 1984]. This pore volume is likely an upper limit, for it seems doubtful that weathering or large-scale ice-segregation will affect more than the upper few kilometers of the crust. Below this depth, the porosity profile will most likely resemble the gravitationally scaled lunar curve. The physical characteristics of both models are summarized in Table 1.

The presence of groundwater could affect estimates of the self-compaction depth and total pore volume in several ways. As discussed by *Hubert and Rubey* [1959] and others [*Byerlee and Brace*, 1968; *Brace and Kohlstedt*, 1980; *Thompson and Connolly*, 1992], the hydrostatic pressure of water within a pore can partially offset the lithostatic pressure acting to close it. Thus, for a "wet" Mars, crustal porosity may persist to depths roughly a third greater than those indicated by the "dry" models in Figure 2. However, groundwater can also reduce crustal porosity by solution, compaction, and cementation [*Maxwell*, 1964; *Rittenhouse*, 1971]. Such processes are of greatest significance under conditions of high temperature and pressure [*Maxwell*, 1964; *Pettijohn*, 1975]. Currently, these conditions are likely to exist only at great depth on Mars, where their impact on the overall porosity of the megaregolith is expected to be small. However, conditions were almost certainly different in the past. For example, models of the thermal history of Mars suggest that 4 billion years ago the planet's internal heat flow was some 3–5 times greater than it is today [*Toksöz and Hsui*, 1978; *Davies and Arvidson*, 1981; *Schubert and Spohn*, 1990]. In addition, the existence of an early atmospheric greenhouse may have permitted liquid water to exist at or near the surface, where it may have reacted with atmospheric CO_2 to form extensive carbonate deposits within the crust [*Kahn*, 1985; *Postawko and Kuhn*, 1986; *Kasting*, 1987; *Pollack et al.*, 1987]. The extent to which such processes may have affected the porosity and depth of the megaregolith is unknown.

Whether Mars once possessed a warmer, wetter climate [*Masursky et al.*, 1977; *Pollack et al.*, 1987], or a climate that has always resembled the conditions we observe today [*Soderblom and Wenner*, 1978], as the interior of the planet gradually cooled, a freezing-front developed within the crust that propagated downward with time [*Carr*, 1979] (see also section 6.2). If the total pore volume of this frozen region grew to exceed the planetary inventory of water, then eventually all of the water on Mars should have been cold-trapped within the frozen near-surface crust [*Soderblom and Wenner*, 1978]. Alternatively, if the pore volume of this region is less than the planetary inventory of outgassed water (defined here as the sum total of chemically unbound water present in the planet's atmosphere, on its surface, or within its crust), then the excess H_2O should have resulted in the formation of extensive bodies of subpermafrost groundwater [*Clifford*, 1981*b*, 1984]. The fate and duration of groundwater on Mars is therefore critically dependent on both the size of the planetary inventory of H_2O and total pore volume of the frozen crust.

TABLE 1. Calculated Megaregolith Characteristics

Surface Porosity $\Phi(0)$, %	Self-Compaction Depth, km	Storage Capacity	
		$\times 10^7$ km^3	m H_2O
20	8.5	7.8	540
50	11.0	20	1400

2.2. *Thermal Structure*

The Martian cryosphere is defined as that region of the crust where the temperature remains continuously below the freezing point of water (Figure 3) [*Fanale*, 1976; *Rossbacher and Judson*, 1981; *Kuzmin*, 1983]. If we assume a solute-free freezing point of 273 K, then at the surface this condition is satisfied at every latitude below the diurnal skin depth, thus defining the cryosphere's upper bound. However, because neither the magnitude of the Martian geothermal heat flux nor the thermal conductivity of the crust are known, the depth to the lower bound of the cryosphere is considerably less certain.

The depth to the base of the cryosphere can be calculated from the steady state one-dimensional heat conduction equation, where

$$z = \kappa \frac{T_{mp} - T_{ms}}{Q_g} \tag{2}$$

and where κ is the thermal conductivity of the crust, T_{mp} is the melting temperature of the ground ice, T_{ms} is the mean annual surface temperature, and Q_g is the value of the geothermal heat flux [*Fanale*, 1976]. At present, only the current latitudinal range of mean annual surface temperature is known to any accuracy (~154–218 K ±5 K), while the remaining variables have associated uncertainties of 20–50%. Plausible ranges for each of these variables are discussed below.

2.2.1. *Thermal conductivity.* Four principal factors influence the thermal conductivity of terrestrial permafrost, they are: bulk density, degree of pore saturation, particle size, and temperature [*Clifford and Fanale*, 1985]. The effect of an increase in bulk density (and/or pore saturation) on the thermal conductivity of permafrost is readily understood because the conductivities of rock and ice are significantly higher than the conductivity of the air they displace. However, the effects of particle size and temperature are a bit more complicated.

Experiments have shown that thin films of adsorbed water remain unfrozen on mineral surfaces down to very low temperatures [*Anderson et al.*, 1967; *Anderson and Tice*, 1973], particularly in the presence of potent freezing point depressors such as

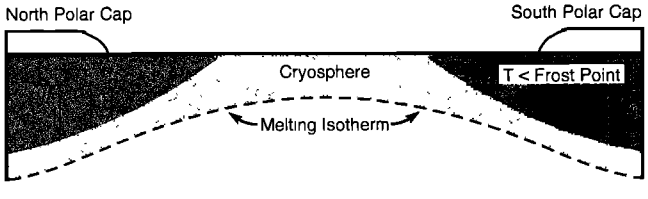

Fig. 3. A pole-to-pole cross section of the Martian crust illustrating the theoretical latitudinal variation in depth of the freezing front at the base of the cryosphere. Note that ground ice can exist in equilibrium with the atmosphere only at those latitudes and depths where crustal temperatures are below the frost point of atmospheric water vapor [~198 K, *Farmer and Doms*, 1979]. Outside these locations, ground ice can only survive if it is diffusively isolated from the atmosphere by a regolith of low gaseous permeability [e.g., *Smoluchowski*, 1968; *Clifford and Hillel*, 1983; *Fanale et al.*, 1986]. Figure adapted from *Fanale* [1976] and *Rossbacher and Judson* [1981].

NaCl and $CaCl_2$ [*Banin and Anderson*, 1974]. Because the thermal conductivity of unfrozen water (~0.54 W m^{-1} K^{-1} [*Penner*, 1970]) is significantly lower than that of ice (2.25 W m^{-1} K^{-1} at 273 K), its presence will necessarily decrease the effective thermal conductivity of silicate-ice mixtures. Since the quantity of H_2O adsorbed per unit surface area is roughly constant for all mineral soils [*Puri and Murari*, 1963], it follows that the conductivity of a frozen soil will be proportional to its content of high specific surface area clay. However, as the temperature of a frozen soil declines, so too does its content of adsorbed water [*Anderson et al.*, 1967; *Anderson and Tice*, 1973]. This results in an increase in the soil's effective conductivity, an increase that is compounded by the strong temperature dependence of the thermal conductivity of ice, which rises from 2.25 W m^{-1} K^{-1} at 273 K, to 4.42 W m^{-1} K^{-1} at 160 K [*Ratcliffe*, 1962].

Although a direct measurement of the bulk thermal conductivity of the Martian megaregolith is lacking, a likely range of values can be inferred by considering terrestrial analogs. Images of the surface taken by the Viking spacecraft suggest that the lithology of the upper few kilometers of the crust varies from a loose fine-grained regolith to meter-sized blocks of ejecta, all intercalated with a significant quantity of volcanics [*Greeley and Spudis*, 1981; *Greeley*, 1987; *Arvidson et al.*, 1989]. If so, then thermal properties of the megaregolith should be closely approximated by those of terrestrial frozen soil and basalt.

Laboratory measurements of the thermal conductivity of 144 samples of frozen soil and 301 samples of basalt are summarized in Table 2 and Figure 4. The samples vary in composition, lithology, porosity, and degree of pore saturation, but all represent conditions that are likely to exist somewhere within the top 10 km of the Martian crust. The thermal conductivities of the soil samples range from 0.08–4.0 W m^{-1} K^{-1}, with an average value of ~1.66 W m^{-1} K^{-1}; while the basalt conductivities exhibit a greater spread, 0.09–5.40 W m^{-1} K^{-1}, with an average value of ~2.06 W m^{-1} K^{-1}.

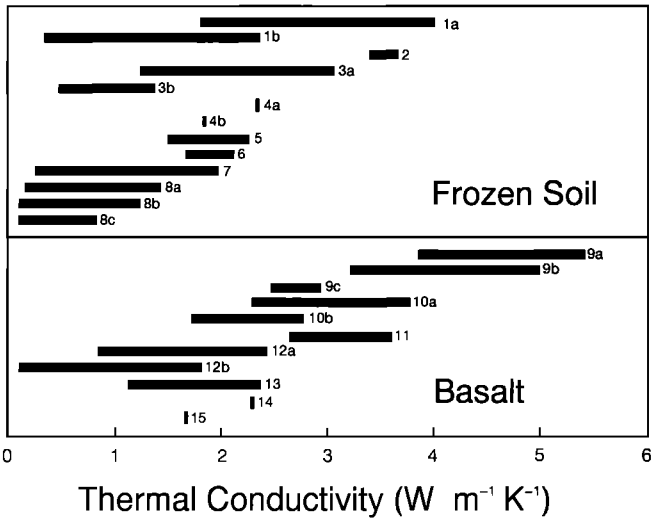

Fig. 4. Thermal conductivities of frozen soil and basalt [*Clifford and Fanale*, 1985].

If our assumptions about the structure and lithology of the outer crust are correct (i.e., Figure 1), then the thermal properties of the megaregolith will be most strongly influenced by basalt. If so, the data in Table 2 suggest a column-averaged thermal conductivity of ~2.0 (±1.0) W m^{-1} K^{-1}, with lower values likely

TABLE 2. Thermal Conductivity of Megaregolith Analogs

Group	Description	Number of Samples	Conductivity Range, W m^{-1} K^{-1}
	Frozen Soil		
1a	Sandy soils, 50–100% saturation [*Sanger*, 1963]	18	1.80–4.00
b	Sandy soils, 3–45% saturation [*Sanger*, 1963]	24	0.33–2.35
2	Poorly graded clean sand, 100% saturation [*Lachenbruch* et al., 1982]	5	3.39–3.67
3a	Clay soils, 50–100% saturation, T = 263 K [*Sanger*, 1963]	21	1.26–3.06
b	Clay soils, 15–45% saturation, T = 263 K [*Sanger*, 1963]	10	0.47–1.38
4a	Generic silt soil, 100% saturation [*Lachenbruch*, 1970]	average of many	2.34
b	Generic clay soil, 100% saturation [*Lachenbruch*, 1970]	average of many	1.84
5	Clay soil, nearly saturated [*Slusarchuk and Watson*, 1975]	24	1.49–2.25
6	Leda clay and Sudbury silty clay soils, 100% saturation, T = 253 K [*Penner, 1970*]	2	1.67–2.09
7	Fairbanks silty clay loam, 5–100% saturation, T = 269 K [*Kersten*, 1963]	13	0.25–1.95
8a	Black cultivated soil, 0–100% saturation, T = 268 K [*Higashi*, 1953]	8	0.18–1.42
b	Brown subsoil, 0–100% saturation, T = 268 K [*Higashi*, 1953]	9	0.08–1.21
c	Yellow brown subsoil, 0–100% saturation, T = 268 K [*Higashi*, 1953]	8	0.10–0.82
		144 (total)	1.66 (average)
	Basalt		
9a	Chloritic Golden Mile basalt, 0% saturation [*Sass*, 1964]	28	3.85–5.40
b	Amphibolitic Golden Mile basalt, 0% saturation [*Sass*, 1964]	11	3.22–4.98
c	Norseman basalt, 0% saturation [*Sass*, 1964]	7	2.47–2.93
10a	Portage Lake lava (amygdaloidal tops), 0% saturation [*Birch*, 1950]	10	2.30–3.77
b	Portage Lake lava (dense flows), 0% saturation [*Birch*, 1950]	27	1.72–2.76
11	Ventersdorp lava, 0% saturation [*Bullard*, 1939]	9	2.64–3.60
12a	Vesicular Hawaiian basalt, 100% saturation [*Robertson and Peck*, 1974]	57	0.84–2.41
b	Vesicular Hawaiian basalt, 0% saturation [*Robertson and Peck*, 1974]	60	0.09–1.80
13	Columbia River Plateau basalt, 0% saturation [*Sass and Munroe*, 1974]	72	1.12–2.38
14	Knippa basalt, 0% saturation [*Horai and Baldridge*, 1972]	1	2.30
15	Deep-Sea Drilling Project leg 37 basalts, 100% saturation [*Hyndman and Drury*, 1976]	19	1.66
		301 (total)	2.06 (average)

near the surface, where fine-grained materials may be present in abundance, and higher values occurring at depth, where the lithology of the crust is likely to be characterized almost exclusively by fractured igneous rock [*Clifford and Fanale*, 1985]. In contrast, previous estimates were often based on the thermal properties of a specific terrestrial analog. For example, *Fanale* [1976] assumed that the properties of the megaregolith were well-represented by a hard-frozen limonitic soil ($\kappa = 0.8$ W m^{-1} K^{-1}), while *Crescenti* [1984] assumed a purely basaltic composition ($\kappa = 2.09$–2.5 W m^{-1} K^{-1}).

2.2.2. *Melting temperature.* The melting temperature of ground ice can be depressed below 273 K by both pressure and solute effects; however, the effect of pressure is minimal (~7.43×10^{-8} K Pa^{-1} [*Hobbs*, 1974]), while the effect of salt can be quite large. The existence of various salts in the regolith is supported by the discovery of a duricrust layer at both Viking Lander sites and by the elemental composition of the soil as determined by the inorganic chemical analysis experiments on board each spacecraft [*Toulmin et al.*, 1977; *Clark*, 1978; *Clark and Van Hart*, 1981]. Among the most commonly cited candidates are NaCl, $MgCl_2$, and $CaCl_2$, which have freezing points at their eutectics of 252 K, 238 K, and 218 K, respectively [*Clark and Van Hart*, 1981]. Indeed, some multicomponent salt solutions have freezing temperatures as low as 210 K [*Brass*, 1980]. It should be noted, however, that serious questions have been raised concerning the chemical and thermodynamic stability of $CaCl_2$ and $MgCl_2$ under ambient Martian conditions, particularly in the presence of abundant sulfates [*Clark and Van Hart*, 1981]. Given these arguments, brines based on NaCl appear to be the most likely candidates to be found within the crust.

2.2.3. *Geothermal heat flux.* Like the other variables in equation (2), estimates of the Martian geothermal heat flux have varied over a wide range (Table 3). *Solomon and Head* [1990] have noted that if Mars loses heat at the same rate per unit mass as the Earth, then it should have a mean global heat flux of ~31 mW m^{-2}, a figure that agrees reasonably well with the independently derived estimates of *Fanale* [1976], *Toksöz and Hsui* [1978], *Turcotte et al.* [1979], and *Stevenson et al.* [1983]. However, other published estimates have been both significantly higher and lower. For example, thermal modeling by *Toksöz et al.* [1978], *Davies and Arvidson* [1981], and *Schubert and Spohn* [1990] suggests a present-day heat flux as high as 40–45 mW m^{-2}; whereas work by *Solomon and Head* [1990], based on rheologic estimates of lithospheric thickness and mantle heat production (inferred from the composition of the SNC meteorites), suggests values as low as 15–25 mW m^{-2}. For comparison purposes, the current best estimates of the average heat flux of the Earth and Moon (the only bodies for which there is any actual data) are 82 mW m^{-2} [*Sclater et al.*, 1980] and 16 mW m^{-2} [*Keihm and Langseth*, 1977], respectively.

TABLE 3. Estimated Globally Averaged Geothermal Heat Flux

Planet	Source	Heat Flux mW m^{-2}
Mars	*Fanale* [1976]	30
	Toksöz and Hsui [1978]	35
	Toksöz et al. [1978]	45
	Turcotte et al. [1979]	33.5
	Davies and Arvidson [1981]	40
	Stevenson et al. [1983]	28–32.4
	Schubert and Spohn [1990]	40
	Solomon and Head [1990]	15–25
Earth	*Sclater et al.* [1980]	82.3
Moon	*Keihm and Langseth* [1977]	14–18

Given the broad range of Martian heat flux estimates, a globally averaged value of 30 mW m^{-2} appears to be a reasonable choice for the present day heat flow. Substituting this estimate, and the current best estimates of crustal thermal conductivity (2.0 W m^{-1} K^{-1}) and ground ice melting temperature (252 K) into equation (2), we find that the depth to the base of the cryosphere should vary from about 2.3 km at the equator to approximately 6.5 km at the poles, an increase that reflects the corresponding poleward decline in mean annual surface temperature (Table 4 and Figure 5). For completeness, maximum and minimum cryosphere depths have also been calculated by combining the appropriate limiting values of geothermal heat flow, thermal conductivity, and melting temperature. Although, the local thermal properties of the crust are likely to display a high degree of variability, on a globally averaged basis it appears unlikely that any geologically reasonable combination will result in cryosphere depths that differ by more than 50% from the values predicted by the nominal model.

By integrating the crustal porosity profile given by equation (1) from the surface down to the melting isotherm depths presented in Table 4, the potential pore volume of the cryosphere is readily determined (Table 5). For the given range of porosities and the likely thermal properties of the crust (i.e., those represented by the nominal model), this amounts to a pore volume sufficient to store a global layer of water some 370–940 m deep. For the extreme conditions represented by the minimum and maximum thermal models, the range in potential storage capacity varies from a global ocean as small as 40 m deep, to one as large as 1400 m. Note that for the thermal conditions defined by the maximum case, the megaregolith should be frozen throughout, a condition that appears incompatible with the geomorphic evidence for abundant groundwater (i.e., the outflow channels) throughout much of Martian geologic history [*Baker*, 1982; *Tanaka*, 1986; *Tanaka and Scott*, 1986; *Carr*, 1986, 1987; *Mouginis-Mark*, 1990; *Baker et al.*, 1992].

2.3. *The Distribution of Groundwater*

Thermodynamically, the primary sink for subsurface H_2O on Mars is the cryosphere; however, once the pore volume of the cryosphere has been saturated with ice, any remaining water will drain to saturate the lowermost porous regions of the crust. But how deep and areally extensive will the resulting zone of saturation be? As a first approximation, Mars can be considered a perfect sphere whose porosity profile is everywhere described by equation (1). The quantity of water required to produce an aquifer of any given thickness can then be calculated by integrating the pore volume of the megaregolith between the self-compaction depth and any shallower region of the crust. For example, a quantity of water equivalent to a global layer 10 m deep is sufficient to saturate the lowermost 0.85 km of the megaregolith (Figure 6), while a quantity of water equivalent to a 100-m layer would create a global aquifer nearly 4.3 km deep [*Clifford*, 1984, 1987*a*].

However, Mars is not a perfect sphere. Its crust has been affected by a variety of geologic processes that have created a surface of considerable heterogeneity and topographic relief. This diversity is undoubtedly reflected in the variability of a number of important hydrologic characteristics, including both the local porosity profile and the depth of self-compaction. Unfortunately without further data, the magnitude of this variation is impossi-

TABLE 4. Latitudinal Variation of Cryosphere Thickness

Latitude	Mean Annual Temperature, K	Depth, km		
		Minimum	Nominal	Maximum
90	154	1.24	6.53	23.8
80	157	1.18	6.33	23.2
70	167	0.96	5.67	21.2
60	179	0.69	4.87	18.8
50	193	0.38	3.93	16.0
40	206	0.09	3.07	13.4
30	211	—	2.73	12.4
20	215	—	2.47	11.6
10	216.5	—	2.37	11.3
0	218	—	2.27	11.0
-10	216.5	—	2.37	11.3
-20	215	—	2.47	11.6
-30	211	—	2.73	12.4
-40	206	0.09	3.07	13.4
-50	193	0.38	3.93	16.0
-60	179	0.69	4.87	18.8
-70	167	0.96	5.67	21.2
-80	157	1.18	6.33	23.2
-90	154	1.24	6.53	23.8

Thermal model properties: Minimum: Q_g = 45 mW m^{-2}, k = 1.0 W m^{-1} K^{-1}, T_{mp} = 210 K; Nominal: Q_g = 30 mW m^{-2}, k = 2.0 W m^{-1} K^{-1}, T_{mp} = 252 K; and Maximum: Q_g = 15 mW m^{-2}, k = 3.0 W m^{-1} K^{-1}, T_{mp} = 273 K.

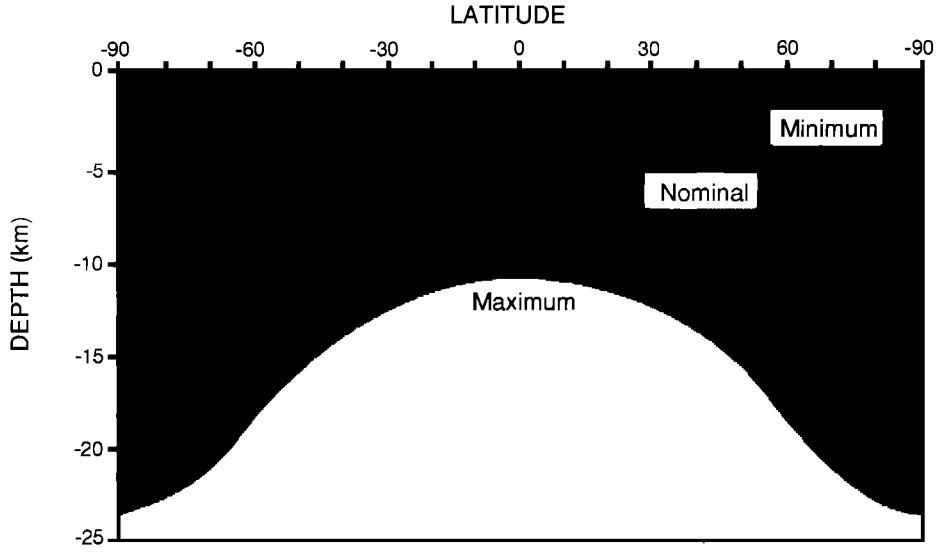

Fig. 5. Extent of the Martian cryosphere for the three thermophysical models defined in the text and in Table 4.

TABLE 5. Storage Potential of Martian Cryosphere

Extent of Cryosphere	Pore Volume, $\times 10^7$ km^3		Equivalent Global Ocean of H_2O, m	
	$\Phi(0)$ = 20%	$\Phi(0)$ = 50%	$\Phi(0)$ = 20%	$\Phi(0)$ = 50%
Minimum	0.57	1.43	39	99
Nominal	5.42	13.6	374	936
Maximum	7.76	20.0	536	1382

Thermal model properties: Minimum: Q_g = 45 mW m^{-2}, k = 1.0 W m^{-1} K^{-1}, T_{mp} = 210 K; Nominal: Q_g = 30 mW m^{-2}, k = 2.0 W m^{-1} K^{-1}, T_{mp} = 252 K; and Maximum: Q_g = 15 mW m^{-2}, k = 3.0 W m^{-1} K^{-1}, T_{mp} = 273 K.

ble to quantify. Thus, although it is clear that the local characteristics of the crust are poorly described by a single set of globally averaged values, they are the best approximation of these properties that we can presently make.

The one improvement that can be made in attempting to model the potential distribution of groundwater on Mars is to consider the effect of topography. If we assume that the local porosity profile of the crust is described everywhere by equa-

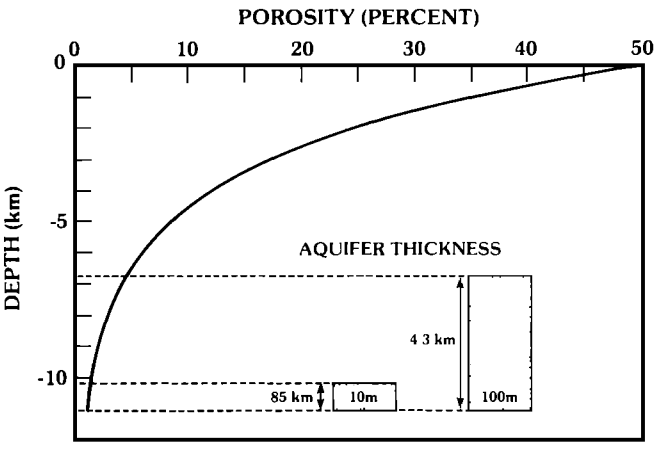

Fig. 6. Resulting saturated thicknesses of groundwater for inventories equivalent to a global ocean 10 and 100 m deep. In this model Mars is considered a perfect sphere whose porosity profile is described everywhere by equation (1) [*Clifford*, 1984, 1987*a*].

tion (1), then the depth of self-compaction will mirror the gross variation of surface topography, defining an irregular, impermeable lower bound for the occurrence of groundwater at a constant depth approximately 10 km beneath the surface. Figure 7 is a pole-to-pole cross section of this crustal model, where the surface elevations and self-compaction depths have been averaged as a function of latitude. This cross section illustrates the potential stratigraphic relationships between surface topography, ground ice, and groundwater, for groundwater inventories ranging from 10 to 250 m. Note that for a groundwater system in hydrostatic equilibrium, the water table conforms to a surface of constant geopotential. In contrast, the distribution of ground ice is controlled by the local surface temperature and the magnitude of the geothermal gradient. As a result, the position of the melting isotherm at the base of the cryosphere will mirror the first-order variations in surface topography, but at a depth several kilometers or more beneath the surface. As illustrated in Figure 7, the differences between these controlling influences (porosity, gravity, and thermal structure) are of considerable importance in determining the state and vertical stratification of H_2O within the crust. For example, beneath topographic highs, the absolute elevation of the local self-compaction depth may exceed the elevation of the global water table; thus, only near-surface ground ice may be present in a vertical section of the crust. Beneath areas of slightly lower elevation, both ground ice and groundwater may be present; however, the vertical distances separating these regions may be substantial, leaving an intervening unsaturated zone that could be many kilometers thick. In still lower regions, the entire crustal column may be saturated with ground ice and groundwater. Indeed, in the very lowest regions, such as the interior of Hellas, the absolute elevation of the global water table may exceed that of the local topography. In such instances the ground ice layer will be under a substantial hydraulic head. As discussed by *Carr* [1979], a rupture of this barrier could lead to a significant discharge of groundwater. However, such a rupture is eventually self-sealing, because as the groundwater erupts onto the surface, it will lower the local hydraulic head until it falls even with the elevation of the basin floor. At that time, the reduced discharge will permit the water-saturated regolith to refreeze at the point of breakout, until the original ground ice thickness is eventually reestablished.

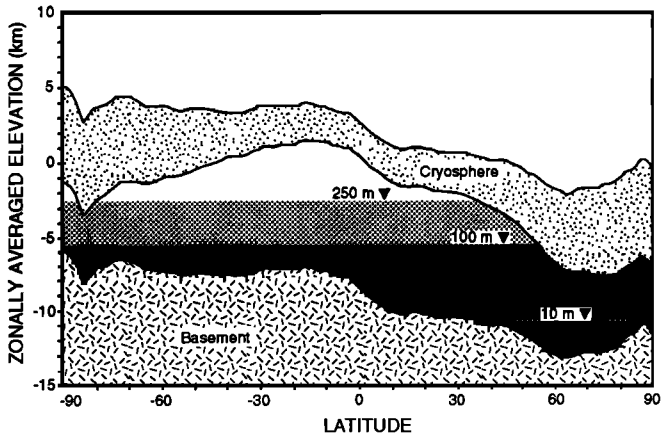

Fig. 7. A pole-to-pole cross section of the Martian crust illustrating the potential relationship between topography, ground ice, and groundwater, for hypothetical groundwater inventories equivalent to a global layer 10, 100, and 250 m deep. Surface elevations are averaged as a function of latitude based on the USGS Mars Digital Terrain Model, while the latitudinal variation in ground ice thickness is based on the nominal model results listed in Table 4. The calculated groundwater depths assume that the groundwater is in hydrostatic equilibrium, that the local porosity profile of the crust is given everywhere by equation (1), and that the self-compaction depth mirrors the gross variation of surface topography at a constant depth of 10 km beneath the surface.

Figure 8*a* illustrates how the areal coverage of groundwater in the crustal model described above should vary as a function of the available inventory of groundwater (i.e., in excess of the H_2O already stored as ground ice in the cryosphere). This relationship is seen more clearly in Plate 1, where the areal coverage of groundwater systems based on available inventories of 10 m, 100 m, and 250 m of water are superimposed on a topographic map of Mars. For the assumed crustal characteristics, the resulting aquifers underlie 34%, 91%, and 98% of the planet's surface (Figure 8*a*), and possess local saturated thicknesses that range from zero to a maximum of 5 km, 10 km, and 13 km, respectively (Figure 8*b*).

To summarize, this analysis suggests that once the pore volume of the cryosphere has been saturated with ice, very little additional water (~10 m) is required to produce a groundwater system of substantial extent. Indeed, given an unlikely combination of low crustal thermal conductivity, high heat flow, and large freezing point depression, a global-scale groundwater system could conceivably result from an outgassed global inventory of H_2O as small as 50 m; however, for more plausible conditions, such as those described by the nominal model, a planetary inventory in excess of 400 m appears necessary.

3. Terrestrial Analogs: The Occurrence of Groundwater and the Permeability of the Earth's Crust

While the calculations presented in the previous section indicate that a planetary-scale groundwater system on Mars is physically possible, is it geologically reasonable? Unfortunately, a clear answer to this question is clouded by the fact that subsurface hydrology remains an inexact science even here on Earth. Much of this uncertainty is attributable to our limited knowledge of the detailed three-dimensional structure of the Earth's crust. It is also due to the subjective and often erroneous way in which this knowledge has historically been interpreted.

Until recently, terrestrial groundwater investigations were driven almost exclusively by a desire to locate easily tapped

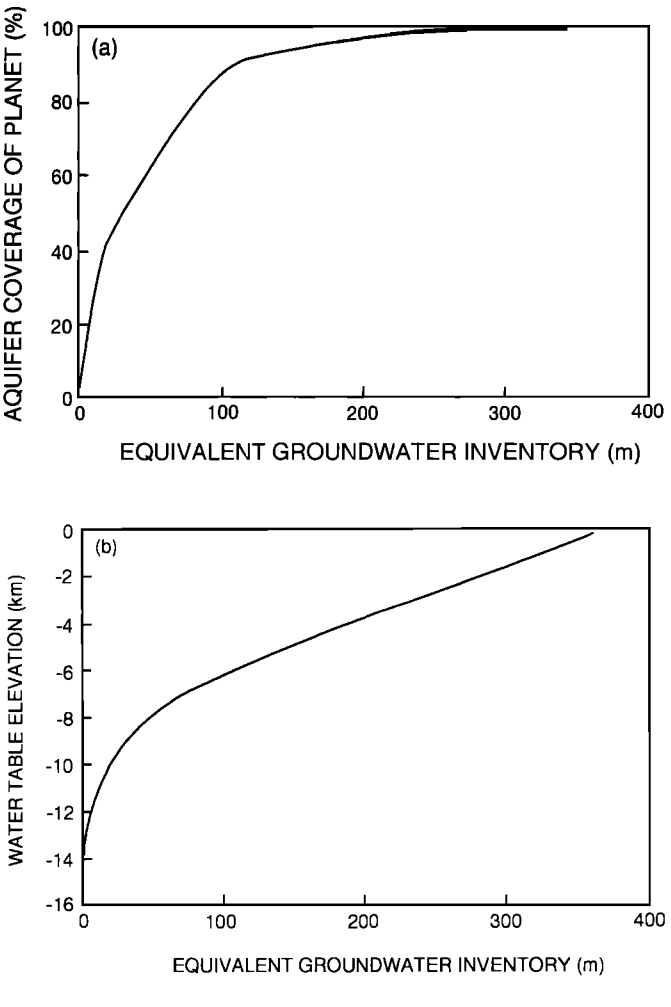

Fig. 8. (*a*) The percent of Mars underlain by groundwater and (*b*) the absolute elevation of the global groundwater table as a function of the planetary inventory of groundwater (expressed as an equivalent global ocean of H_2O). This model is based on the same data set and assumptions as Figure 7.

sources of water for human, industrial, and agricultural consumption. As a result, little effort was spent to characterize the nature and extent of groundwater systems whose development was perceived as economically prohibitive or whose water quality was poor. This limited perspective has contributed to a number of misconceptions about the nature of the subsurface hydrologic environment, a problem that has been further aggravated by the frequent and often uncritical use of terms like "aquifer" and "aquiclude", that lack precise definitions. For example, a water-bearing formation that may be considered an aquifer in one region (such as a desert), might well be considered an aquiclude (i.e., essentially impervious) in a region where other significantly higher-yielding formations are present [*Davis and De Wiest*, 1966]. The evaluation of groundwater systems by such subjective standards has led to the widespread perception that groundwater flow on Earth is restricted to shallow, local aquifers with well-defined impermeable boundaries. However, over the past 30 years, numerous detailed subsurface hydrologic investigations have clearly demonstrated the inaccuracy of this picture. In this section, some of the key findings of these investigations will be summarized, providing the necessary terrestrial background for evaluating the likelihood, potential extent, and subsequent evolution, of a global groundwater system on Mars.

3.1. *The Occurrence of Groundwater*

Deep well observations indicate that groundwater is present, at some depth, virtually everywhere beneath the Earth's surface [*Waltz*, 1969; *de Marsily et al.*, 1977; *Fetter*, 1980]. According to *Brace* [1971], this zone of saturation generally extends to a depth that is at least 4–5 km below the regional water table. However, there is considerable evidence that groundwater persists to even greater depths. Some of this evidence comes from studies of the electrical conductivity of the top 20 km of the Earth's crust, a conductivity that is several orders of magnitude higher than that of dry rock studied under similar conditions of temperature and pressure [*Hyndman and Hyndman*, 1968; *Brace*, 1971; *Nekut et al.*, 1977; *Thompson et al.*, 1983; *Shankland and Ander*, 1983]. Although a wide variety of explanations have been proposed to account for these observations, laboratory studies and theoretical arguments both strongly suggest that the high electrical conductivity of the crust owes its origin to the existence of water-saturated permeable rock at depth [*Hyndman and Hyndman*, 1968; *Brace*, 1971; *Shankland and Ander*, 1983; *Gough*, 1992].

More direct evidence for the existence of groundwater at depth comes from deep borehole studies, such as the Russian "superdeep" research well located in the Kola Peninsula [*Kozlovsky*, 1982, 1984]. The Kola well, which is part of an extensive Russian program to study the deep structure and evolution of the continental crust, has penetrated to a depth of over 12 km. Throughout the interval of 4.5–9 km, the well encountered numerous zones of intensely fractured crystalline rock from which large flows of hot, highly mineralized water were released. These flows occurred despite confining pressures in excess of 3 kbar [*Kozlovsky*, 1982]. Flow under these conditions is thought to be possible only when the permeability of the host rock is low enough for pore fluid pressures to reach lithostatic values; transport may then occur by the propagation of fluid-filled microfractures in response to tectonic stress [*Thompson and Connolly*, 1992]. Such an argument has been proposed to explain the isotopic (δD and $\delta^{18}O$) composition of groundwater found in deep fault zones, which indicates that surface-derived water has circulated to depths as great as 10–15 km [*Kerrich et al.*, 1984; *McCaig*, 1988].

3.2. *The Large-Scale Permeability of the Earth's Crust*

Numerous borehole and seismic investigations have established that the Earth's crust consists largely of fractured rock [*LeGrand*, 1979; *Brace*, 1980, 1984; *Mair and Green*, 1981; *Seeburger and Zoback*, 1982]. While some early studies suggested that the density of fractures declines appreciably with depth [e.g., *Snow*, 1968], more recent investigations indicate that this correlation is limited to the weathered, near-surface layer. Indeed, in numerous wells drilled in various parts of the world, fractures are invariably found down to the limit of exploration, with little or no evidence of a significant decline in fracture density [*Seeburger and Zoback*, 1982; *Haimson and Doe*, 1983; *Kozlovsky*, 1982, 1984].

Although independent of depth, the variability of fracture density within a given borehole, or between boreholes, is often considerable. For example, one hole may exhibit a fairly uniform distribution of fractures throughout its length, while another, just a few kilometers away, may display concentrations of fractures in densely fractured intervals [*Seeburger and Zoback*, 1982; *Haimson and Doe*, 1983]. As a result, neighboring wells may some-

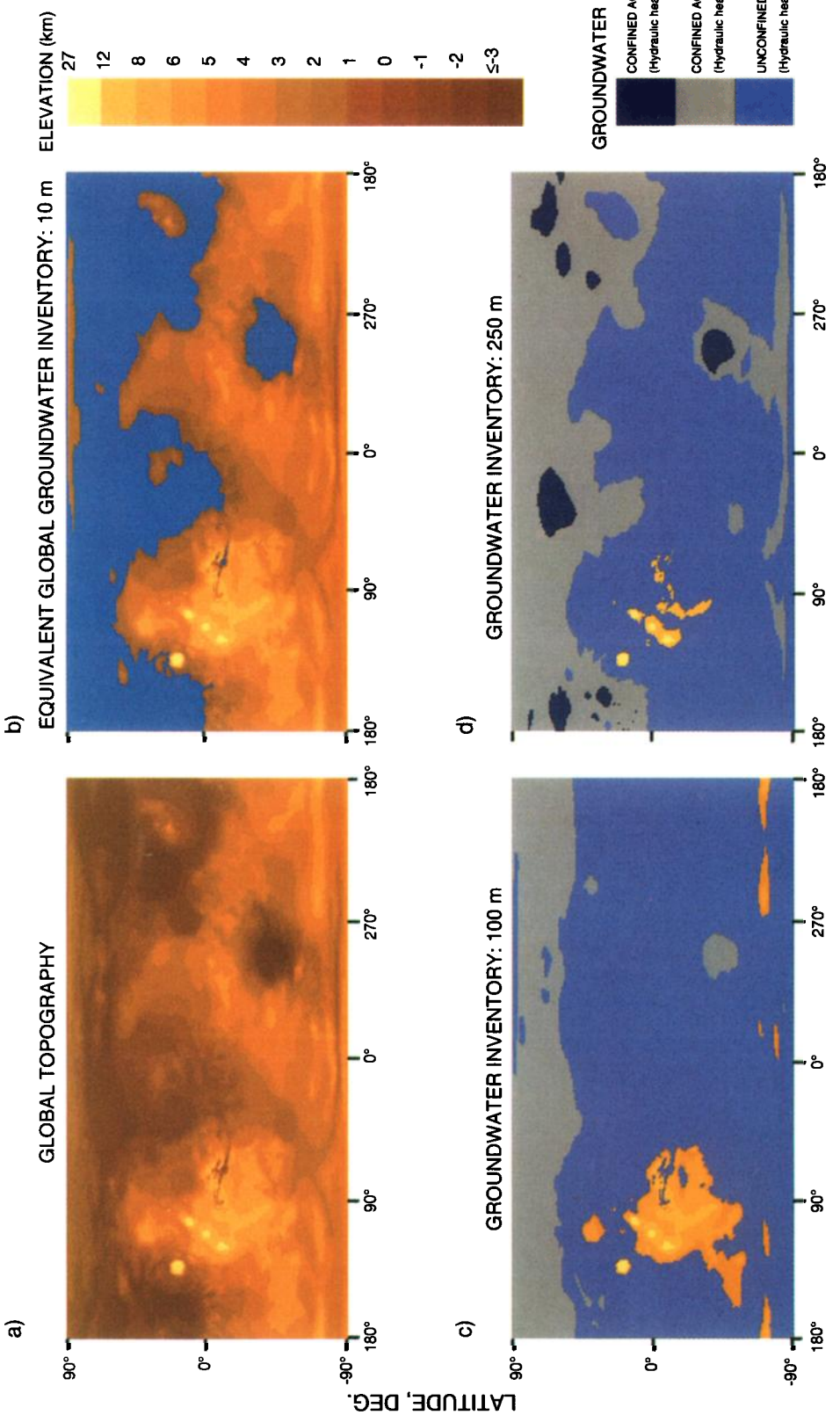

Plate 1. (*a*) The USGS Mars Digital Terrain Model and (*b-d*) the geographic distribution of groundwater on Mars for global groundwater inventories of (*b*) 10 m, (*c*) 100 m, and (*d*) 250 m. The crustal model is the same as that depicted in Figure 7, where: the latitudinal variation in ground ice thickness is given by the nominal model in Table 4, the groundwater is assumed to be in hydrostatic equilibrium, the local porosity profile of the crust is given everywhere by equation (1), and the self-compaction depth mirrors the gross variation of surface topography at a constant depth of 10 km beneath the surface.

times show as much as a four-order-of-magnitude difference in permeability over the same depth interval [*Brace*, 1980].

Because of the spatial variability of fractures, the effective permeability of crustal rocks is critically dependent on the scale of the sample under consideration (Figure 9). For example, laboratory measurements of samples several centimeters in size generally indicate only the minimum permeability of a rock mass [*Brace*, 1984]. However, at the scale of interest for most hydrogeologic studies (generally 10^2–10^3 m), virtually all crustal rocks have undergone a considerable degree of fracturing, dramatically increasing their effective permeabilities [*Streltsova*, 1976; *LeGrand*, 1979; *Seeburger and Zoback*, 1982; *Brace*, 1980, 1984].

Despite the low porosity of fractured rock (~1%), its permeability is often quite high [*LeGrand*, 1979; *Brace*, 1980; *Fetter*, 1980]. This is because the pore geometry of a fracture is inherently more efficient at conducting a fluid per unit porosity than the geometry of an intergranular pore network; thus, a rock with a fracture porosity of only 0.011% can have the same permeability as a silt with a porosity of 50% [*Snow*, 1968].

The pervasive nature of crustal fractures means that few, if any, large-scale geologic formations can be considered impermeable [*de Marsily et al.*, 1977; *Fetter* 1980; *Brace*, 1980, 1984]. Indeed, *Brace* [1980, 1984] has summarized the results of in situ borehole permeability measurements, as well as permeabilities inferred from large-scale geologic phenomena (such as earthquakes triggered by fluid injection from nearby wells), and has concluded that, on a size scale of 1 km, the average permeability of the top 10 km of the Earth's crust is roughly 10^{-2} darcies (where 1 darcy is the permeability necessary to permit a specific discharge of 1 cm s^{-1} for a fluid with a viscosity of 1 centipoise under a hydraulic pressure gradient of 1 bar cm^{-1}; 1 darcy = 10^{-12} m^2). Thus, at this size scale, virtually all groundwater systems on Earth may be considered hydraulically interconnected. The extent of this interconnection has become increasingly apparent as detailed hydrogeologic studies have demonstrated the potential for contamination of groundwater supplies by migrating chemical and radioactive wastes [*de Marsily et al.*, 1977; *Anderson*, 1987].

3.3. *Local and Regional Groundwater Flow*

On Earth, the smallest and most dynamic element of a groundwater flow system is typically a shallow unconfined aquifer located within a small topographic basin. Because the aquifer is recharged by atmospheric precipitation, the water table generally conforms to the shape of the local terrain (Figure 10). The elevated water table that occurs at the boundary between basins is called a groundwater divide. The extent to which infiltration from the surface contributes to groundwater flow in neighboring basins is based solely on which side of the divide the infiltration occurs. The resulting variation in hydraulic head then drives the flow of groundwater to the basin interior, where it evaporates from the water table or is discharged to the surface as a lake or spring-fed stream.

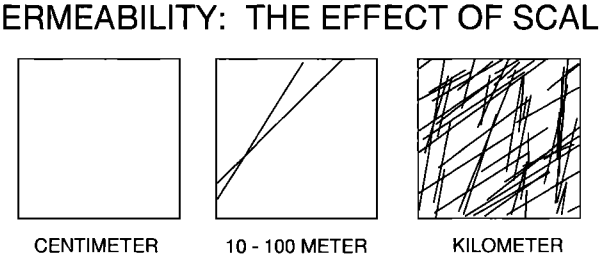

Fig. 9. The effect of scale on crustal permeability measurements (after *Brace* [1984]). Laboratory studies of rock samples only a few centimeters in size generally yield only the minumum permeability of a rock mass. However, on a size scale of kilometers, the pervasive nature of crustal faults and fractures yields a mean permeability of ~10^{-2} darcies for the top 10 km of the Earth's crust.

Although most basin aquifers are modeled as if they were hydraulically independent, virtually all are part of larger intermediate and regional groundwater flow systems (Figure 11) [*Toth*, 1963, 1978; *Ambroggi*, 1966; *Freeze and Witherspoon*, 1967; *Mifflin and Hess*, 1979; *Habermehl*, 1980; *Castany*, 1981; *Issar*, 1985]. In such systems, neighboring basins are linked by networks of intersecting faults and fractures. In practice, the extent of this interconnection is not often recognized because the volume of water that participates in interbasin flow usually represents only a small fraction of a basin's total hydrologic budget. Exceptions are noted when there are sizable differences in precipitation between neighboring basins and/or the fracture permeability of the intervening formation is high.

3.4. *Examples of Large-Scale Terrestrial Groundwater Flow Systems*

In areas that experience frequent precipitation, both the shape of the water table and the direction of groundwater flow are strongly influenced by the local topography, making any evidence of regional or interbasin flow difficult to recognize. However, in arid regions, the long intervals between atmospheric recharge often provide sufficient time for the topographic influence on the shape of the water table to decay, making evidence of large-scale hydraulic continuity considerably easier to identify. For this reason, the best recognized examples of regional groundwater flow on Earth are all found in arid environments.

3.4.1. *The Great Basin Carbonate Aquifer System, USA.* Some of the very first evidence for interbasin groundwater flow came from Death Valley, California, where it was observed that the discharge of certain springs far exceeded that which could be explained by local recharge [*Hunt and Robinson*, 1960]. This discovery suggested that groundwater derived from the higher intermontane basins to the east was reaching Death Valley via an extensive network of interconnected fractures through a thick intervening formation of carbonate rock. Convincing support for this hypothesis came from the near identical chemical composition of spring water in Death Valley and that found ~70 km to the east in the intermontane valley of Ash Meadows, Nevada.

The discovery of interbasin flow between Ash Meadows and Death Valley raised concern about the possibility of groundwater contamination from underground nuclear tests conducted at the nearby Nevada Test Site [*Winograd*, 1962]. Although the three large basins encompassed by the Test Site are topographically isolated, the well water levels in all three are essentially identical, a result that argues strongly for hydraulic interconnection. Shortly after this discovery, another regional groundwater system was discovered to the east of the Test Site that linked 13 intermontane valleys into a regional flow system measuring roughly 385 by 115 km [*Eakin*, 1966]. Indeed, as investigations continue, it is now believed that most of western Utah, eastern and southern Nevada, and the southeastern corner of California are underlain by one or more deep regional flow systems that extend from Great Salt Lake to Death Valley. The host rock is a thick (6–9 km) accumulation of Paleozoic limestone and dolomite that underlies ~1.6 × 10^5 km^2 of the Great Basin province [*Mifflin*

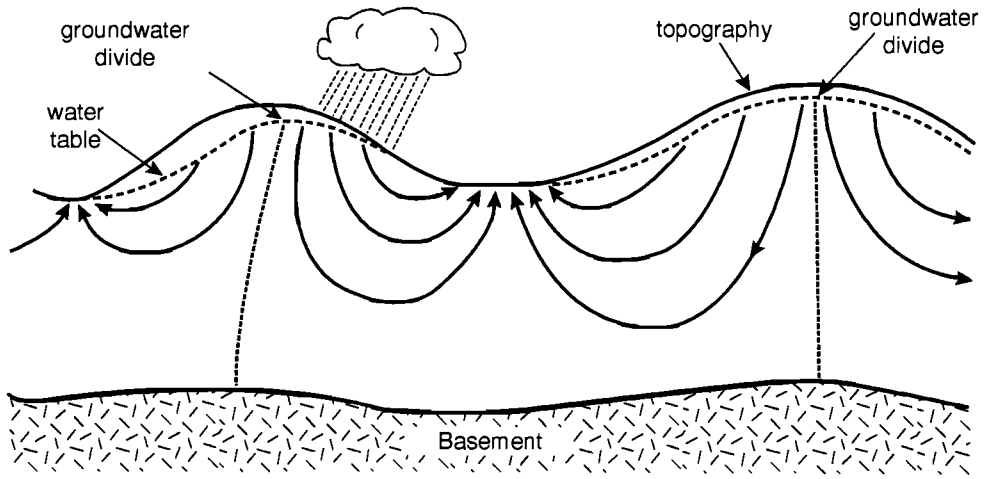

Fig. 10. A sketch of a local groundwater flow system, illustrating the relationship between topography, the shape of the water table, and the direction of subsurface flow.

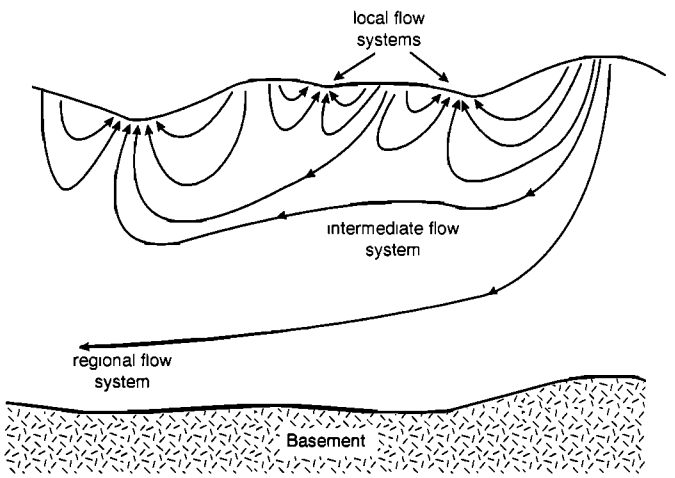

Fig. 11. An illustration of the nested nature, lateral extent, and relative depth of flow of local, intermediate, and regional groundwater flow systems.

and Hess, 1979; *Harrill*, 1984; *Thomas and Mason*, 1986]. Because little data has been collected below the upper zone of saturation, the full extent of hydraulic continuity within the system has yet to be established. However, at depth, the limited evidence that does exist suggests that solution-widened fractures and caverns have created widespread regions of high permeability, a characteristic that has made carbonate aquifers among the most extensive and productive in the world [*LeGrand and Stringfield*, 1973; *Mifflin and Hess*, 1979].

3.4.2 *The Great Artesian Basin, Australia.* The Great Artesian Basin underlies ~1.7 × 10^6 km^2 of the eastern half of Australia, an arid to semi-arid region that represents over one-fifth the land area of the entire continent [*Habermehl*, 1980]. Structurally, the basin is a bowl-shaped depression that contains up to 3 km of sedimentary deposits. These deposits form a multilayer confined aquifer system consisting of sandstone aquifers sandwiched between less permeable layers of siltstone and mudstone [*Habermehl*, 1980; *Cathles*, 1990].

The basin is recharged along its eastern margin by precipitation on the elevated slopes of the Great Dividing Range. Discharge by natural springs occurs primarily in a region 900 km to the southwest, in the vicinity of Lake Eyre [*Habermehl*, 1980]. Numerical models and isotopic data suggest that the natural flow velocity through the basin's principal aquifer is ~1.0 m yr^{-1}, with a total east-west transit time in excess of 1 million years [*Bentley et al.*, 1986; *Cathles*, 1990].

Unlike the Great Basin Carbonate Aquifer System in the United States, the geologic simplicity of the Great Artesian Basin Aquifer led to early recognition of both its physical dimensions and the extent of groundwater flow [e.g., *Pittman*, 1914]. To this day, it remains the largest recognized single-basin groundwater system on Earth.

3.4.3. *The Nubian Aquifer System of the Eastern Sahara.* The groundwater resources of the Sahara Desert in North Africa are divided among eight major sedimentary basins [*Ambroggi*, 1966; *Burdon*, 1977; *Margat and Saad*, 1984]. Two of these, the Dakhla Basin of Egypt and the Kufra Basin of Libya, form the Nubian Aquifer System of the Eastern Sahara, a regional aquifer with an area of ~2 × 10^6 km^2 [*Schneider*, 1986; *Hesse et al.*, 1987]. The aquifer's principal water-bearing formation is the Nubian Sandstone, which varies in thickness from less than 500 m to more than 3000 m [*Shata*, 1982]. In the northern portion of the system (i.e., between ~25°N and the southern shore of the Mediterranean Sea) the sandstone is intercalated with shales and clays and overlain by fractured carbonate rock, creating a confined multilayered system of considerable complexity [*Shata*, 1982; *Hesse et al.*, 1987].

From a human and agricultural resource perspective, the Nubian Aquifer is generally considered hydraulically isolated; however, there is considerable evidence of hydraulic continuity far beyond the system's recognized boundaries. For example, the northern limit of the aquifer is usually defined by the location of the saline-fresh water interface that occurs up to several hundred kilometers inland from the Mediterranean Sea [*Shata*, 1982; *Thorweihe*, 1986]. Although the location of this chemical transition is important in the context of water quality, it has no bearing on the extent of hydraulic continuity. Indeed, exploration wells in northern Egypt have established that the Nubian sandstone persists and deepens as it extends northward beneath the Mediterranean's southern shore [*Shata*, 1982; *Thorweihe*, 1986].

The remaining boundaries of the Nubian Aquifer are similarly vague. For example, along most of its eastern margin, the Nubian Aquifer is bounded by an outcrop of basement between the Nile Valley and Red Sea. However, further north, where the outcrop disappears, there is evidence of a connection to a major aquifer in the Sinai peninsula [*Shata*, 1982; *Issar*, 1985]. To the south, water table contours suggest hydraulic continuity with the Blue Nile-Main Nile Basin [*Hesse et al.*, 1987] as well as groundwater

inflow from northeastern Chad [*Ambroggi*, 1966; *Edmunds and Wright*, 1979]. Finally, in the west, there is evidence of a hydraulic link between the Nubian Aquifer and the Sirte Basin in Libya [*Edmunds and Wright*, 1979]. Because detailed hydrologic information is scarce throughout the Eastern Sahara, the degree of the hydraulic interconnection between these neighboring systems is difficult to assess. It is clear, however, that as the area of recognized hydraulic continuity expands, the likelihood of additional links with neighboring basins increases as well.

In summary, the distribution and flow of groundwater on Earth exhibits several characteristics that are of potential importance in understanding the subsurface hydrology of Mars. First, given a global inventory of H_2O that exceeds the pore volume of the cryosphere by as little as a few percent, groundwater is likely to be found virtually everywhere beneath the Martian surface. Second, as on Earth, it is likely that such groundwater will persist and circulate to depths far in excess of the 10 km self-compaction depth assumed in this study. Third, in the absence of atmospheric precipitation, the hydraulic boundaries of a groundwater system on Mars will be determined, not by the local topography or the presence of groundwater divides, but by the continuity of pore space beneath the water table. Fourth, given a km-scale permeability of the Martian crust no greater than that of the Earth ($\sim 10^{-2}$ darcies), the extent of hydraulic continuity, and thus the potential areal extent of a Martian groundwater system, is essentially global.

4. The Stability and Replenishment of Equatorial H_2O

Theoretical considerations and various lines of morphologic evidence suggest that, in addition to the normal seasonal and climatic exchange of H_2O that occurs between the Martian polar caps, atmosphere, and mid- to high-latitude regolith [e.g., *Jakosky*, 1985; *Zent et al.*, 1986], large volumes of water have been introduced into the atmospheric leg of the planet's long-term hydrologic cycle by the sublimation of equatorial ground ice, impacts, catastrophic flooding, and volcanism. In this section both endpoints of the proposed cycle are discussed, beginning with the loss of water from crustal reservoirs at equatorial and temperate latitudes and concluding with its possible replenishment by subsurface sources of H_2O. The intermediate steps of the proposed cycle, including polar deposition, basal melting, and pole-to-equator groundwater flow, are discussed at length in section 5.

4.1. *The Stability of Equatorial Ground Ice*

Although mean annual surface temperatures are below freezing everywhere on Mars, observations made by the Viking Orbiter Mars Atmospheric Water Detectors (MAWD) indicate a globally averaged frost point temperature of ~198 K. Therefore, given the present latitudinal range of mean annual surface temperatures (~154–218 K), any subsurface reservoir of H_2O is unstable with respect to the water vapor content of the atmosphere at latitudes equatorward of ±40° (Figure 3) [*Farmer and Doms*, 1979].

Despite this fact, there is a considerable body of morphologic evidence that suggests that both ground ice and groundwater have survived at some depth within the equatorial regolith throughout much of Martian geologic history. At latitudes poleward of 30°, this evidence is based on the identification of Martian analogs to cold-climate features found on Earth, such as debris flows, table mountains, and thermokarst. These features have been reviewed by a number of investigators [*Carr and Schaber*, 1977; *Allen*, 1979*a*; *Rossbacher and Judson*, 1981; *Lucchitta*, 1981, 1985; *Squyres and Carr*, 1986; *Carr*, 1986; *Squyres*, 1989; and others]; their common conclusion has been that of the possible mechanisms that might explain the presence of these features, those involving ground ice appear the most reasonable. Additional evidence (found at all latitudes) for the presence of subsurface H_2O, is provided by the occurrence of rampart craters, whose distinctive lobate ejecta morphology is thought by many investigators to originate from the fluidization of ejecta material during an impact into a water- or ice-rich crust [*Carr et al.*, 1977; *Johansen*, 1978; *Allen*, 1979*b*; *Mouginis-Mark*, 1979, 1987; *Blasius and Cutts*, 1981; *Kuzmin*, 1983; *Kuzmin et al.*, 1988; *Costard*, 1989; *Barlow and Bradley*, 1990]. Finally, the survival of a significant reservoir of subsurface water in the equatorial region is also supported by the presence of the outflow channels, whose episodic development appears to have spanned much of Martian geologic history [*Carr*, 1981; *Baker*, 1982; *Tanaka*, 1986].

The above evidence presents a problem, for it is difficult to account for both the initial origin and continued survival of H_2O in a region where the present mean annual surface temperature exceeds the frost point by more than 20 K. Indeed, under current climatic conditions, any subsurface H_2O should experience a net annual depletion, resulting in its preferential transfer from the "hot" equatorial region to the colder latitudes poleward of ±40° [*Flasar and Goody*, 1976; *Toon et al.*, 1980; *Clifford and Hillel*, 1983; *Fanale et al.*, 1986].

Currently, the most widely accepted explanation for the existence of a subsurface reservoir of equatorial H_2O is that it is a relic, emplaced very early in Martian geologic history (> 3.5 b.y.) and under substantially different climatic conditions. This explanation is based in part on the work of *Smoluchowski* [1968], who showed that under certain restricted conditions of porosity, pore size, temperature, and depth of burial, the diffusion-limiting properties of a fine-grained regolith could preserve equatorial ground ice for billions of years.

The stability of ground ice is governed by the rate at which H_2O molecules can diffuse through the regolith and into the atmosphere. This process is complicated by the fact that the collisional mean free path of an H_2O molecule in the Martian atmosphere is ~10 μm. When the ratio of the pore radius to the mean free path of the diffusing molecules is large ($r/\lambda > 10$), bulk molecular diffusion is the dominant mode of transport (i.e., where diffusion occurs in response to the repeated collisions that happen with other molecules present in the soil pores). However, for very small pores ($r/\lambda < 0.1$), collisions between the diffusing molecules and the pore walls greatly outnumber those that occur with other molecules, a process known as Knudsen diffusion. Because the frequency of pore wall collisions increases with decreasing pore size, small pores can substantially reduce the efficiency of the transport process. For pores of intermediate size ($0.1 < r/\lambda < 10$), the contributions of both diffusive processes must be taken into account [*Younquist*, 1970; *Clifford and Hillel*, 1983, 1986].

The effect of a 10 μm mean free path on the diffusion of H_2O through the regolith is clearly seen in Figure 12, where the effective diffusion coefficient of water vapor D_{eff} has been plotted as a function of pore size. D_{eff} is given by

$$D_{eff} = \frac{D_{AB}\, D_{KA}}{D_{KA} + D_{AB}} \tag{3}$$

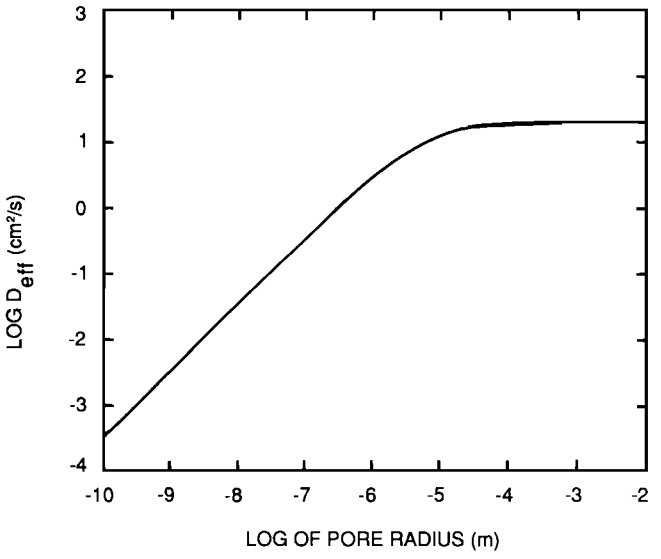

Fig. 12. The effective diffusion coefficient of water vapor in the Martian regolith plotted as a function of pore size [*Clifford and Hillel*, 1983].

where D_{AB} and D_{KA} are the bulk and Knudsen diffusion coefficients respectively [*Scott and Dullien*, 1962; *Rothfield*, 1963]. After *Wallace and Sagan* [1979], the bulk diffusion coefficient of H_2O through an atmosphere of CO_2 (in $cm^2\ s^{-1}$) is given by

$$D_{AB} = 0.1654\ (T/273.15)^{3/2}\ (1.013 \times 10^6/P) \quad (4)$$

where T is the temperature and P is the total pressure (in dynes cm^{-2}). However, as discussed by *Clifford and Hillel* [1986], the expression for calculating D_{KA} is dependent on the specific shape of the soil pores. For the simple case of a straight cylindrical pore of radius r, we have

$$D_{KA} = \frac{2}{3}\, r \left(\frac{8\,T\,R}{\pi\,M_A}\right)^{1/2} \quad (5)$$

where R is the universal gas constant and M_A is the molecular weight of H_2O. Of course, most soils generally exhibit a broad spectrum of pore sizes. The impact of this characteristic on vapor transport is illustrated in Figure 13, where the differential and cumulative flux of H_2O is plotted for three hypothetical pore size distributions.

The survival of equatorial ground ice was considered in detail by both *Clifford and Hillel* [1983] and *Fanale et al.* [1986]. They found that, for reasonable values of porosity and pore size, the near-equatorial crust has probably been desiccated to a depth of 300–500 m over the past 3.5 billion years. However, because the sublimation of H_2O is sensitively dependent on temperature, the quantity of ice lost from the regolith is expected to decline with increasing latitude, falling to perhaps a few tens of meters at a latitude of 35° (Figure 14) [*Clifford and Hillel*, 1983; *Fanale et al.*, 1986].

Of course, a variety of factors are likely to complicate this simple picture of equatorial desiccation. For example, if the effective pore size of the regolith is larger than 10 μm, or if the regolith has a specific surface area $\gtrsim 10^3\ m^2\ g^{-1}$ (a condition that would give rise to a diffusive surface flux greater than any likely pore gas flux [*Clifford and Hillel*, 1983]), the actual depth of desiccation could well exceed the values calculated by *Clifford and Hillel* [1983] and *Fanale et al.* [1986]. Alternatively, shallower depths of desiccation will result if the gound ice is replenished (section 4.5), the effective regolith pore size is less than 1 μm, or if its porosity is less than the 50% value assumed in these two studies. Considerations that argue in favor of a spatially variable (and generally lower) porosity include: igneous re-

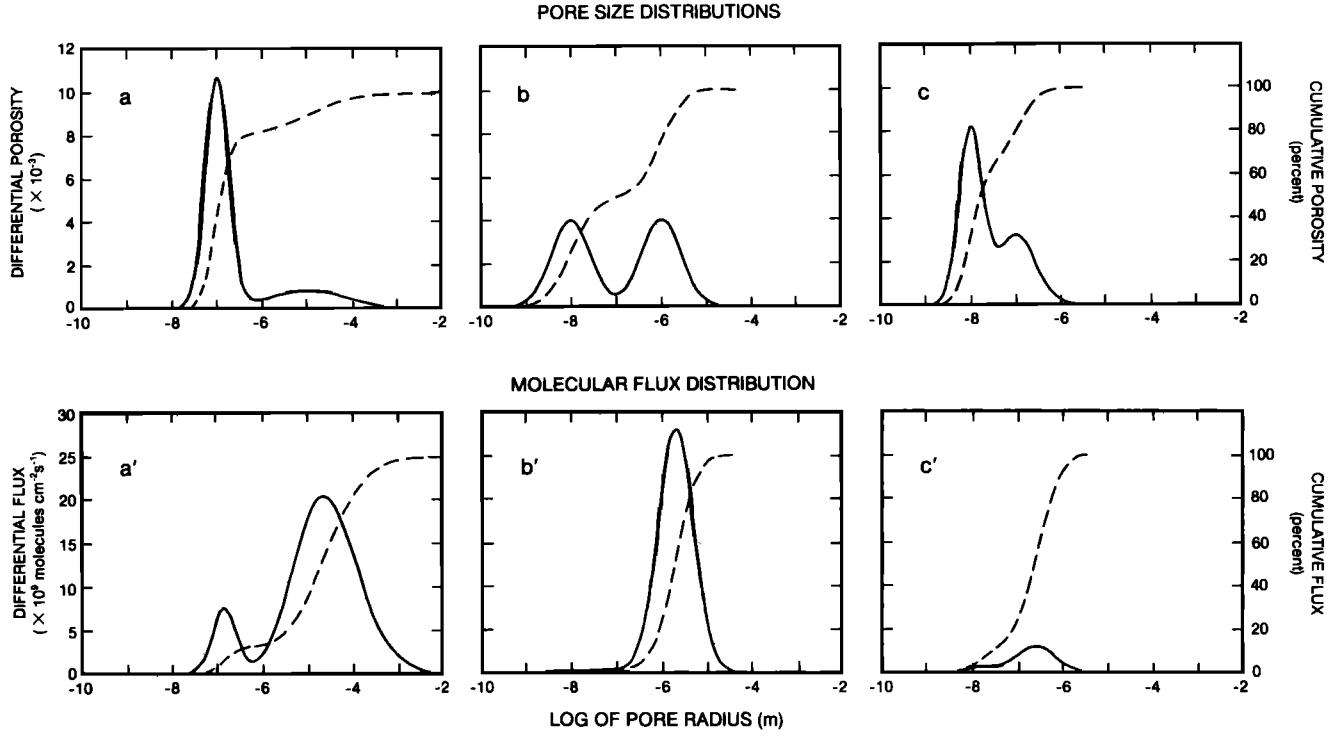

Fig. 13. (*a–c*) The differential and cumulative porosities of three hypothetical soils and (*a'–c'*) the corresponding diffusive flux of H_2O that results from these pore size distributions [*Clifford and Hillel*, 1986].

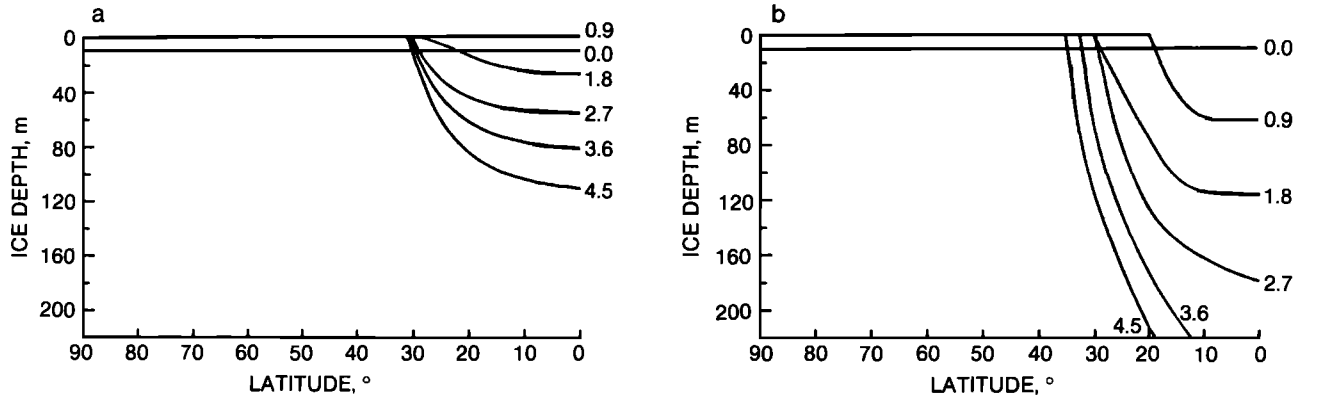

Fig. 14. The recession of equatorial ground ice on Mars as a function of latitude and time (b.y.). The regolith models adopted for these calculations differ only in assumed pore size: (*a*) $r = 1$ μm, and (*b*) $r = 10$ μm (from *Fanale et al.* [1986]).

consolidation, duricrust formation, and the self-compaction of the regolith with depth. Perhaps more importantly, variations in the local thermophysical properties of the surface (versus the globally averaged values assumed in Figure 14) can affect mean annual temperatures, causing significant differences in both the geographic stability of ground ice and its predicted depth of desiccation [*Paige*, 1992; *Mellon and Jakosky*, 1993]. A final caveat regards the potential effect of quasi-periodic changes in Martian obliquity and orbital elements, the primary drivers of climate change. Recent studies suggest that the obliquity of Mars is chaotic and may vary from a minimum of 0° to a maximum of 50° or higher [*Bills*, 1990; *Touma and Wisdom*, 1993; *Laskar and Robutel*, 1993]. Although these extremes exceed the 10.8°–38° obliquity range considered by *Fanale et al.* [1986], their short duration and limited effect on equatorial temperatures suggests that their potential impact on the loss of equatorial ground ice will be minimal. More pronounced effects are likely at the poles, where the increased insolation associated with high obliquities could have a considerable effect on the stability of the ice caps. (A more detailed discussion of the polar mass balance and high obliquities is contained in section 7.2.)

By integrating the total pore volume between the Martian surface and the desiccation depths presented in Figure 14, *Fanale et al.* [1986] have estimated that over the course of geologic history as much as 2.7–5.6 × 10^6 km^3 of H_2O (equivalent to a global ocean ~20–40 m deep) may have been sublimed from the equatorial regolith and cold-trapped at the poles. As seen in Table 6, however, the sublimation of equatorial ground ice is just one of several potential processes that may have episodically introduced large volumes of water into the atmosphere.

4.2. *Other Crustal Sources of Atmospheric Water*

Perhaps the clearest evidence that the crust has been a major source of atmospheric water are the outflow channels. The abrupt emergence of these features from regions of collapsed and disrupted terrain, suggests that they were formed by a massive and catastrophic release of groundwater [*Sharp and Malin*, 1975; *Carr*, 1979; *Baker*, 1982; *Baker et al.*, 1992]. Channel ages, inferred from the density of superposed craters, indicate at least several episodes of flooding, the oldest dating back as far as the Late Hesperian (~3 billion years ago), while the youngest may have formed as recently as the Mid-to-Late Amazonian (i.e., within the last 1 billion years) [*Tanaka*, 1986; *Tanaka and Scott*, 1986; *Parker et al.*, 1989; *Mouginis-Mark*, 1990; *Rotto and Tanaka*, 1991; *Baker et al.*, 1992]. Based on a conservative estimate of how much material was eroded to form the channels in Chryse Planitia (~5 × 10^6 km^3) and the maximum sediment load that the flood waters could have carried (~40% by volume), *Carr* [1987] has estimated a minimum cumulative channel discharge of 7.5 × 10^6 km^3 of H_2O (equivalent to a global ocean ~50 m deep). However, if the channels were formed by multiple episodes of outbreak and erosion, then the flood waters may have been less turbulent and carried less sediment than generally assumed [*Baker et al.*, 1992]. If so, the total volume of water required to erode the channels may have been many times the estimate of *Carr* [1987]. Indeed, *Baker et al.* [1991] suggest that the total discharge may have been sufficient to flood the northern plains with as much as 6.5 × 10^7 km^3 of water (equal to a global layer 450 m deep).

Impacts into the Martian crust are another potential source of atmospheric water [*Carr*, 1984]. Assuming a representative cry-

TABLE 6. Crustal Sources and Potential Contributed Volumes of Atmospheric Water

Crustal Source	Volume, km^3	Equivalent Layer, m H_2O
Sublimation of ground ice [*Fanale et al.*, 1986]	2.7–5.6 × 10^6	20–40
Catastrophic floods [*Carr*, 1987; *Baker et al.*, 1991]	0.75–6.5 × 10^7	50–450
Volcanism [*Greeley and Schneid*, 1991]	2.3 × 10^6	15
Impacts [*this work*]		
Excavation/volatization*	1.5–3.0 × 10^7	100–200
Hydrothermal circulation†	1.9 × 10^7	130
Totals	0.47–1.2 × 10^8 km^3	315–830 m

*Calculation assumes a crustal inventory of 500–1000 m of water within the top 10 km of the crust and a global crater density equivalent to that found in the cratered highlands.

†Figure represents the potential quantity of water brought to the surface by impact-generated hydrothermal systems alone (section 4.4.3).

osphere thickness of 2.5 km, an ice content of 20%, and a transient crater diameter given by equation (11) (see section 4.4.2), the volume of water excavated and/or volatilized by individual impacts will range from ~34 km^3 for a crater 10 km in diameter to in excess of 2.8×10^5 km^3 for a major impact basin like Hellas (D ~2000 km). Note that because craters with diameters ≥ 40 km have excavation depths that exceed the predicted 10 km self-compaction depth of the megaregolith, the volume of water excavated by large impacts depends on neither the state nor the depth of the subsurface reservoir of H_2O, but solely on the quantity of water stored per unit area in the crust. Therefore, given a global crater size-frequency distribution equivalent to that preserved in the cratered highlands [e.g., *Barlow*, 1990] and a crustal water inventory of 500–1000 m [*Carr*, 1987], we find that the cumulative volume of water injected into the atmosphere by impacts over geologic time is ~$1.5–3.0 \times 10^7$ km^3 (or roughly 100–200 m). However, this figure represents only the water that was physically excavated by the impacts. As discussed in section 4.4.3, the subsequent development of impact melt-driven hydrothermal systems could have brought as much as an additional 130 m of water to the surface. This possibility is supported by both the evidence for hydrothermal activity associated with terrestrial impact craters and the observed association of many valley networks with the outside rims of craters throughout the Martian cratered highlands [*Newsom*, 1980; *Brakenridge et al.*, 1985].

Finally, as discussed by *Greeley* [1987] and *Plescia and Crisp* [1991], it is likely that volcanism also injected large volumes of water into the atmosphere. For example, *Plescia and Crisp* [1991] estimate that during the emplacement of the volcanic plains in southeastern Elysium (5° N, 195° W), lavas may have exsolved between 10^3–10^4 km^3 of H_2O, assuming a water content comparable to that of terrestrial mafic to ultramafic lavas (~1% by weight). *Greeley* [1987] has taken a more global perspective, calculating the total volume of juvenile water released from the planet's interior by estimating the extent and thickness of all volcanic units visible on the planet's surface. However, *Greeley*'s [1987] estimate of extrusive magma production has recently been revised downward by *Greeley and Schneid* [1991]. Substituting this revised figure for that in *Greeley*'s [1987] original analysis suggests that volcanic processes have released a total of 2.3×10^6 km^3 (~15 m) of H_2O into the atmosphere. It should be noted, however, that in light of our inability to accurately assess both the extent of plutonic activity and the magnitude of ancient (≥ 4 billion year old) volcanism, this estimate is likely a minimum. Note also that, unlike water derived from other crustal sources (which simply undergoes an exchange from one volatile reservoir to another), water released by volcanism represents an actual addition to the planet's outgassed inventory. However, once this water has been introduced into the atmosphere, its fate is governed by the same processes that affect water derived from any other crustal source, leading to a slow but inexorable transfer from equatorial and temperate latitudes to the poles [*Clifford and Hillel*, 1983; *Fanale et al.*, 1986].

4.3. *Evidence of Ground Ice Replenishment*

Under the climatic conditions that have apparently prevailed on Mars throughout most of its history, the loss of equatorial ground ice appears irreversible; thus, once ice has sublimated, or been removed by some other process (e.g., impact cratering), it is difficult to see how the depleted crust could be replenished by any atmospheric means [*Clifford and Hillel*, 1983; *Fanale et al.*, 1986]. Yet, regardless of the actual process by which it may have occurred, consideration of the valley networks, outflow channels and the crustal mass balance of H_2O argues strongly for some type of crustal resupply [*Clifford*, 1980*b*, 1984; *Carr*, 1984; *Jakosky and Carr*, 1985; *Baker et al.*, 1991]. This conclusion is further supported by geomorphic evidence which suggests that, at least in some locations within the latitude band of ±30°, ground ice has indeed been replenished.

Consider first the consequences of a major impact at equatorial latitudes. As noted by *Allen* [1979*a*] and *Clifford and Johansen* [1982], the production of a crater many tens of kilometers in diameter should result in the excavation of any ground ice that existed, prior to the impact, within the region interior to the crater walls (Figure 15). While backfilling and melting of nearby ground ice may partially replenish some of the H_2O lost near the crater periphery, it appears unlikely that its lifetime would be very long given the high temperature and porosity of the post-impact environment.

It is interesting to note, therefore, that within many large equatorial impact craters there exist clearly defined rampart craters [*Allen*, 1979*a*; *Clifford and Johansen*, 1982]. If the morphology of this type of crater does indeed arise from an impact into an ice-rich crust, then the occurrence of rampart craters within the interiors of numerous older impacts presents a problem, for it is difficult to conceive of a scenario by which any ground ice that existed prior to the original cratering event could have survived to produce the well-defined fluidized ejecta pattern often seen as the result of a second and sometimes third consecutive and concentric impact (Figure 16).

There are at least two explanations that may account for these observations. First, contrary to popular belief, rampart craters may not be specific indicators of ground ice. Experiments by *Schultz* [1992] and *Schultz and Gault* [1979, 1984] have demonstrated that when an impact occurs in the presence of an atmosphere, the effects of drag and turbulence can modify the emplacement of ejecta, reproducing many of the features generally associated with Martian rampart craters. This effect is clearly seen in the recent Magellan radar images of Venus, where craters with multilobate, fluidized ejecta morphologies are abundant despite the absence of water [*Phillips et al.*, 1991].

Although laboratory impact experiments and the Magellan radar images both suggest that the presence of an atmosphere may play a role in rampart crater formation, they do not exclude the possibility that, on Mars, water and ice may have contributed to the process as well. Indeed, three lines of evidence lend credence to the original proposal of a link between rampart craters and subsurface volatiles. The first is the observed latitudinal dependence of several Martian rampart crater ejecta morphologies, which vary from an apparent high-viscosity single-rampart style at polar latitudes to a highly fluidized multilobate-style near the equator [*Johansen*, 1978; *Mouginis-Mark*, 1979; *Saunders*

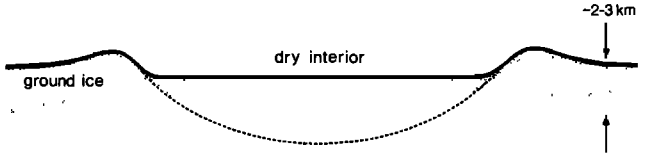

Fig. 15. The probable ground ice distribution resulting from a major impact in the equatorial region of Mars. The production of a crater many tens of kilometers in diameter should result in the excavation of any ground ice which existed, within the region interior to the crater walls, prior to the impact [*Clifford and Johansen*, 1982].

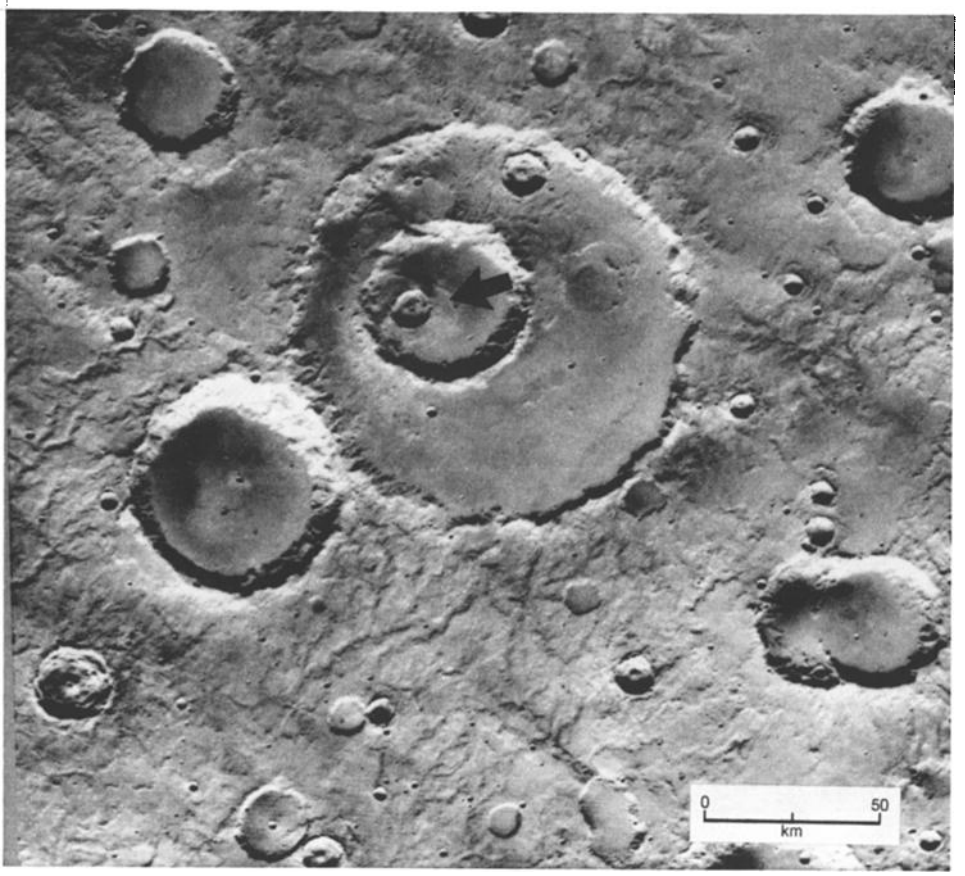

Fig. 16. A rampart crater within two earlier and concentric impacts (20° S, 203° W) [*Clifford and Johansen*, 1982]. The oldest crater in the sequence (Hadley) is approximately 110 km in diameter, while the innermost crater (arrow) has a diameter of roughly 13 km.

and Johansen, 1980; *Blasius et al.*, 1981; *Kuzmin et al.*, 1988; *Costard*, 1989; *Barlow and Bradley*, 1990]. Advocates of the ground ice hypothesis suggest that this latitudinal dependence is consistent with the pole-to-equator thinning of frozen ground predicted by thermal models of the crust (e.g., Figure 3). A second, but complementary, observation has been reported by *Kuzmin et al.* [1988], who have found that rampart crater onset diameters increase with decreasing latitude, a relationship that may reflect the greater depth of crustal desiccation expected from the instability of ground ice at these latitudes (e.g., Figure 14). The third and final line of evidence is the tentative identification of single-rampart ("pedestal") craters on Ganymede [*Horner and Greeley*, 1982], an observation that is difficult to reconcile with an atmospheric origin, but one that is fully compatible with an origin based on an impact into an ice-rich crust.

If rampart crater ejecta morphology does indeed arise from an impact into a volatile-rich target, then perhaps the most reasonable explanation for the occurrence of rampart craters within the theoretically ice-free interiors of numerous older craters is that, at some time following the original loss of ground ice, it was replenished. Given our present understanding of Martian geology and climate history, it appears that such replenishment could have only occurred from sources of water residing deep within the crust.

4.4. *Processes of Replenishment*

It has been proposed that equatorial ground ice on Mars may be episodically or continuously replenished by water derived from a subpermafrost aquifer [*Clifford*, 1980*a*, 1984]. However, as illustrated in Figure 7, the vertical distance separating the groundwater table from the base of the cryosphere may in some regions be many kilometers; thus, for replenishment to occur, some process for the vertical transport of H_2O between a deep-lying source region and the base of the cryosphere must exist. In this section, three possible mechanisms for this type of transport are considered.

4.4.1. *Thermal vapor diffusion.* Although less dramatic and energetic than the other two processes discussed in this section, perhaps the most important mechanism for the vertical transport of H_2O in the Martian crust has been the process of thermal vapor diffusion [*Clifford*, 1980a; 1983]. Clearly, given the existence of a water-rich crust, the presence of a geothermal temperature gradient will give rise to a corresponding vapor pressure gradient. As a result of this pressure difference, water vapor will diffuse from the higher temperature (high vapor pressure) depths to the colder (lower vapor pressure) near-surface regolith.

It has been known for over 75 years that vapor transport in excess of that predicted by Fick's law will occur in a moist porous medium under the influence of a temperature gradient [*Bouyoucos*, 1915]. More recently, *Philip and deVries* [1957] and *Cary* [1963] have proposed two different but widely used models for calculating the magnitude of this type of thermally driven vapor transfer. The *Philip and deVries* [1957] approach is based on a mechanistic description of the transport process. They suggest that the exchange of water vapor in an unsaturated soil occurs between numerous small "islands" of liquid that exist at the con-

tact points of neighboring particles. The existence of a temperature gradient causes water from the warmer liquid islands to evaporate, diffuse across the intervening pore space, and condense on the cooler liquid islands at the opposite end of the pore. In this fashion both moisture and latent heat are transferred through the soil.

The *Cary* [1963] model of H_2O transport differs from the Philip and deVries approach in that it makes no assumptions regarding the actual mechanism of vapor transport but merely attempts to provide a phenomenological description of the process based on the thermodynamics of irreversible processes. Despite this difference, it has been shown that the final form of the flux equations for both models are identical [*Taylor and Cary*, 1964; *Jury and Letey*, 1979]. After *Cary* [1966], the thermally driven vapor flux is given by

$$q_v = - \frac{\beta D_{eff} P_{H_2O} L_v}{\rho R_v^2 T^3} \frac{dT}{dZ} \quad (6)$$

where D_{eff} is the effective diffusion coefficient of H_2O in CO_2, P_{H_2O} is the saturated vapor pressure of H_2O at a temperature T, L_v is latent heat of vaporization (= 2.3×10^6 J kg^{-1}), R_v is the gas constant for water vapor (= 461.9 J kg^{-1} K^{-1}), ρ is the density of liquid water, and β is an empirical dimensionless factor that has been found to have a mean value of 1.83 ± 0.79 when measured over geologically reasonable ranges of temperature (276–314 K), porosity (0.3–0.5), saturation (0–100%), and soil type [*Jury and Letey*,1979].

The physical basis for the vertical transport of water vapor in response to the geothermal gradient is perhaps best understood by considering first the equilibrium distribution of vapor in an isothermal crust. Under this condition, the vapor pressure of H_2O at any height z above the water table is given by the barometric relation

$$P_{H_2O}(z) = P_{H_2O}(0) \exp(-z/H) \quad (7)$$

where $P_{H_2O}(0)$ is the saturated vapor pressure of water at $z = 0$, and H is the water vapor scale-height (= $kT/m_{H_2O}\, g \cong 36$ km, where $T = 290$ K and k is the Boltzmann constant). Thus, at a height of 1 km above the water table, the resulting hydrostatic reduction in vapor pressure is ~3% (Figure 17). However, over this same interval, a geothermal gradient of 15 K km^{-1} reduces the equilibrium saturated vapor pressure by 68%. Because the thermally induced gradient in saturated vapor pressure greatly exceeds the isothermal/gravitationally induced gradient, water vapor will diffuse upward in an effort to achieve an equilibrium barometric profile. However, as the rising vapor encounters the colder regions of the crust, the associated reduction in saturated vapor pressure forces some of the rising vapor to condense, ultimately draining back to the water table as a liquid. As a result, the flux of vapor that leaves the groundwater table greatly exceeds that which finally reaches the freezing front at the base of the cryosphere. As shown by *Jackson et al.* [1965], once a closed system has been established (i.e., the pore volume of the cryosphere has been saturated with ice), a dynamic balance of opposing fluxes is achieved, creating a circulation system of rising vapor and descending liquid condensate (Figure 18).

In Figure 19, the vapor flux resulting from a geothermal gradient of 15 K km^{-1} has been calculated from equation (6) and plotted as a function of crustal temperature for pore sizes of 1 and 10 μm. Under these conditions, the flux of vapor (per unit

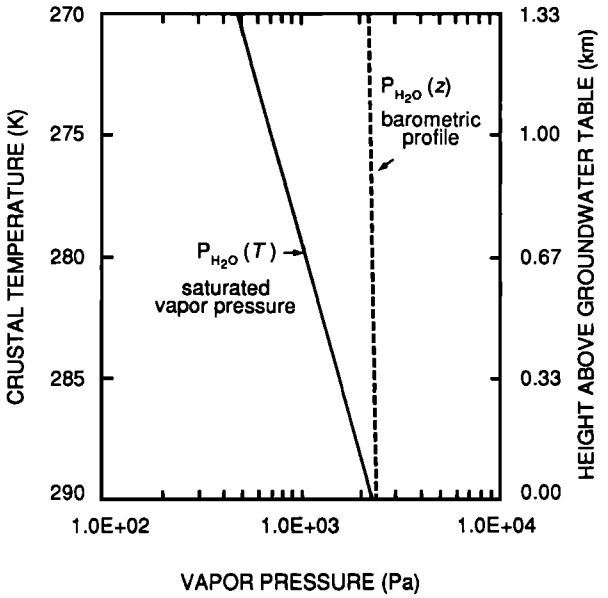

Fig. 17. The saturated vapor pressure of water $P_{H_2O}(T)$ as a function of crustal temperature T compared with the barometric profile of vapor in an isothermal crust, $P_{H_2O}(z)$, where, for illustrative purposes, the temperature at the surface of the water table has an assumed value of 290 K.

area) reaching the freezing front at the base of the cryosphere is ~8.3×10^{-5}–2.8×10^{-4} m H_2O yr^{-1}. This flux is equivalent to the vertical transport of 1 km of water every 10^6–10^7 years, or roughly 10^2–10^3 km of water over the course of Martian geologic history. However, there is reason to believe that this thermally induced vapor flux was even greater in the past. Recall that models of the thermal history of Mars suggest that 4 billion years ago the planet's internal heat flow was ~3–5 times larger than it is today [e.g., *Davies and Arvidson*, 1981, *Schubert and Spohn*, 1990]. Since the flux rate predicted by equation (6) is directly proportional to the temperature gradient, this implies a similar increase in the volume of water cycled through the early crust. (Note: The flux rates reported here are ~10^3 times greater than those previously published by *Clifford* [1983, 1984]. These ear-

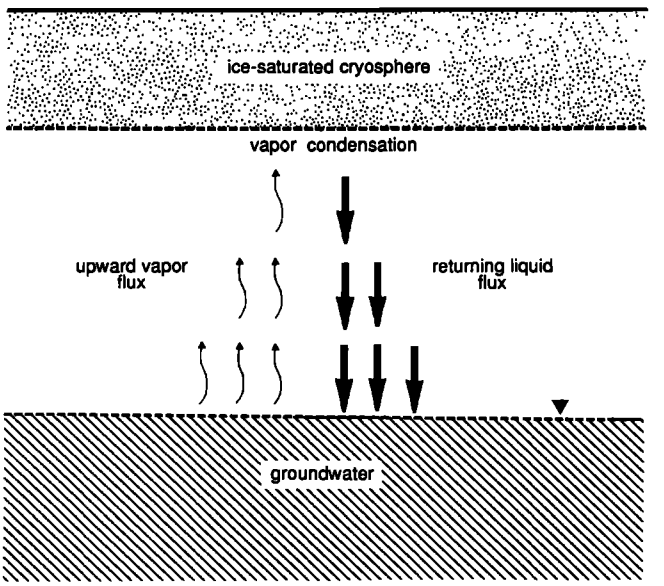

Fig. 18. An example of low-temperature hydrothermal circulation driven by the Martian geothermal gradient.

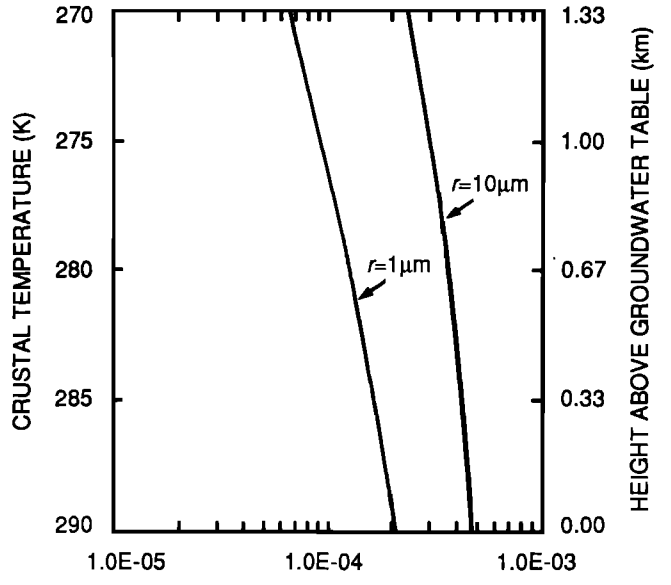

Fig. 19. Thermal vapor fluxes calculated from equation (6) for pore sizes of 1 μm and 10 μm, and a geothermal gradient of 15 K km^{-1}. Note that in a closed system (such as that illustrated in Figure 18) the rising vapor flux at any level is countered by an equal and opposite downward flux of liquid condensate.

lier calculations are incorrect, the result of a unit conversion error.)

4.4.2. *Seismic pumping.* In light of the density of impact craters preserved in the cratered highlands, perhaps the most obvious mechanism for the vertical transport of H_2O in the crust is seismic pumping. Shock waves generated by earthquakes, impacts, and explosive volcanic eruptions can produce a transient dilatation and compression of water-bearing formations that can force water to the surface through crustal fractures and pores. During the great Alaska earthquake of 1964, this process resulted in water and sediment ejection from shallow aquifers as far as 400 km from the earthquake's epicenter, with some eruptions rising over 30 m into the air [*Grantz et al.*, 1964; *Waller*, 1968]. In addition, seismically induced water level fluctuations were observed in over 700 wells worldwide, the most notable being a 2.3-m variation recorded in an artesian well in Perry, Florida, located some 5500 km from the quake [*Cooper et al.*, 1968; *Gabert*, 1968]. The Martian cratering record provides abundant evidence that Mars has witnessed numerous events of a similar, and often much greater, magnitude.

After *Bath* [1966], the seismic energy E_s associated with an earthquake of magnitude M can be calculated from the Gutenberg-Richter relation, where

$$\log_{10} E_s = 1.44\,M + 5.24 \tag{8}$$

For the 8.4 magnitude 1964 Alaska earthquake, equation (8) yields a corresponding seismic energy of ~2.2×10^{17} J. However, according to *Schultz and Gault* [1975*a*,*b*], only about 10^{-4} of a projectile's initial kinetic energy is converted into seismic energy upon impact. Thus, to match the seismic output of the Alaska earthquake, an impacting projectile must have an initial kinetic energy in excess of 10^{21} J.

The size of the crater produced by a projectile of kinetic energy E_k can be calculated from the crater volume-scaling relationship of *Schmidt and Housen* [1987], as revised by *Grieve and Cintala* [1992]. Their expression for the maximum diameter of the transient cavity (i.e., before gravitational slumping of the cavity walls) written as a function of projectile diameter D_p is given by

$$D_{tc} = 2.89 \left(\frac{\delta_p}{\rho_t}\right)^{1/3} D_p^{0.78} U^{0.44} g^{-0.22} \tag{9}$$

where δ_p and ρ_t are the projectile and target densities, U is the impact velocity and g is the acceleration of gravity at the planet's surface (all in SI units). In their analysis, *Grieve and Cintala* [1992] assume a chondritic projectile density of 3.58×10^3 kg m^{-3} and target density of 2.73×10^3 kg m^{-3}. Adopting these same values, and making the appropriate substitution for D_p ($= 2(3m_p/4\pi\delta_p)^{1/3}$, where $m_p = 2E_k/U^2$), equation (9) can be rewritten to yield the relationship between transient crater diameter and projectile kinetic energy where

$$D_{tc} = 0.219\ E_k^{0.26} U^{-0.09} g^{-0.22} \tag{10}$$

The corresponding final crater diameter D_f can then be found through the empirical scaling relation of *Croft* [1985], which is given by

$$D_{tc} \cong D_c^{0.15\pm0.04} D_f^{0.85\pm0.04} \tag{11}$$

where D_c is the transition diameter between simple and complex crater morphology, which on Mars occurs at a diameter of ~6 km [*Pike*, 1980].

The foregoing analysis suggests that a projectile with a kinetic energy of 2.2×10^{21} J will produce a final crater roughly 33 km in diameter, assuming a characteristic Mars impact velocity of 10 km s^{-1} [*Hartmann*, 1977]. Therefore, if the crater size-frequency distribution preserved in the cratered highlands is representative of the cratering flux experienced over the entire planet (Table 7), then a minimum of ~10,000 impact events with seismic energies greater than or equal to that of the 1964 Alaska earthquake have occurred throughout Martian geologic history. At the lower end of this size range, the forceful closure of water-filled fractures by impact generated shock waves may have resulted in surface eruptions of water and sediment at distances of up to several crater radii from the impact. However, at the high end, the seismic energies associated with the impacts that formed Hellas (~2000 km), Isidis (~1900 km), and Argyre (~1200 km), are as much as four to six orders of magnitude greater [*O'Keefe and Ahrens*, 1975; *Gault et al.*, 1975]. Seismic energies this large may have been sufficient to disrupt subpermafrost aquifers and vent groundwater on a global scale.

4.4.3. *Hydrothermal convection.* Given the widespread evidence of volcanism [*Greeley and Spudis*, 1981; *Greeley and Schneid*, 1991] and large impacts [*Schultz et al.*, 1982] on Mars, hydrothermal activity has long been recognized as a potentially important process in the mineralogic and geomorphic evolution of the planet's surface [*Allen*, 1979*b*; *Schultz and Glicken*, 1979; *Pieri*, 1980; *Newsom*, 1980; *Morris*, 1980; *Clifford*, 1982]. For example, hydrothermal circulation has been discussed in connection with the development of the small valleys found on the flanks of Alba Patera and five other major volcanoes [*Gulick and Baker*, 1990], while *Allen* [1979*a*], *Hodges and Moore* [1979], *Schultz and Glicken* [1979], *Squyres et al.* [1987] and *Wilhelms*

TABLE 7. Crater Statistics, Impact Energies, and Melt Volumes for the Crater-Size Frequency Distribution of the Martian Highlands

D_{min}, km	D_{max}, km	D_{mean}, km	D_{tc}, km	E_k, J	N	log R	N_g	V_m, km^3	V_t (= N_g * V_m), km^3	Equivalent Global Melt Layer, m
8.00	11.31	9.51	8.88	2.72E + 19	946	−1.55	15705	1.07E + 00	1.01E + 03	0.01
11.31	16.00	13.45	11.92	8.44E + 19	777	−1.34	12735	3.31E + 00	2.57E + 00	0.02
16.00	22.63	19.03	16.00	2.62E + 20	582	−1.16	9638	1.02E + 01	5.96E + 03	0.04
22.63	32.00	26.91	21.48	8.14E + 20	499	−0.93	8184	3.16E + 01	1.58E + 04	0.11
32.00	45.25	38.05	28.84	2.53E + 21	417	−0.71	6791	9.77E + 01	4.08E + 04	0.28
45.25	64.00	53.82	38.73	7.84E + 21	227	−0.67	3723	3.02E + 02	6.86E + 04	0.47
64.00	90.51	76.11	51.99	2.44E + 22	119	−0.65	1949	9.33E + 02	1.11E + 05	0.77
90.51	128.00	107.63	69.80	7.56E + 22	51	−0.72	830	2.88E + 03	1.47E + 05	1.01
128.00	181.02	152.22	93.72	2.35E + 23	14	−0.98	228	8.91E + 03	1.25E + 05	0.86
181.02	256.00	215.27	125.82	7.29E + 23	11	−1.74	20	2.75E + 04	3.03E + 05	2.09
256.00	362.04	304.44	168.93	2.26E + 24	8	−1.57	15	8.51E + 04	6.81E + 05	4.70
362.04	512.00	430.54	226.79	7.03E + 24	9	−1.22	16	2.63E + 05	2.37E + 06	16.33
512.00	724.08	608.87	304.49	2.18E + 25	4	−1.27	7	8.13E + 05	3.25E + 05	22.42
724.08	1024.00	861.08	408.80	6.78E + 25	2	−1.27	4	2.51E + 06	5.02E + 06	34.65
1024.00	1448.15	1217.75	548.84	2.10E + 26	2	−0.97	4	7.76E + 06	1.55E + 07	107.07
1448.15	2048.00	1722.16	736.86	6.53E + 26	2	−0.67	4	2.40E + 07	4.80E + 07	330.89
Global Totals									7.56E + 07	521.72

Read 2.72E + 19 as 2.72×10^{19}, for instance.

The statistical data on the crater size-frequency distribution of the martian highlands is taken from *Barlow* [1990]. The data have been binned and analyzed using the relative (R plot) procedure recommended by the *Crater Analysis Techniques Working Group* [1978]. The R plot technique highlights any deviation from a power law distribution function by presenting the crater size-frequency data in differential form (where log R is plotted against log D_{mean}). $R = (D_{mean})^3 N/A(D_{max} - D_{min})$ where N is the number of craters within the diameter range D_{min} to D_{max} ($D_{max} = D_{min}\sqrt{2}$), D_{mean} is the geometric mean diameter of the bin ($= \sqrt{D_{min}D_{max}}$ and A is the surface area over which the craters are counted ($A = 8.8 \times 10^6$ km^2 for $D_{max} < 181$ km and $A = 8.0 \times 10^7$ km^2 for $D_{max} > 181$ km). Assuming that the differential crater size-frequency distribution preserved in the cratered highlands (i.e., R) is representative of the cratering flux experienced over the entire planet, the global number of impacts that have occurred within a particular size range can be calculated by setting A equal to the surface area of Mars ($= 1.45 \times 10^8$ km^2) and solving for N (listed under N_g in the table). E_k is the projectile kinetic energy, V_m is the melt volume produced per impact, and V_t is the total volume of impact melt produced by the impacts within a given bin size.

and Baldwin [1989], have considered how volcanic eruptions and igneous sills may have interacted with ground ice to form the outflow channels and the small valleys that dissect the ancient heavily cratered terrain.

An alternative mechanism for the origin of the small valleys invokes an impact-generated heat source. As discussed by *Newsom* [1980], a major impact will result in the production of a large quantity of impact melt. The interaction of groundwater with such a long-lived (up to 10^4 years) heat source will result in the development of a large-scale hydrothermal circulation system centered on the impact. Cool water will enter the system from the base of the aquifer, rise as its heated, and then flow radially away as it reaches the top. Directly beneath the impact, the groundwater may boil, carrying away heat through the convection of super-heated water and steam. Fractures around the impact may then serve as conduits to the surface, allowing the steam and boiling water to discharge as hot-springs and geysers around the periphery of the crater. Such a scenario may well explain the association of valley networks with the outside rims of large craters throughout the cratered highlands [*Pieri*, 1980; *Schultz and Glicken*, 1979; *Newsom*, 1980; *Clifford*, 1982; *Brakenridge et al.*, 1985; *Brakenridge*, 1990].

After *Newsom* [1980] and *Brakenridge et al.* [1985], the volume of water that is vertically discharged by an impact-generated hydrothermal system can be estimated from the quantity of melt produced by the impact. However, because large discrepancies exist between the observed and theoretically predicted melt volumes of many terrestrial impact craters, reliable estimates of impact melt production have been difficult to make. To address this problem *Grieve and Cintala* [1992] have recently presented a revised scaling relationship that provides a better fit to the observed data. Their expression for the volume of melt produced by the vertical impact of a chondritic projectile (gravitationally scaled for Mars) is

$$V_m = 7.55 \times 10^{-7} D_{tc}^{3.84} \quad (12)$$

which, as before, assumes a characteristic impact velocity of 10 km s^{-1}.

Given a global crater size-frequency distribution equivalent to that preserved in the cratered highlands (e.g., *Barlow* [1990]), and melt volumes calculated from equation (12), the cumulative volume of impact melt generated over the course of Martian geologic history is readily estimated. The results of these calculations, for craters in the 8–2048 km size-range, are summarized in Table 7. They indicate that the cumulative flux of impacts on Mars has produced a volume of melt equivalent to a global layer over 0.5 km thick, more than 85% of which has been contributed by impacts with final diameters greater than 10^3 km.

The total heat, ΔQ_{melt}, released per unit area by the cooling of an impact melt sheet from an initial temperature T_i to a final temperature T_f can be calculated from

$$\Delta Q_{melt} = \rho C_p (T_i - T_f) \Delta z \quad (13)$$

where ρC_p is the volumetric heat capacity of the melt , and Δz is its thickness. From this relationship, the quantity of heat represented by a 520-m thick global layer of impact melt (cooling from an initial temperature of 1473 K to a final temperature of 473 K) is found to be $\sim 2.2 \times 10^{12}$ J m^{-2}. Of this energy, only a small fraction (~20%) will go into driving hydrothermal convection, the remainder will be lost to the surface by radiation and conduction, and by heating much of the surrounding medium to a temperature that falls short of the boiling point [*Onorato et al.*, 1978; *Newsom*, 1980; *Brakenridge et al.*, 1985].

Newsom [1980] and *Brakenridge et al.*[1985] assume that any steam generated by the interaction of groundwater with the im-

pact melt must be superheated by at least 300 K to reach the surface. Thus, if the initial temperature of the groundwater is 273 K, the heat from the melt must provide enough energy to elevate the temperature a total of 400 K and drive a phase change from liquid to steam. Based on these assumptions, the mass of steam reaching the surface is given by

$$\Delta m_{steam} = \frac{0.2\,\Delta Q_{melt}}{C_{pw}\,\Delta T_{water} + L_v + C_{ps}\,\Delta T_{steam}} \quad (14)$$

where C_{pw} and C_{ps} are the heat capacities of water and steam; ΔT_{water} and ΔT_{steam} are the corresponding temperature intervals over which each phase is heated; and L_v is the latent heat of vaporization (adopted values for all variables are listed in Table 8). This model suggests that the total mass of water that was brought to the surface by impact-generated hydrothermal systems was equivalent to a global ocean ~130 m deep. For several reasons, however, this is likely a conservative estimate. For example, the crater statistics of *Barlow* [1990] do not include any correction for erosion or obliteration; therefore, they likely underestimate the cumulative number of impacts the highlands have experienced. Nor do *Barlow's* [1990] statistics include any of the six "megabasins" (i.e., *D*> Hellas) that have recently been reported in the literature [*Schultz et al.*, 1982; *McGill*, 1989; *Schultz and Frey*, 1990]. The omission of these basins reflects both the tentative nature of their identification, and the clear geometric and scaling difficulties associated with estimating the amount of impact melt produced by basins whose diameters approach or exceed the radius of Mars. It appears likely, however, that their inclusion would increase both the estimated production of impact melt and the resulting cumulative flux of water by as much as an order of magnitude.

Finally, no attempt has been made to quantify the contribution of igneous intrusions or volcanic eruptions to hydrothermal activity. Although a large quantity of volcanic material has been extruded onto the Martian surface (estimated by *Greeley and Schneid* [1991] to be equivalent to a global layer ~0.5 km thick), its emplacement over the preexisting topography is not conducive to the hydrothermal convection of water from deep within the crust. However, around volcanic vents and igneous intrusions, the potential for the development of deeply circulating hydrothermal systems is greatly increased. To date, the best quantitative analyses of the interaction of dikes, sills, and lava flows with ground ice are those of *Squyres et al.* [1987] and *Gulick* [1991]. Unfortunately, the lack of a reasonable basis for estimating the number, extent, and emplacement geometry, of deeply penetrating magma bodies on Mars precludes any global assessment of the quantity of water circulated by such activity.

4.5. *Transport Through the Cryosphere*

Although thermal vapor diffusion, seismic pumping, and hydrothermal convection are all capable of transporting large volumes of H_2O between the local water table and the base of the cryosphere, it seems reasonable to expect that the subsequent freezing of this water will create a barrier that precludes any further rise of water beyond the base of the frozen crust. However, as discussed in section 4.4.1, the presence of a geothermal gradient can have a profound influence on both the state and redistribution of crustal H_2O, a fact that is equally true whether the temperature is above or below the freezing point. Indeed, there are at least three different processes, involving all three phases of water, that will contribute to the thermally induced transport of H_2O through the cryosphere.

TABLE 8. Adopted Values for Hydrothermal Calculations

Variable	Description	Value
ρC_p	volumetric heat capacity of melt	4.2×10^6 J m^{-3} K^{-1}
C_{pw}	heat capacity of water	4188 J kg^{-1} K^{-1}
C_{ps}	heat capacity of steam	2092 J kg^{-1} K^{-1}
δT_{water}	373 K–273 K	100 K
δT_{water}	673 K–373 K	300 K
L_v	latent heat of vaporization	2.3×10^6 J Kg^{-1}

In the gas phase, the transport of H_2O through unsaturated frozen ground occurs by the familiar process of thermal vapor diffusion where, as before, the presence of a temperature gradient creates a corresponding vapor pressure gradient that drives the diffusion of vapor from the warmer depths to the colder near-surface crust. However, subfreezing temperatures affect this process in two important ways. First, because the vapor flux at any depth is proportional to the local saturated vapor pressure, the magnitude of vapor transport necessarily declines as the diffusing vapor rises higher in the frozen crust. Second, as a consequence of this decline in temperature and saturated vapor pressure, a portion of the ascending vapor flux will condense and freeze, preferentially blocking the smallest pores present in the pore system. This condensation can both substantially retard diffusion and choke off much of the pore network long before the larger pores are filled with ice. With time, however, these blockages succumb to the same thermal process that led to their forma tion. Thus, vapor will sublime from the ice plugs formed in the warmer, deeper regions of the cryosphere and redistribute itself (through a repeated process of condensation, sublimation, and diffusion) to the colder near-surface crust. In this way, the process of thermal vapor diffusion will continue until the cryosphere is ultimately saturated with ice.

The possibility of liquid phase transport arises from the fact that both adsorbed water and water in small capillaries can survive in frozen soil down to very low temperatures (see section 2.2). Under conditions where the unfrozen water content is high enough to provide thin film continuity, the presence of a temperature gradient creates a corresponding gradient in soil water potential $\Delta\psi$, a quantity that reflects the difference in effective pressure between the phases of ice and unfrozen water present in the soil. Under atmospheric conditions (i.e., in the absence of a confining pressure), the magnitude of this pressure difference can be calculated from a form of the Clausius-Clapeyron equation [*Edlefsen and Anderson*, 1943; *Williams and Smith*, 1989], given by

$$\frac{dP_w}{dT} = \frac{L_f}{T V_w} \quad (15)$$

where P_w is the pressure (or hydraulic head) of soil water, L_f is the latent heat of fusion (= 3.35×10^5 J kg^{-1}), and V_w is the specific volume of water (= $1/\rho$) at the crustal temperature T. Equation (15) indicates that the pressure difference between ice and water in the soil increases by ~1.2×10^6 Pa K^{-1} for crustal temperatures below 273 K. After *Smith and Burn* [1987] and *Williams and Smith* [1989], the liquid flow (per unit area) that occurs in response to this temperature-induced pressure difference is given by

$$q_l = - \frac{k_f g}{\nu} \frac{d\psi}{dT} \frac{dT}{dz} \quad (16)$$

where k_f is the permeability of the frozen soil, g is the acceleration of gravity, ν is the kinematic viscosity, and $d\psi/dT$ ($\cong dP_w/dT$) is the temperature-dependent gradient in soil water potential. Assuming a geothermal gradient of 15 K km^{-1}, a value of $d\psi/dT = 1.2 \times 10^6$ Pa K^{-1} (from equation (15)), and a frozen permeability of $\sim 2 \times 10^{-7}$ darcies (a value appropriate to a silty clay soil at a temperature just below freezing [*Smith*, 1985; *Williams and Smith*, 1989]), the resulting vertical flux of liquid water through the base of the cryosphere is found to be $\sim 4.3 \times 10^{-5}$ m yr^{-1}, or roughly 0.4 km every 10^7 years. It should be cautioned, however, that this flux is highly sensitive to both the local lithology and effective confining pressure of the crust; therefore, because these conditions are so poorly constrained at the base of the cryosphere, this estimate has an inherent uncertainty of as much as two orders of magnitude. Note also, that because the permeability of frozen soil declines with decreasing temperature, the magnitude of liquid transport will necessarily decline as the water reaches the colder and shallower regions of the crust.

Finally, in addition to the movement of H_2O vapor and liquid through the cryosphere, transport in the solid phase can occur by the process of thermal regelation; where, as before, the direction of transfer is from warm to cold [*Miller et al.*, 1975; *Miller*, 1980]. As discussed by *Williams and Smith* [1989], the process of regelation involves the movement of both ice and unfrozen water through a saturated (or nearly saturated) frozen soil. Fundamental to this process is the thermodynamic relationship between freezing point depression and the effective pressure difference between the ice and water phases present in the pores. As the geothermal gradient drives the flow of water through the unfrozen films that permeate the cryosphere, the entry of liquid water at the warm end of the pores causes a local increase in water pressure that decreases the effective pressure difference between the ice and water phases. This reduction in effective pressure increases the local freezing point by an amount sufficient to cause a small quantity of water to freeze at the warm end of the pore. The addition of this ice also increases the effective pressure at the pore's cold end, where it lowers the local freezing point. Water released by the subsequent melting of ice from the cold end of the pore then becomes part of the thin-film flow that enters the colder ice-filled pores located higher in the crust, following which the whole process is repeated again.

Note that because each of the three thermal processes discussed here operate by driving the movement of water from warmer to colder regions of the crust, the transport of H_2O through the cryosphere is necessarily a one-way street. That is, if one attempts to introduce water into the cryosphere via the atmosphere, the maximum depth of penetration is necessarily limited to the maximum depth at which surface temperature variations are sufficient to overwhelm the influence of the local geothermal gradient. For the surface temperature variations expected at equatorial latitudes from the periodic changes in Martian obliquity and orbital elements [e.g., *Toon et al.*, 1980; *Fanale et al.*, 1986], this depth is not likely to exceed more than ten meters.

In contrast, when water is supplied to the cryosphere from below, the processes of thermal vapor diffusion, thermal liquid transport, and regelation, will permit its eventual redistribution throughout the frozen crust. This fact has a number of important consequences. For example, should an ice-rich region be buried by lavas, sediments, or some other type of deposit, the resulting increase in insulation provided by the depositional layer will cause local crustal temperatures to rise, permitting the buried ground ice to be thermally redistributed into the overlying mantle.

The ability of H_2O to thermally migrate through the cryosphere also has implications for the sublimation of equatorial ground ice. As the sublimation front propagates deeper into the crust (e.g., Figure 14), it may ultimately reach a depth where the diffusive loss of ground ice is exactly balanced by the upward thermal migration of H_2O through the cryosphere, a condition that could significantly limit the depth of equatorial desiccation predicted by current models [*Clifford and Hillel*, 1983; *Fanale et al.*, 1986]. Unfortunately, the processes governing the transport of H_2O, both to and from the sublimation front, are sufficiently complex that calculating a specific depth at which this equilibrium condition is reached is virtually impossible without a more detailed knowledge of a number of crustal parameters (e.g., lithology, porosity, pore size, specific surface area, heat flow, and salt content).

In summary, various lines of evidence suggest that, over the course of Martian geologic history, at least four processes have introduced substantial amounts of water into the atmosphere, these include: the sublimation of equatorial ground ice, catastrophic floods, impacts, and volcanism. Under the climatic conditions that have apparently prevailed on Mars throughout its history, the atmospheric loss of this H_2O from equatorial and temperate latitudes appears irreversible. However, if Mars is water-rich, then these depleted crustal reservoirs may have been replenished by sources of groundwater residing deep within the crust. At least three processes (thermal vapor diffusion, seismic pumping, and hydrothermal convection) appear viable for driving the vertical transport of H_2O from the local water table to the base of the cryosphere. While the calculations presented in section 4.4 indicate that all three processes are potentially important, the flux arising from thermal vapor diffusion alone is sufficient to supply the equivalent of ~1 km of water to the base of the cryosphere every 10^6–10^7 years. Thermal vapor diffusion, aided by thermal liquid transport and regelation, may then redistribute this H_2O throughout much of the frozen crust. Note that these thermal processes will occur on a global basis, wherever there exists a crustal temperature gradient, a subsurface reservoir of H_2O, and the continuity of pore space between the source region and the near-surface crust. In this way, ground ice that was removed by impacts or sublimation to the atmosphere may have been replenished on a global scale (e.g., Figure 20), without the need to invoke exotic scenarios of climate change.

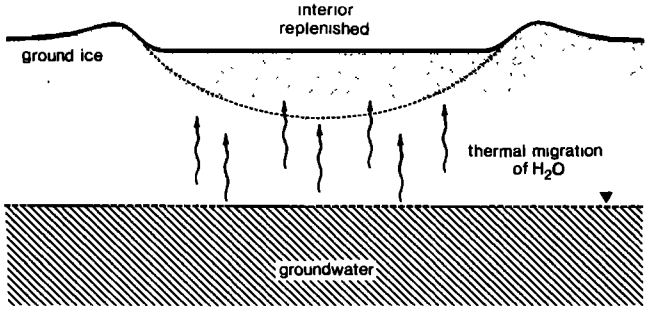

Fig. 20. A geothermal gradient as small as 15 K km^{-1} could supply the equivalent of 1 km of water to the freezing front at the base of the cryosphere every 10^6–10^7 years, a process that may explain how the interiors of equatorial craters were recharged with ground ice.

5. Polar Deposition, Basal Melting, and the Physical Requirements for Pole-to-Equator Groundwater Flow

With mean annual temperatures that are ~40 K below the atmospheric frost point of water vapor, the Martian polar regions represent the dominant thermodynamic sink for H_2O on the planet. As a result, any water that is introduced into the atmosphere, above its normal saturation level, is eventually cold-trapped at the poles. *Pollack et al.* [1979] have suggested that this process of polar deposition is intimately tied to the fate of atmospheric dust and the formation of the seasonal polar caps. They propose that airborne dust particles, raised by local and global dust storms, may serve as nucleation centers for the condensation of water ice. As either hemisphere enters the fall season, the suspended dust particles receive an additional coating of CO_2 that makes them heavy enough to precipitate from the atmosphere, contributing to the formation of the seasonal caps. In the spring the CO_2 sublimes away; however, at high latitudes it leaves behind a residual deposit of H_2O ice and dust that adds to the perennial caps [*Cutts*, 1973; *Pollack et al.*, 1979]. Insolation changes due to axial precession and periodic variations in obliquity and orbital eccentricity [e.g., *Ward*, 1974, 1979; *Bills*, 1990] may alter the erosional and depositional balance at the poles, as well as the mixing ratio of ice to dust in the annual depositional layer [*Murray et al.*, 1973; *Toon et al.*, 1980; *Cutts and Lewis*, 1982]. Such a scenario may well explain the origin of the numerous horizontal layers that comprise the stratigraphy of both polar caps [*Murray et al.*, 1972; *Soderblom et al.*, 1973; *Squyres*, 1979*b*; *Howard et al.*, 1982].

In this section, the effect of polar deposition on the thermal evolution of the cryosphere and polar caps is considered. Given an initially ice-saturated condition, the deposition of ice and dust at polar latitudes will result in a situation where the equilibrium depth to the melting isotherm has been exceeded, melting ice at the base of the cryosphere until thermodynamic equilibrium is once again established. The drainage of the resulting meltwater into the underlying global aquifer will then cause the local water table to rise in response, creating a gradient in hydraulic head that will drive the flow of groundwater away from the poles. In the discussion which follows, the process of basal melting, the rise of the polar water table, and the physical requirements for pole-to-equator groundwater flow are analyzed in detail.

5.1. *Polar Basal Melting*

In studies of terrestrial glaciers, the term "basal melting" is used to describe any situation where the local geothermal heat flux, as well as any frictional heat produced by glacial sliding, is sufficient to raise the temperature at the base of an ice sheet to its melting point. In this regard, the process is always discussed with reference to the interface between an ice sheet and the bed on which it rests. However, as discussed by *Clifford* [1980*b*, 1987*b*] and as illustrated in Figure 21, it appears appropriate to broaden the use of this term as it applies to Mars.

Figure 21*a* is an idealized cross section of the Martian polar crust prior to the deposition of any dust or ice. Given a cryosphere that is initially saturated with ice, the deposition of any material at the surface will result in a situation where the equilibrium depth to the melting isotherm has been exceeded (Figure 21*b*). In response to this added layer of insulation, the position of the melting isotherm will rise in the crust until thermal equilibrium is once again established. Thus, while melting will not occur at the actual base of the polar deposits, it will occur at the base of the cryosphere in response to any increase in polar deposit thickness. Should deposition persist, the polar deposits may eventually reach the thickness necessary for melting to occur at their physical base (Figure 21*c*) [*Clifford*, 1980*b*, 1987*b*]. Under such conditions, the deposits may then reach a state of equilibrium, whereby the deposition of any additional ice at the surface is offset by the melting of an equivalent layer at the base of the cap. Since this last stage is merely the endpoint in the evolution of a single continuous process, the use of the term "basal melting" is broadened here to include any situation where pore or glacial ice is melted as the result of a rise in the position of the melting isotherm, regardless of whether such melting oc-

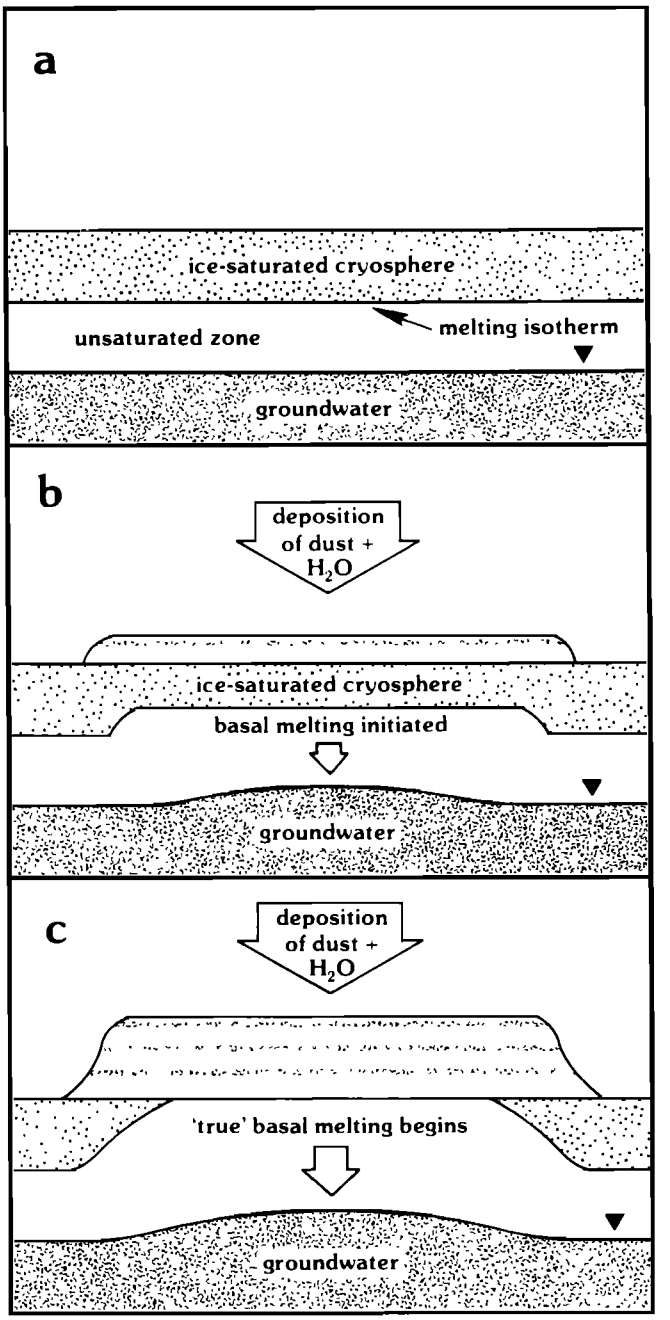

Fig. 21. An idealized cross section of the polar crust illustrating the possible time evolution of basal melting [*Clifford*, 1987*b*]. The sequence depicts (*a*) a time prior to the deposition of any dust and ice, (*b*) the onset of deposition and basal melting, and (*c*) melting at the actual base of the deposits.

curs at the actual base of the deposits or at the base of the cryosphere within the underlying terrain.

As with the cryosphere calculations discussed in section 2.2, the polar deposit thickness required for basal melting can be calculated by solving the one-dimensional steady state heat conduction equation. After *Weertman* [1961] and *Clifford* [1987*b*], this thickness is given by

$$H = \kappa \frac{T_{mp} - T_{ms}}{Q_g + Q_f} \quad (17)$$

where κ is the effective thermal conductivity of the polar deposits, T_{mp} is the melting temperature of the ice, T_{ms} is the mean polar surface temperature, Q_g is the geothermal heat flux, and Q_f is the frictional heat due to glacial sliding. With the exception of the frictional heat term, all of these variables are discussed at length in section 2.2. However, because of differences in the degree of homogeneity, particle size, and ice content, the thermal conductivity of the polar deposits is likely to differ from that which characterizes the regolith or crust as a whole. For this reason, both the thermal conductivity of the polar ice and the potential role of glacial sliding are discussed here in greater detail.

The thermal conductivity of the Martian polar deposits is determined by such factors as the volumetric mixing ratios of ice and dust, their spatial variability, temperature-dependent thermal properties, and the presence of other contaminants, such as salts. While a comprehensive analysis of these factors is beyond the scope of this paper, a reasonable range of values can be inferred from the available data. For example, the light-scattering properties of the dust suspended in the Martian atmosphere indicate grain diameters in the range of 0.2–2.5 μm [*Pang et al.*, 1976; *Pollack et al.*, 1979; *Chylek and Grams*, 1978]. If this size range is representative of the dust entrained in the polar ice, then the thermal properties of the polar deposits should be closely approximated by laboratory mixtures of ice and clay.

In Figure 22 the thermal conductivities of various clay-ice mixtures are plotted as a function of their volumetric ice content. Additional information about these mixtures is presented under the "frozen soil" heading of Table 2. Note that roughly half the mixtures have thermal conductivities comparable to that of ice (i.e., >2.25 W m^{-1} K^{-1}), while the rest have values as much as 60% lower. Since the conductivities of most clay minerals equal or exceed that of ice [*Clark*, 1966; *Horai and Simmons*, 1969], it is difficult to explain how any mixture of these two components could have a lower value. As discussed in section 2.2.1, this discrepancy may be explained by the presence of low-conductivity adsorbed water on high specific area clay.

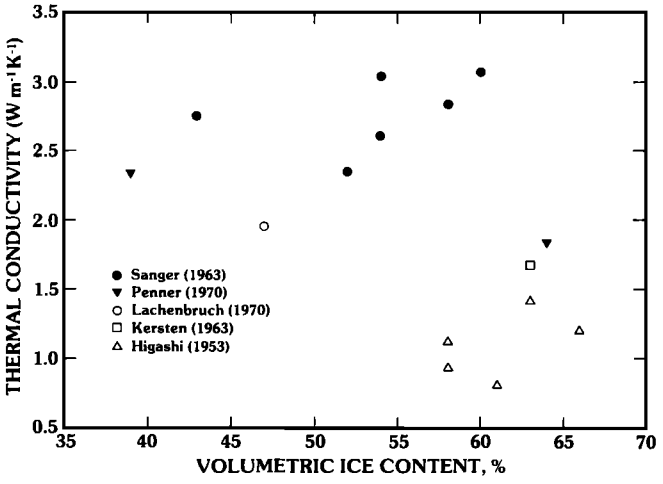

Fig. 22. The thermal conductivities of various terrestrial clay-ice mixtures plotted as a function of their ice content [*Clifford*, 1987*b*]. Additional information is presented in Table 2.

In Table 9, basal melting thicknesses have been calculated based on a mean polar surface temperature of 154 K, thermal conductivities of 1.0–3.0 W m^{-1} K^{-1}, and melting temperatures of 252 and 273 K. In addition, to assess the potential for basal melting at earlier epochs, calculations have also been carried out for heat flows of 90 and 150 mW m^{-2} [e.g., *Toksöz and Hsui*, 1978; *Davies and Arvidson*, 1981; *Schubert and Spohn*, 1990]. For these calculations, no pressure-induced freezing point depression or frictional heat input due to glacial sliding was assumed.

Based on an analysis of Mariner 9 radio occultation data, *Dzursin and Blasius* [1975] have determined that the Martian polar caps reach a maximum thickness of 4–6 km in the northern hemisphere and 1–2 km in the southern. Therefore, only in the north does the total thickness of the cap overlap the potential range of present-day (i.e., Q_g = 30 mW m^{-2}) basal melting thicknesses listed in Table 9. In the south, the deposits appear sufficiently thin that any melting is likely to be relegated to a depth that lies well below the regolith-polar cap interface. Of course, given the higher geothermal heat flow that likely characterized the planet's early history, the conditions for basal melting (at both poles) were almost certainly more favorable in the past. However, even under current conditions, given an initially ice-saturated regolith, melting at the base of the cryosphere (Figure 21*b*) appears to be an inevitable consequence of polar deposition.

For basal ice at the melting point, the thickness of the layer Δz that can be melted per unit area by a geothermal heat flux Q_g is given by

$$\Delta z = \frac{Q_g}{\rho L_f} \Delta t \quad (18)$$

where L_f is the latent heat of fusion and Δt is the elapsed time. Thus, a geothermal heat flux of 30 mW m^{-2} has the potential for melting as much as 3×10^{-3} m of ice from beneath the polar caps

TABLE 9. Calculated Basal Melting Thicknesses

Geothermal Heat Flux, mW m^{-2}	Polar Deposit Thermal Conductivity W m^{-1} k^{-1}	Thickness, km	
		252 K	273 K
30	1.0	3.27	3.97
	2.0	6.53	7.93
	3.0	9.80	11.90
90	1.0	1.09	1.32
	2.0	2.18	2.64
	3.0	3.27	3.97
150	1.0	0.65	0.79
	2.0	1.31	1.59
	3.0	1.96	2.38

These results assume a mean polar surface temperature of 154 K.

each year. Of course, if glacial sliding should occur, the resulting frictional heat could both substantially reduce the required thickness for basal melting and increase the production of meltwater. For a given basal sliding velocity V_b the frictional heat flux Q_f can be calculated from

$$Q_f = V_b \tau_b = V_b \rho_i g h \frac{dh}{dx} \quad (19)$$

where τ_b is the basal shear stress, ρ_i is the density of the polar ice (including any component of entrained dust), g is the acceleration of gravity, h is the local thickness of the cap, and dh/dx is the local slope at the polar cap's surface [*Weertman*, 1961; *Clifford*, 1987*b*]. As seen in Figure 23, a sliding velocity of 10 m yr^{-1}, driven by a basal shear stress of 100 kPa (a value typical of terrestrial glaciers and ice sheets [*Paterson*, 1981]), generates sufficient heat (~30 mW m^{-2}) to halve the thicknesses necessary for basal melting during the present epoch.

Possible evidence of past basal melting has been discussed by several investigators. For example, *Carr et al.* [1980], *Howard* [1981], and *Kargel and Strom* [1992] have noted the resemblance of the braided ridges of the Dorsa Argentea region (78° S, 40° W, Figure 24) to terrestrial eskers, landforms created by the deposition of fluvial sediments beneath glaciers and ice sheets that have undergone basal melting. In addition, *Clifford* [1987*b*] has cited the geomorphic similarities between the major polar reentrant Chasma Boreale (85° N, 0° W) and the outflow channel Ravi Vallis (1° S, 43° W), suggesting that Chasma Boreale, and similar features found elsewhere in the polar regions, may have formed as the result of a jökulhlaup, the catastrophic drainage of a large subglacial reservoir of basal meltwater. A terrestrial example of this process is the recurrent catastrophic drainage of Grimsvötn, a large subglacial lake in the center of the Vatnajökull ice cap in Iceland [*Nye*, 1976].

Given the presence of a subpermafrost aquifer and geologically reasonable values of crustal permeability, the deep infiltration of basal meltwater will result in the rise of the local water table in the form of a groundwater mound (Figure 21*c*). The gradient in hydraulic head created by the presence of the mound will then drive the flow of groundwater away from the poles. The two principle factors that will govern the magnitude of this transport are the size of the groundwater mound and the effective permeability of the crust. In the following discussion, the relative importance of these factors is assessed through the use of well established terrestrial hydrogeologic models.

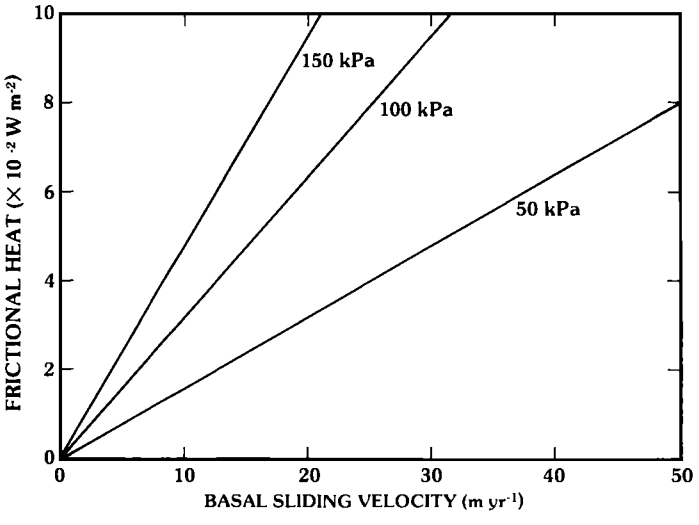

Fig. 23. The frictional heat produced by basal sliding under an applied basal shear stress of 50, 100, and 150 kPa [*Clifford*, 1987*b*].

5.2. *Growth of a Polar Groundwater Mound*

The development of a groundwater mound in response to polar basal melting is analogous to a problem frequently studied on Earth: the artificial recharge of an aquifer beneath a circular spreading basin [*Hantush*, 1967; *Marino*, 1975; *Schmidtke et al.*, 1982]. To obtain an analytical expression for the growth of a groundwater mound beneath a recharging source, a number of simplifying assumptions must be made, i.e., (1) the aquifer is homogeneous, isotropic, infinite in areal extent, and rests upon an impermeable horizontal base; (2) the hydraulic properties of the aquifer are invariant in both space and time; and (3) the constant downward percolation of water proceeds at a rate which is sufficiently small (compared to the aquifer permeability) that the influx is almost completely refracted in the direction of the local slope of the water table when it reaches the mound [*Hantush*, 1967; *Marino*, 1975; *Schmidtke et al.*, 1982].

After *Hantush* [1967], the governing equation for the development of a groundwater mound beneath a circular recharging source is

$$\frac{\partial^2 Z}{\partial r^2} + \frac{1}{r}\frac{\partial Z}{\partial r} + \frac{2 w \nu}{k g} = \frac{\varepsilon \nu}{\bar{h} k g}\frac{\partial Z}{\partial t} \quad (20)$$

where $Z = h^2 - h_i^2$, h is the height of the water table above the base of the aquifer after an elapsed time t, h_i is the initial saturated thickness of the aquifer, $\bar{h}$ is a constant of linearization ($= 0.5(h + h_i)$) which represents the weighted mean depth of saturation [*Hantush*, 1964], r is the radial distance from the center of the mound, w is the recharge rate per unit area, k is the aquifer permeability, g is the acceleration of gravity, ν is the kinematic viscosity, and ε is the effective porosity.

The boundary and initial conditions that apply to equation (20) are

$$Z(r, 0) = 0$$
$$\partial Z(0, t)/\partial r = 0$$
$$w = w \quad (0 \le r \le a)$$
$$= 0 \quad (r > a)$$
$$Z(\infty, t) = 0$$

These conditions correspond to four basic assumptions: (1) the water table is initially horizontal, (2) the groundwater mound is symmetric about its vertical axis, (3) the recharge is limited to a circular region of radius a, and (4) the effect of the recharge on the shape of the water table is negligible at large radial distances [*Hantush*, 1967; *Marino*, 1975; *Schmidtke et al.*, 1982].

After *Hantush* [1967], equation (20) can be solved using Laplace and zero-ordered Hankel transforms to obtain the following expression for the maximum height h_m of the water table (evaluated at $r = 0$) at any time t

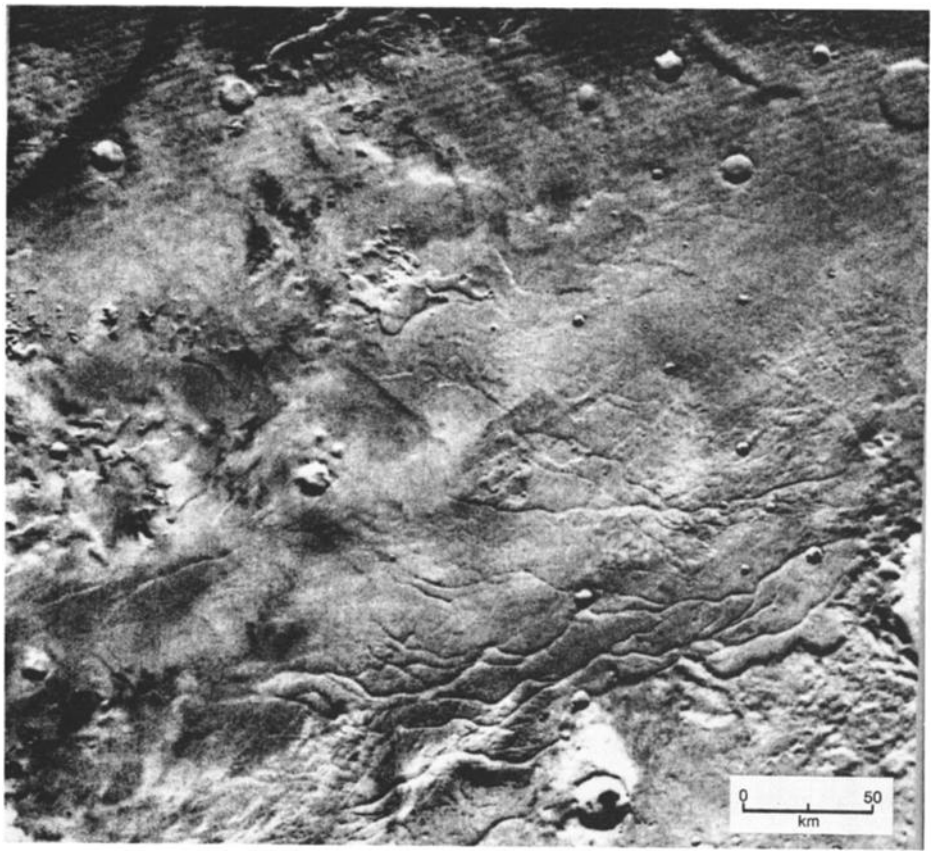

Fig. 24. Braided ridges, in the Dorsa Argentea region (77°S, 44°W), that have been interpreted as possible analogs of terrestrial eskers (Viking Orbiter frame 421B14).

$$h_m^2 - h_i^2 = \frac{Q_r \nu}{2\pi kg}\left(W(u_o) + \frac{1 - e^{-u_o}}{u_o}\right) \quad (21)$$

where the recharge volume $Q_r = \pi a^2 w$, $u_o = a^2 \nu\varepsilon/4kgh\,t$, and where $W(u_o)$ is the well function for a nonleaky aquifer given by

$$W(u_o) = \int_{u_o}^{\infty} \frac{e^{-u_o}}{u_o}\,du_o = -0.5772 - \log_e u_o + \sum_{i=1}^{n} (-1)^{1+n} \frac{u_o^{\,n}}{n \cdot n!} \quad (22)$$

Note that the solution given by equation (21) is valid for groundwater mound heights (h_m–h_i) up to 50% of the initial depth of saturation (h_i) [*Hantush*, 1967].

Development times for groundwater mounds from 100 m to 2500 m in height are presented in Table 10 and Figure 25. These times were calculated for four recharge volumes, ranging in size from 0.01–2.2 km^3 H_2O yr^{-1}, and are based on hydraulic properties that might reasonably characterize the Martian crust. The calculations assume saturated aquifer thicknesses of 1 km and 5 km, an effective porosity of 0.1, and a permeability of 1 darcy. For comparison purposes, a second set of development times were calculated for a recharge volume of 0.01 km^3 H_2O yr^{-1} and

TABLE 10. Groundwater Mound Heights as a Function of Time

Initial Aquifer Thickness h_i, m	Groundwater Mound Height $h_m - h_i$, m	Time t, years				
		Q = 2.2 km^3 yr^{-1}	Q = 1 km^3 yr^{-1}	Q = 0.1 km^3 yr^{-1}	Q = 0.01 km^3 yr^{-1}	
					k = 1 darcy	k = 10 mdarcies
1000	100	3.54E3	7.84E3	9.95E4	1.47E9	7.85E5
	200	7.08E3	1.57E4	3.75E5	—	1.57E6
	300	1.06E4	2.38E4	1.31E6	—	2.38E6
	400	1.42E4	3.25E4	4.78E6	—	3.25E6
	500	1.78E4	4.22E4	1.91E7	—	4.22E6
5000	100	3.54E3	8.18E3	1.46E6	—	8.18E5
	500	2.39E4	1.23E5	—	—	1.23E7
	1000	1.00E5	2.08E6	—	—	2.08E8
	2500	8.33E6	—	—	—	—

Unless otherwise noted, development times are based on an effective porosity of 0.1 and a crustal permeability of 1 darcy (=10^{-12}m^2). Read 3.54E3 as 3.54×10^3, for instance. No entry indicates a development time greater than the age of the solar system.

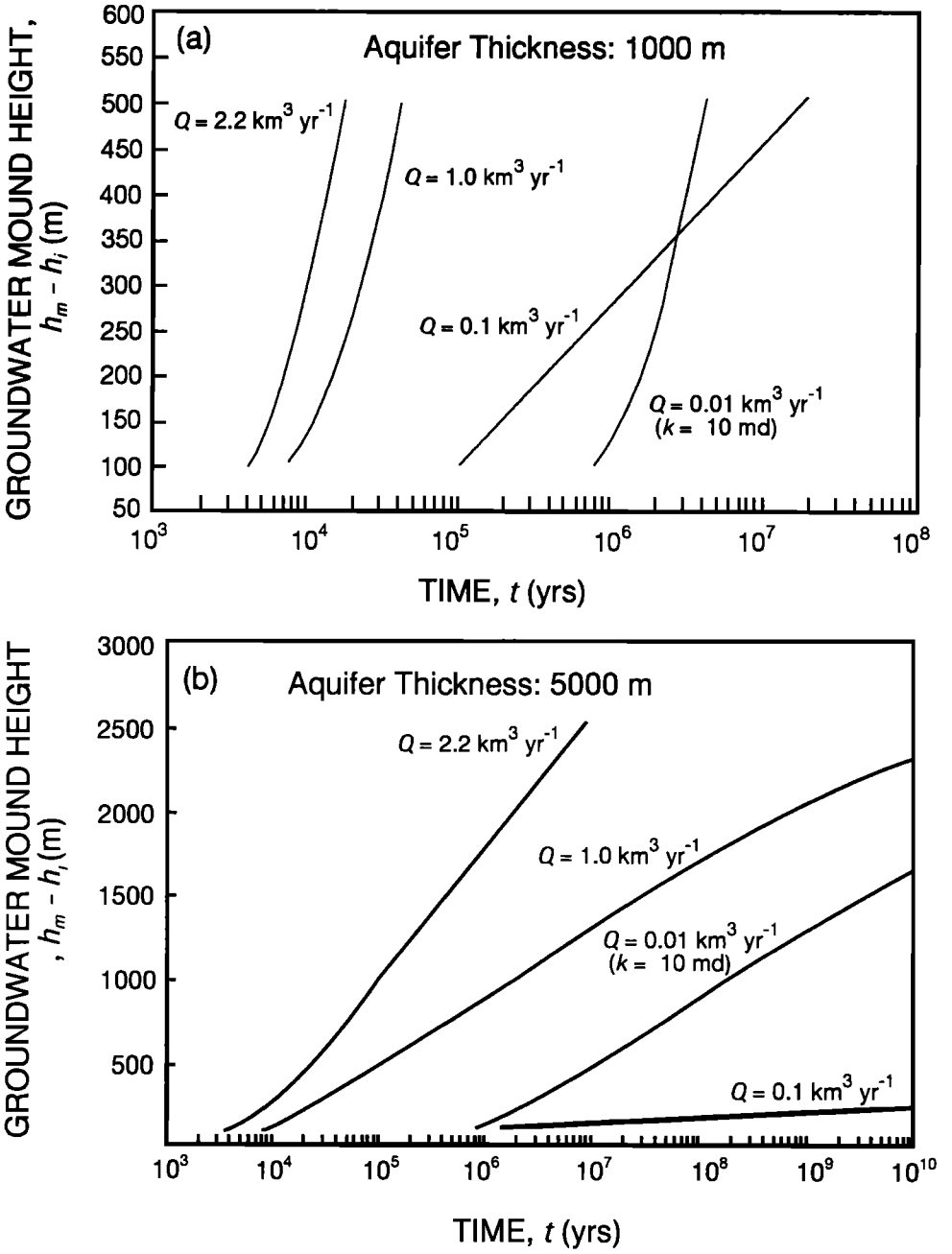

Fig. 25. Groundwater mound development times for recharge volumes between 0.01 and 2.2 km^3 H_2O yr^{-1} and aquifer thicknesses of (*a*) 1000 m and (*b*) 5000 m. Unless otherwise noted, the calculations assume a crustal permeability of 1 darcy and a basal melting radius equal to that of the permanent north polar cap ($a = 5 \times 10^5$ m).

a permeability of 10^{-2} darcies. In all cases, the radius of the basal melting area was taken to be equal to that of the permanent north polar cap ($a = 5 \times 10^5$ m).

For an aquifer with an initial saturated thickness of 1 km and a recharge volume of 2.2 km^3 H_2O yr^{-1} (equal to the maximum volume of ice that could be melted per year from beneath the north polar cap by a geothermal heat flux of 30 mW m^{-2}), the results summarized in Table 10 indicate that a groundwater mound will grow to a height of 100 m in less than 4×10^3 years and reach a height of 500 m in a little over 10^4 years. Although these growth times lengthen considerably as the initial saturated thickness of the aquifer is increased, even in a 5-km-thick aquifer, a groundwater mound 2500 m high will develop in less than 10^7 years [Figure 25*b*].

Groundwater mound development times also lengthen if the recharge volume is reduced. For example, cutting the recharge volume from 2.2 km^3 to 0.01 km^3 H_2O yr^{-1} increases the growth time for a 100 m mound in a 1-km-thick aquifer to over 10^9 years. In contrast, a reduction in crustal permeability shortens development times. This is illustrated by reducing the permeability in the preceding example from 1 to 10^{-2} darcies, thereby shortening the development time for a 100 m mound to less than 10^6 years.

The difference in development time that results from a change in aquifer thickness, permeability, or recharge volume, simply reflects a change in the relative mass balance of water between vertical recharge Q_r, storage (i.e., the volume of water contained in the mound), and radial discharge Q_d, which is given by

$$Q_d = 2\pi a h v \tag{23}$$

where h is the saturated thickness of the aquifer at $r = a$, and v is the specific discharge (the discharge per unit area) given by Darcy's law

$$v = - \frac{kg}{\nu} \frac{\partial h}{\partial r} \tag{24}$$

Of course, when the radial discharge of the mound finally balances the vertical recharge, a steady state condition is reached. The permeability requirements necessary to support such steady state flow are discussed in the following section.

5.3. *The Effect of Crustal Permeability on Pole-to-Equator Groundwater Flow*

Given the presence of a global interconnected groundwater system on Mars, the development of a groundwater mound in response to polar basal melting will create a gradient in hydraulic head that will drive the flow of groundwater away from the pole. The effect of crustal permeability on the magnitude of this flow can be readily assessed on the basis of established models of unconfined and confined steady state well flow. In this analysis, the well radius, a, is equivalent to the radius of the recharge (or basal melting) area discussed in the previous analysis; while, as before, the groundwater mound height is taken to be the difference between the maximum and minimum hydraulic heads (h_m–h_i). The distance R to the region of lowest hydraulic head represents the separation between the regions of net vertical recharge (the poles) and discharge (the equator), and is taken here to be of the order of the planetary radius of Mars. These relationships are illustrated in Figures 26 and 27.

The governing equation and appropriate boundary conditions for steady unconfined well flow are [after *Todd*, 1959]

$$\frac{\partial}{\partial r}\left(r \frac{\partial (h^2)}{\partial r} \right) = 0 \tag{25}$$

$$h^2 = h_i^2 \qquad (r = R)$$
$$Q_r = 2\pi r h v \qquad (\text{i.e., } Q_r = Q_d)$$

where as before, v is the specific discharge (the discharge per unit area) given by equation (24). Solving equation (25) in light of the above boundary conditions, we obtain

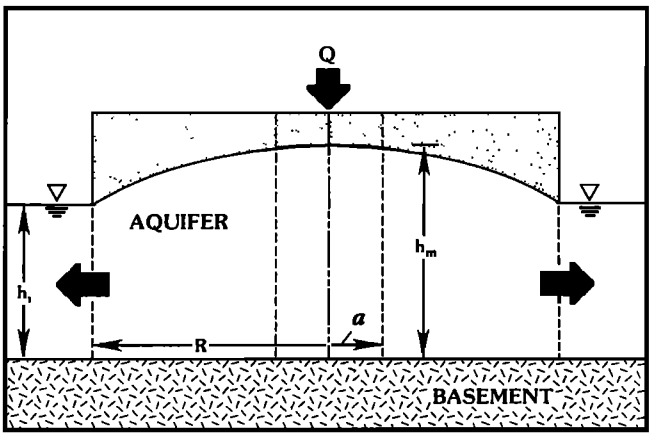

Fig. 26. A schematic diagram of unconfined steady state well flow.

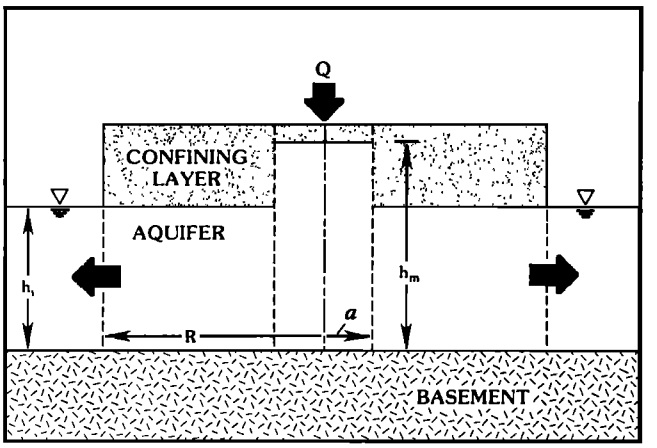

Fig. 27. A schematic diagram of confined steady state well flow.

$$h^2 = h_i^2 + \frac{Q_r \nu}{\pi k g} \ln (R / r) \tag{26}$$

Evaluated at $r = a$, equation (26) yields an expression for the maximum hydraulic head which can then be solved for k to find the permeability necessary to sustain unconfined steady state flow

$$k = \frac{Q_r \nu}{\pi g (h_m^2 - h_i^2)} \ln (R / a) \tag{27}$$

Of course, the possibility exists that, in an initially unconfined aquifer, a polar groundwater mound could grow to the point of contact with the base of the caps; in this event, the aquifer will undergo a transition between confined conditions at the poles to unconfined conditions closer to the equator. It is also possible that the polar aquifer has been confined from the very outset of basal melting (i.e., see Figure 7). Given either case, the solution presented in equation (27) is no longer valid.

The possibility of confined flow can be analyzed by solving the steady confined well equation, which, after *Todd* [1959], is given by

$$\frac{\partial}{\partial r}\left(r \frac{\partial h}{\partial r} \right) = 0 \tag{28}$$

and which is subject to the following boundary conditions

$$h = h_i \, (r = R)$$
$$Q_r = 2\pi r h_i v$$

Solving for the permeability of the crust in the same manner as before, yields

$$k = \frac{Q_r \nu}{2\pi g h_i (h_m - h_i)} \ln (R / a) \tag{29}$$

In Table 11 and Figure 28, crustal permeabilities necessary for steady state flow (calculated from equations (27) and (29)) are presented for a reasonable range of polar recharge volumes and net hydraulic heads. The results indicate that a recharge volume of 1 km^3 H_2O yr^{-1}, introduced into a 1-km-thick aquifer

TABLE 11. Permeability Required for Steady State Flow

Initial Aquifer Thickness h_i, m	Groundwater Mound Height $h_m - h_i$, m	Permeability k, darcies							
		Q = 2.2 km^3 yr^{-1}		Q = 1 km^3 yr^{-1}		Q = 0.1 km^3 yr^{-1}		Q = 0.01 km^3 yr^{-1}	
		Unconfined	Confined	Unconfined	Confined	Unconfined	Confined	Unconfined	Confined
1000	100	102.0	107.0	45.96	48.25	4.60	4.83	0.46	0.48
	200	48.69	53.56	21.93	24.13	2.19	2.41	0.22	0.24
	300	31.05	35.71	13.99	16.08	1.40	1.61	0.14	0.16
	400	22.32	26.78	10.05	12.06	1.01	1.21	0.10	0.12
	500	17.14	21.42	7.72	9.65	0.77	0.97	0.08	0.10
5000	100	21.21	21.42	9.56	9.65	0.96	0.97	0.10	0.10
	500	4.08	4.28	1.84	1.93	0.18	0.19	0.02	0.02
	1000	1.95	2.14	0.88	0.97	0.09	0.10	0.01	0.01
	2500	0.69	0.86	0.31	0.39	0.03	0.04	0.003	0.004

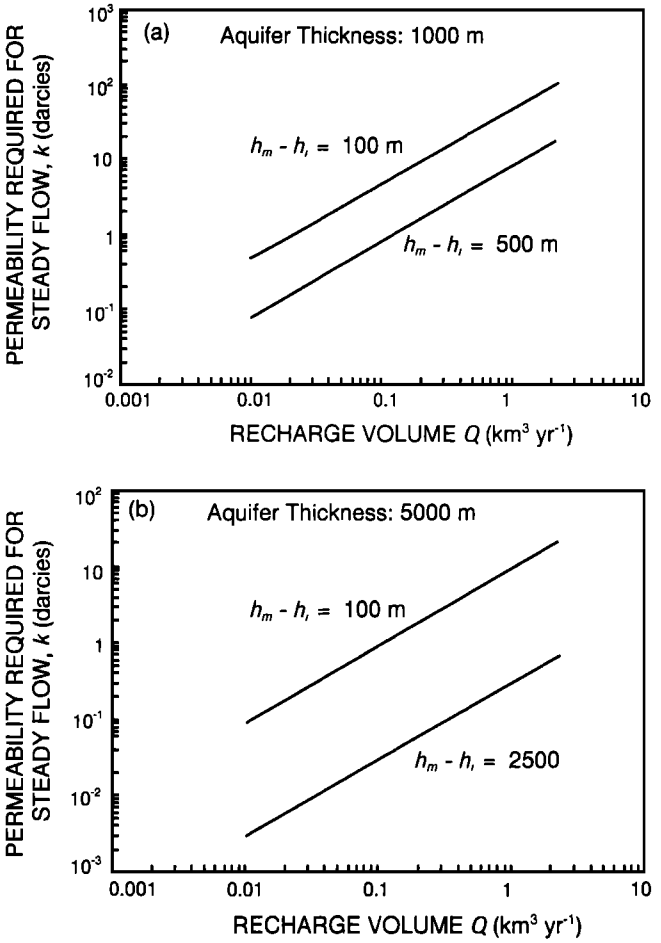

Fig. 28. Permeability required for pole-to-equator steady state flow for various recharge volumes and groundwater mound heights in aquifers (*a*) 1000 m and (*b*) 5000 m thick. Unless otherwise noted, the calculations assume a crustal permeability of 1 darcy and a basal melting radius equal to that of the permanent north polar cap ($a = 5 \times 10^5$ m).

at the poles, could drive the flow of a similar volume of water to the equator, given a crustal permeability of ~100 darcies and a groundwater mound height of 100 m. If the recharge volume is lowered to 0.01 km^3 H_2O yr^{-1}, and if we permit a net hydraulic head of 2500 m (equivalent to the lithostatic pressure exerted by a 1.5-km thickness of ice-rich permafrost), then the minimum permeability required to support steady state flow falls to less than 5×10^{-3} darcies, a value that lies within the lower extreme of measured permeabilities for fractured igneous and metamorphic rock (Figure 29). Note that even this low value of crustal permeability permits the pole-to-equator transport of as much as 4.5×10^7 km^3 of groundwater (from each pole) over the course of Martian geologic history, or ~10^8 km^3 H_2O (equivalent to a global ocean ~600 m deep) when the potential contribution of both poles is taken into account.

5.4. *The Large-Scale Permeability of the Martian Crust*

The significance of the steady state permeabilities presented in Table 11 can be placed in perspective by comparing them with the crustal values assumed by *Carr* [1979] in his discussion of the origin of the outflow channels. Based on both the size of the channels and the assumption that each was formed by a single catastrophic event, *Carr* [1979] calculated that discharges of ~10^7 to 5×10^8 m^3 s^{-1} were necessary to produce the observed erosion. To achieve rates this high requires large-scale permeabilities on the order of 10^3 darcies, permeabilities that *Carr* [1979] argued were only reasonable if the Martian crust was intensely fractured and/or possessed numerous unobstructed lava tubes, characteristics similar to those of certain Hawaiian basalts [*Davis*, 1969].

Arguments for crustal permeabilities of 10^3 darcies or higher have also been advanced by *MacKinnon and Tanaka* [1989].

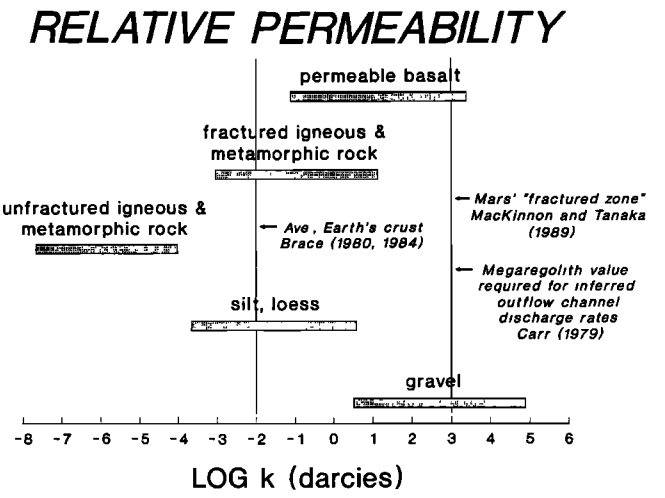

Fig. 29. Relative permeability of typical terrestrial geologic formations (after *Freeze and Cherry* [1979]).

Based on gravity studies of terrestrial and lunar impact craters, and borehole observations of terrestrial impact and explosion craters, they suggest that porosities as high as 20% may characterize the Martian fractured basement. They further suggest that much of this impact-generated porosity may occur as open planar fractures having widths of 1–5 mm and associated permeabilities as great as 10^4 darcies.

Although local permeabilities as high as 10^3 darcies undoubtedly occur on Mars, on a globally averaged basis, an effective permeability this large seems difficult to reconcile with the five order-of-magnitude smaller value inferred for the near surface of the Earth [*Brace*, 1980, 1984]. Therefore, given the general importance of this parameter to understanding the subsurface hydrology of Mars, just how reliable are these higher estimates?

As noted by *Carr* [1979], much of the need to invoke high discharge rates (and thus high permeabilities) to account for the origin of the outflow channels is based on the assumption that each channel was carved by a single catastrophic event. However, if the channels were created by multiple episodes of outbreak and erosion, or by continuous shallow flows acting over a prolonged period of time, then the need for high crustal permeabilities is significantly reduced.

Similar qualifications apply to the high permeabilities inferred by *MacKinnon and Tanaka* [1989]. The validity of their analysis rests on two key assumptions: (1) that the gravity anomalies associated with terrestrial and lunar craters are almost exclusively due to an increase in the fracture porosity of the surrounding basement, and (2) that the geometry of these fractures is both open and planar. As discussed below, there are good reasons to question both assumptions.

First, contrary to the assertion by *MacKinnon and Tanaka* [1989], the largest contributor to the gravity anomalies recorded over terrestrial and lunar craters is not the fracture porosity of the surrounding basement, but the increase in porosity associated with the breccia lens at the bottom of the crater [*Dvorak and Phillips*, 1978]. As discussed by *Shoemaker* [1963], *Short* [1970], and *Grieve and Garvin* [1984], the breccia lens consists of country rock that is pulverized along the wall of the transient cavity and then slumps to the bottom later in the cratering event. As such, its lithology consists of boulder-sized fragments imbedded in a substantial matrix of more finely divided debris. The hydrologic properties of such a mix are more closely related to those of a low-permeability glacial till than to a regular network of open planar fractures. Second, shock waves generated by subsequent impacts will help to eliminate any sizable openings in the fractured basement by both shifting and compacting the overlying debris (i.e., see Figure 1) and by rupturing additional material off the fracture walls as the shock waves are reflected along the fracture boundaries [*Short*, 1970].

Finally, as noted in section 2.1, the presence of groundwater can also contribute to a significant reduction in crustal porosity and permeability. On Earth, groundwater that resides in the crust for millions of years generally evolves into a highly mineralized brine consisting of a saturated mixture of chlorides, carbonates, sulfates, silica, and a variety of other dissolved species [*White*, 1957]. On Mars, this geochemical evolution will likely be accelerated by the influx of minerals leached from the crust by low-temperature hydrothermal circulation (see section 4.4.1 and Figure 18). The convective cycling of 10^2–10^3 km of water (per unit area) between the water table and the base of the cryosphere will deplete the intervening crust of any easily dissolved substances, concentrating many of them in the underlying groundwater to levels far in excess of their respective saturation points. The resulting precipitation of these minerals beneath the water table should lead to widespread diagenesis and to the development of a distinct geochemical horizon within the crust [*Soderblom and Wenner*, 1978]. Where exposed by subsequent faulting or erosion, this horizon should appear as a relatively competent layer whose upper boundary conforms to a surface of constant geopotential. Although not diagnostically unique, such an observation is consistent with mineral deposition in an unconfined aquifer in hydrostatic equilibrium.

In summary, although previous estimates of the large-scale permeability of the Martian crust have run as high as 10^3 darcies, consideration of the mean permeability of the Earth's crust [*Brace*, 1980, 1984], and the potential for extensive diagenesis, suggests that a more reasonable value may be 3–5 orders of magnitude smaller. As discussed in section 5.3, even permeabilities this low will permit the pole-to-equator transport of a significant volume of groundwater ($\geq 10^8$ km^3) over the planet's history. It should be noted, however, that even if only a few percent of the Martian crust possesses permeabilities as high as those estimated by *Carr* [1979] and *MacKinnon and Tanaka* [1989], the potential for pole-to-equator groundwater flow will be vastly increased.

6. The Early Evolution of the Martian Hydrosphere and Climate

The way in which the Martian crust was initially charged with H_2O is critically dependent on the nature of the planet's early climate. Was Mars was warm and wet, as suggested by the valley networks? Or has it always resembled the frozen state we observe today? And, finally, if the climate did start warm, how was the planet's hydrologic cycle affected by the onset of colder temperatures? These, and several related questions about the development of the early hydrosphere and climate, are addressed in the following discussion.

6.1. *The Evolution of the Early Martian Climate and the Initial Emplacement of Crustal H_2O*

Given the geomorphic evidence for the widespread occurrence of water and ice in the early crust, and the difficulty involved in accounting for this distribution given the present climate, it has been suggested that the Martian climate was originally more Earth-like, permitting the global emplacement of crustal H_2O by direct precipitation as snow or rain [e.g., *Masursky et al.*, 1977; *Pollack et al.*, 1987]. The resemblance of the valley networks to terrestrial runoff channels, and their almost exclusive occurrence in the planet's ancient (~4 billion year old) heavily cratered terrain, is often cited as evidence of just such a period.

Clearly, if the valley networks did originate from an early episode of precipitation and surface runoff, it required atmospheric pressures and surface temperatures far higher than those observed today. For this reason, it has been suggested that early Mars possessed a greenhouse climate, a condition that would have required in excess of 5 bars of CO_2 and the presence of other potent greenhouse gasses, such as methane and ammonia, to maintain surface temperatures above freezing [*Postawko and Kuhn*, 1986; *Pollack et al.*, 1987; *Kasting*, 1987, 1991]. Although this amount of CO_2 is ~10^2–10^3 times more than contained in the present atmosphere, it is well within current estimates of the planet's total volatile budget [*Pepin*, 1987]. The surface erosion expected from such a massive early atmosphere may also

explain the early episode of crater obliteration inferred from crater diameter-frequency plots of the ancient cratered highlands [*Mutch et al.*, 1976; *Arvidson et al.*, 1980; *Carr*, 1981].

However, if Mars did possess an early greenhouse, then what caused the atmospheric inventory of CO_2 to fall from an initial value of 5 bars to its present level of 6.1 mbar? At least four processes appear likely. Calculations by *Watkins and Lewis* [1985] suggest that shock waves from large impacts may have blown off a significant portion of the early atmosphere. This process was probably most effective during the heavy bombardment period, when large impacting bodies were still prevalent in the solar system. The depletion of the atmosphere was likely further enhanced by the interaction of the solar wind with the ionosphere. Particle velocities within the resulting plasma flow could have easily exceeded the planet's 5 km s^{-1} escape velocity. Calculations indicate that this process alone could have reduced a dense early atmosphere to its present state in less than a billion years [*Perez-de-Tejada*, 1987]. Finally, atmospheric CO_2 may have been lost to the regolith by both adsorption [*Fanale et al.*, 1986] and by reaction with surface and subsurface liquid water to form carbonate rocks [*Booth and Kieffer*, 1978; *Kahn*, 1985; *Pollack et al.*, 1987]. Ultimately, all four processes may have contributed to reducing the atmospheric pressure and temperature to the point where liquid water was no longer stable at the surface. Proponents of this idea suggest that this transition occurred some 4 billion years ago; thus, ending the period of valley network formation.

An alternative school of thought suggests that the early Martian climate did not differ substantially from that of today. Advocates of this view [e.g., *Pieri*, 1979, 1980; *Carr*, 1983] find no compelling reason to invoke a warmer, wetter period to explain the origin of the valley networks. Rather, they cite evidence that the primary mechanism of valley formation was groundwater sapping [*Sharp and Malin*, 1975; *Pieri*, 1980; *Baker*, 1982; *Carr*, 1983; *Brakenridge et al.*, 1985; *Baker and Partridge*, 1986], a process that does not require that surface water exist in equilibrium with the atmosphere. According to this scenario, as groundwater seeped onto the surface, the heat removed by its rapid vaporization led to the formation of a protective and thickening cover of ice, beneath which water may have continued to flow for considerable distances even under current climatic conditions [*Wallace and Sagan*, 1979; *Carr*, 1983; *Brakenridge et al.*, 1985].

Of course, if the early climate was similar to the present one, why are the valley networks found almost exclusively in the ancient cratered highlands? As discussed in section 4.4, the association of most small valleys with the rims of large craters suggests a genetic relationship, whereby the melt generated by large impacts resulted in the formation of local hydrothermal systems whose discharge then formed the valleys [*Newsom*, 1980; *Brakenridge et al.*, 1985]. Because only large impacts may have produced sufficient melt to establish the necessary hydrothermal activity, the decline in valley network formation might then simply reflect the early decline in the number of large impactors.

However, while groundwater sapping may successfully explain the origin of the small valleys, it fails to address how the crust was initially charged with H_2O. Indeed, even advocates of the sapping hypothesis sometimes sidestep this issue by suggesting that the groundwater involved in the formation of the networks was emplaced during a period of precipitation that occurred so early that no physical record of that period remains [*Pieri*, 1979, 1980].

Although it is possible that evidence of an ancient period of global precipitation has been lost by erosion and resurfacing, it seems equally reasonable to take this lack of evidence at face value and consider the possibility that such an episode may never have occurred. In this regard, *Soderblom and Wenner* [1978] suggest that the emplacement of crustal H_2O was the result of the direct injection and migration of juvenile water derived from the planet's interior. There are at least two ways in which this emplacement may have occurred. First, by the process of thermal vapor diffusion, water exsolved from cooling magmas will migrate from warmer to colder regions of the crust. As a result, any part of the cryosphere that overlies or surrounds an area of magmatic activity, will quickly become saturated with ice. The introduction of any additional water will then result in its accumulation as a liquid beneath the cryosphere, where, under the influence of the growing local hydraulic head, it will spread laterally in an effort to reach hydrostatic equilibrium.

However, the fate of water released to the cold Martian atmosphere is significantly different. The rapid injection of a large quantity of vapor into the atmosphere (e.g., by volcanism) will lead to its condensation as ice on, or within, the surrounding near-surface regolith. As the available pore space in the upper few meters of the regolith is saturated with ice, it will effectively seal off and eliminate any deeper region of the crust as an area of potential storage. From that point on, any excess water vapor that is introduced into the atmosphere will be restricted to condensation and insolation-driven redistribution on the surface until it is eventually cold-trapped at the poles.

Should the deposition of ice at the poles continue, it will ultimately lead to basal melting, recycling water back into the crust beneath the caps. As the meltwater accumulates beneath the polar cryosphere, it will create a gradient in hydraulic head that will drive the flow of groundwater away from the poles. As the flow expands radially outwards, it will pass beneath regions where, as a result of vapor condensation from the atmosphere, only the top few meters of the cryosphere have been saturated with ice. As before, the presence of a geothermal gradient will then lead to the vertical redistribution of H_2O from the underlying groundwater to the cryosphere until its pore volume is saturated throughout (see section 4.5). In this way, and by these processes, the early crust may have been globally charged with water and ice without the need to invoke an early period of atmospheric precipitation.

6.2. *The Hydrologic Response of Mars to the Thermal Evolution of Its Early Crust*

Although unambiguous evidence that Mars once possessed a warmer, wetter climate is lacking, a study of the transition from such conditions to the present climate can benefit our understanding of both the early development of the cryosphere and the various ways in which the current subsurface hydrology of Mars is likely to differ from that of the Earth. Viewed from this perspective, the early hydrologic evolution of Mars is essentially identical to considering the hydrologic response of the Earth to the onset of a global subfreezing climate.

If the valley networks did result from an early period of atmospheric precipitation, then Mars must have once possessed near-surface groundwater flow systems similar to those currently found on Earth, where, as a consequence of atmospheric recharge, the water table conformed to the shape of the local terrain (Figure 30*a*). However, with both the transition to a colder

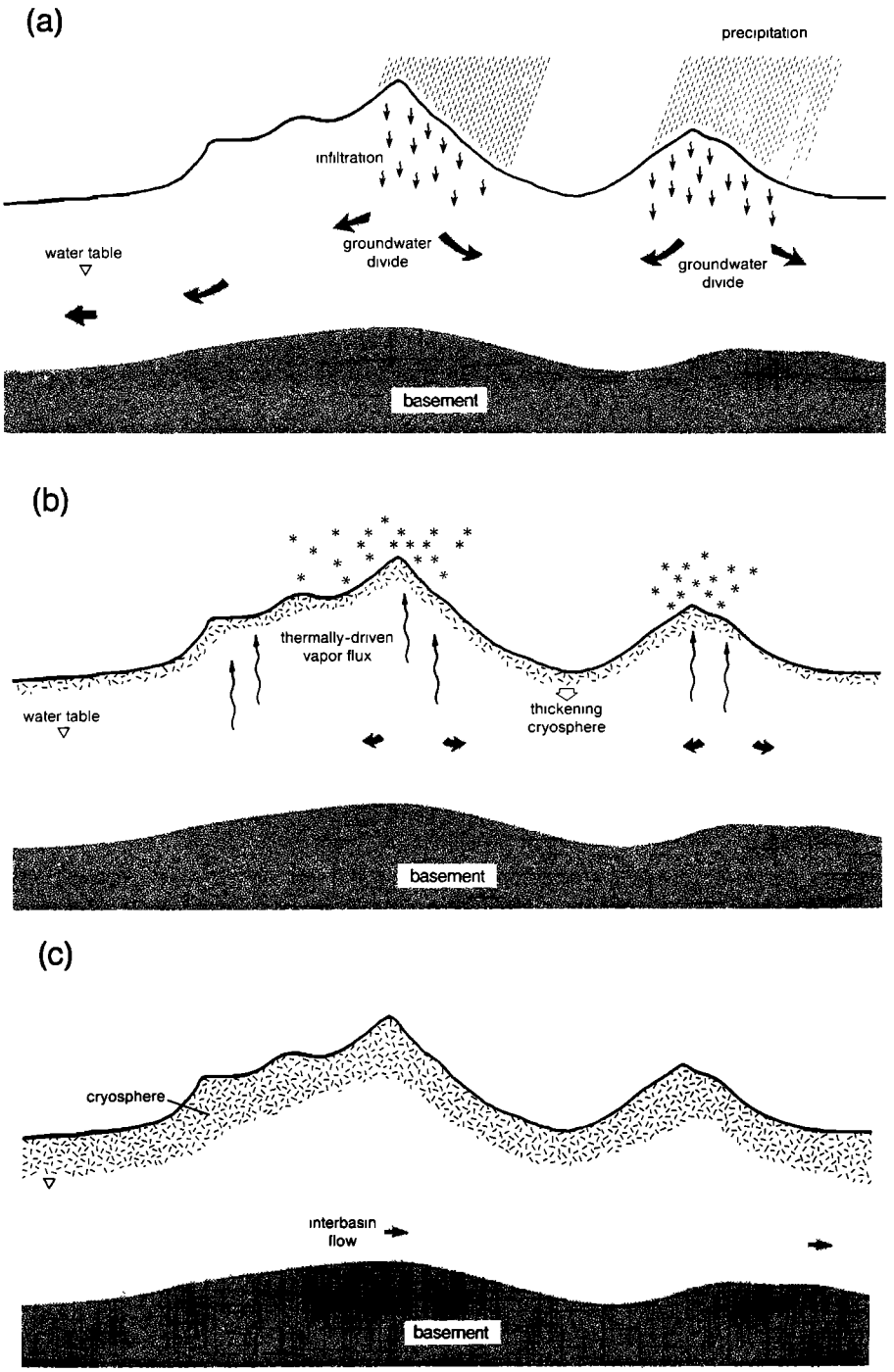

Fig. 30. The hydrologic response of Mars to the onset of a colder climate. (*a*) If Mars once had a warmer, wetter climate, it may have had near-surface groundwater flow systems similar to those found on Earth which, as a result of atmospheric precipitation, had water tables that followed the local topography. (*b*) As the temperature fell below freezing, the condensation of ice in the near-surface crust eliminated any further replenishment of the underlying groundwater, leading to the decay of the precipitation and topographically induced groundwater divides. (*c*) Ultimately, as the groundwater reached hydrostatic equilibrium, it saturated the lowermost porous regions of the crust, resulting in a groundwater table that conformed to a surface of constant geopotential.

climate and the decline in Mars' internal heat flow, a freezing front eventually developed in the regolith that propagated downward with time, creating a thermodynamic sink for any H_2O within the crust. Initially, water may have entered this developing region of frozen ground from both the atmosphere and underlying groundwater. However, as ice condensed within the near-surface pores, the deeper regolith was ultimately sealed off from any further atmospheric supply. From that point on, the only source of water for the thickening cryosphere must have been the thermally driven upward flux of vapor from the underlying groundwater (Figure 30*b*).

With the elimination of atmospheric recharge, the elevated water tables that once followed the local topography eventually decayed. The continuity of pore space provided by sediments,

breccia, and interbasin faults and fractures should have then allowed the water table to hydrostatically readjust on a global scale until it ultimately conformed to a surface of constant geopotential (Figure 30*c*). This conclusion is supported by investigations of areally extensive groundwater systems on Earth that experience little or no precipitation [e.g., *Mifflin and Hess*, 1979; *Cathles*, 1990].

The time required for the development of the cryosphere can be calculated by solving the transient one-dimensional heat conduction equation for the case of a semi-infinite half-space with internal heat generation, where

$$\frac{\partial^2 T}{\partial z^2} + \frac{S}{\kappa} = \frac{1}{\alpha}\frac{\partial T}{\partial t} \qquad (30)$$

and where T is the crustal temperature, z is the depth, t is time, κ is the crustal thermal conductivity, α is the thermal diffusivity ($= \kappa/\rho c$), and S is the heat generation rate per unit volume ($= 3Q_g/R$, where Q_g is the geothermal heat flux an R is the radius of Mars) [*Fanale et al.*, 1986]. An upper limit can be placed on how rapidly the cryosphere evolved if we assume that the surface temperature of Mars underwent an instantaneous transition from a mean global value of 273 K to its current latitudinal range of 154–218 K. Given this assumption, the boundary and initial conditions that apply to equation (30) are

$$T(0, 0) = 273 \text{ K}$$
$$T(0, t) = 218 \text{ K (at the equator)}$$
$$= 154 \text{ K (at the poles)}$$

$$\frac{\partial T}{\partial z} = -\frac{Q_g}{\kappa}$$

For the conditions described above, equation (30) was solved numerically using the method of finite-differences. The results indicate that, given a present-day geothermal heat flux of 30 mW m^{-2}, the freezing front at the base of the cryosphere will reach its equilibrium depth at the equator in ~4.6×10^5 years, while at the poles it will take roughly 1.5×10^6 years (Figure 31). Given the elevated geothermal conditions that likely characterized the planet 4 billion years ago (i.e., $Q_g \sim 150$ mW m^{-2}), the corresponding development times are 2×10^4 years and 1.3×10^5 years, respectively. These calculations are based on a thermal conductivity of 2.0 W m^{-1} K^{-1}, a freezing temperature of 273 K, and a maximum latent heat release (due to the condensation of H_2O vapor as ice in the pores) that does not exceed Q_g, a limit that is imposed by the geothermal origin of the vapor flux reaching the base of the cryosphere (e.g., Figure 30*b*; see also section 4.4.1). Note that although these development times assume an initially dry crust, they would not be significantly different even if the crust were initially saturated throughout. Although the early growth of the cryosphere would be slowed by the ready supply of latent heat, this period represents only a small fraction of the total time required for the cryosphere to reach equilibrium. In the later stages of growth, which are controlled almost exclusively by conduction through the frozen crust, the rate of heat loss is sufficiently small that the effect of latent heat release can be virtually ignored.

Although the assumption that Mars underwent an instantaneous transition from a warm to cold early climate is clearly incorrect, this extreme example serves to illustrate an important point, that is: on a time scale greater than ~10^6 years, the base of the cryosphere is essentially in thermal equilibrium with mean temperature environment at the surface. As a result, for any reasonable model of climate evolution, the growth of the cryosphere is not controlled by the rate of conduction through the crust, but by

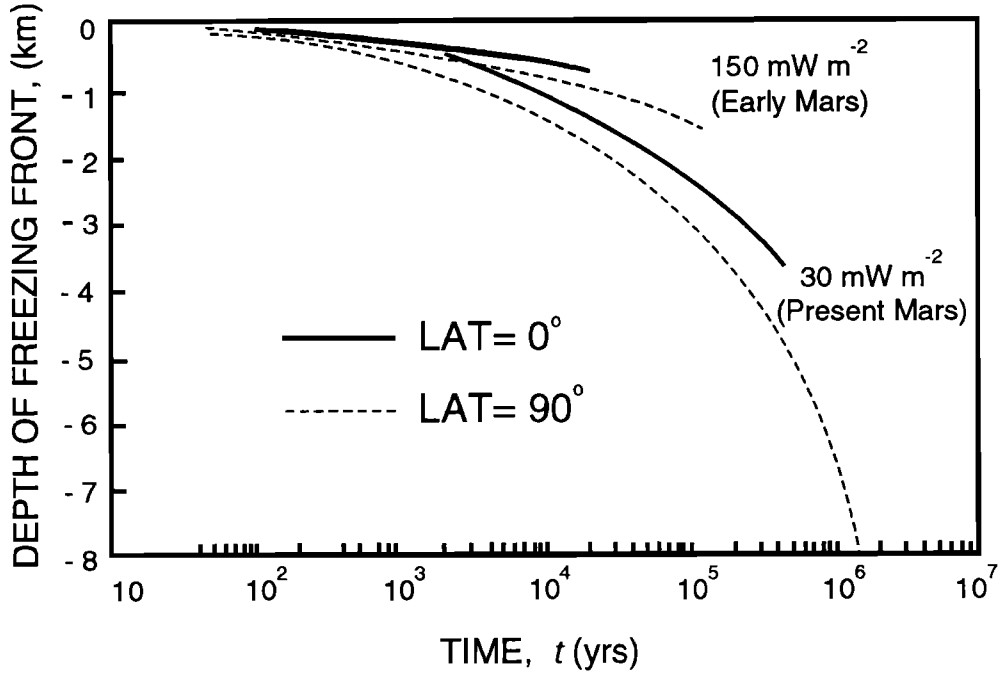

Fig. 31. Development times for the Martian cryosphere at the equator (T_s = 218 K) and poles (T_s = 154 K), assuming an instantaneous transition from a previous warm early climate (T_s = 273 K). The calculations are based on a crustal thermal conductivity of 2.0 W m^{-1} K^{-1}, a basal freezing temperature of 273 K, and geothermal heat fluxes of 30 and 150 mW m^{-2}. The resulting equilibrium depths at the equator and poles for the two values of geothermal heat flux are, respectively, 3670 m and 7930 m, and 730 m and 1590 m.

how rapidly the mean surface temperature environment changes with time. *Pollack et al.* [1987] estimate that if the primary mechanism driving climate change was the removal of a massive (1–5 bar) CO_2 atmosphere by carbonate formation, then the transition from a warm to cold early climate must have taken between 1.5×10^7 to 6×10^7 years. For transition times this slow, the downward propagation of the freezing front at the base of the cryosphere proceeds at a rate that is sufficiently small (when compared with the geothermally-induced vapor flux arising from the groundwater table) that the geothermal gradient should have no trouble supplying enough vapor to keep the cryosphere saturated with ice throughout its development.

From a mass balance perspective, the thermal evolution of the early crust effectively divided the subsurface inventory of water into two reservoirs: (1) a slowly thickening zone of near-surface ground ice and (2) a deeper region of subpermafrost groundwater [*Carr*, 1979]. Regardless of how rapid the transition to a colder climate actually was, the cryosphere has continued to thicken as the geothermal output from the planet's interior has gradually declined. One possible consequence of this evolution is that, if the planet's initial inventory of outgassed water was small, the cryosphere may have eventually grown to the point where all of the available H_2O was taken up as ground ice [*Soderblom and Wenner*, 1978]. Alternatively, if the inventory of H_2O exceeds the current pore volume of the cryosphere, then Mars has always had extensive bodies of subpermafrost groundwater.

Because the pore volume of the cryosphere was likely saturated with ice throughout its early development, the thermally driven vapor flux arising from the reservoir of underlying groundwater could have led to the formation and maintenance of near-surface perched aquifers, fed by the downward percolation of condensed vapor from the higher and cooler regions of the crust (Figure 32). Eventually the hydrostatic pressure exerted by the accumulated water may have been sufficient to disrupt the overlying ground ice, allowing the stored volume to discharge onto the surface. Such a scenario may have been repeated hundreds of times during the planet's first half-billion years of geologic history, possibly explaining (in combination with local hydrothermal systems driven by impact melt [*Newsom*, 1980] and volcanism [*Gulick*, 1991]) how some valley networks may have evolved in the absence of atmospheric precipitation [*Pieri*, 1979, 1980; *Carr*, 1983]. However, as the internal heat flow of the planet continued to decline, the thickness of the cryosphere may have grown to the point where it could no longer be disrupted by the limited hydrostatic pressure that could develop in a perched aquifer, thus terminating the potential contribution of low-temperature hydrothermal convection to valley network formation.

Finally, the postcryosphere groundwater hydrology of Mars will differ from its possible precryosphere predecessor (and therefore from present-day terrestrial groundwater systems) in at least one other important way. In contrast to the local dynamic cycling of near-surface groundwater that may have characterized the first half-billion years of Martian climate history (e.g., Figures 11 and 30*a*), the postcryosphere period will necessarily be dominated by deeper, slower interbasin flow (e.g., Figure 30*c*). Aside from polar basal melting, there are at least three other processes that are likely to drive flow under these conditions, they are (1) tectonic uplift (essentially the same mechanism proposed by *Carr* [1979] to explain the origin of the outflow channels east of Tharsis), (2) gravitational compaction of aquifer pore space (perhaps aided by the accumulation of thick layers of sediment and basalt on the surface), and (3) regional-scale hydrothermal convection (e.g., associated with major volcanic centers such as Tharsis and Elysium). Note that, with the exception of active geothermal areas, the flow velocities associated with these processes are likely to be orders of magnitude smaller than those that characterize precipitation-driven systems on Earth.

7. Further Considerations

A unique feature of the hydrologic model presented in this paper is that, with regard to the transfer of H_2O between its long-term sources and sinks, it is essentially a closed loop (Figure 33). That is, given an inventory of outgassed water that is sufficient to both saturate the pore volume of the cryosphere and form a subpermafrost groundwater system of global extent, the loss of crustal water from any region on the planet is ultimately balanced by surface deposition, basal melting, and subsurface replenishment. Further, given a geologically reasonable description of the crust, this cycle appears to be an inevitable consequence of both basic physics and the climatic conditions that have apparently prevailed on Mars throughout the past 3.5–4.0 billion years. For this reason, the model has important implications for a variety of problems associated with the planet's hydrologic and climatic history. In this section two examples that illustrate the relevance and potential importance of this model are considered: (1) the recharge of the valley networks and outflow channels, and (2) the polar mass balance of H_2O.

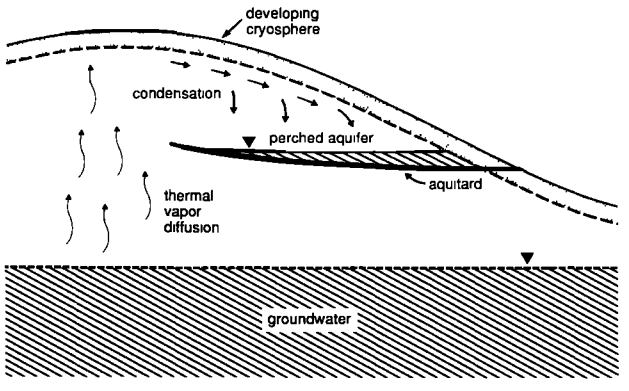

Fig. 32. An illustration of how the process of thermal vapor diffusion may have led to the development and maintenance of near-surface perched aquifers in the absence of atmospheric precipitation.

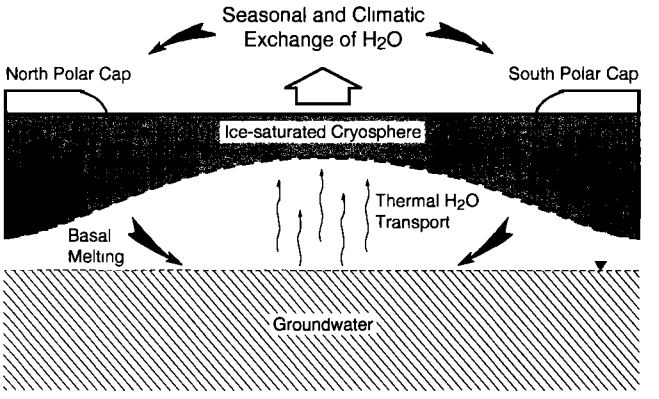

Fig. 33. A model of the climatic behavior of water on Mars.

7.1. *Recharge of the Valley Networks and Outflow Channels*

A recurrent issue regarding the origin of the valley networks and outflow channels is that the amount of water required to erode these features is so large, compared with the storage capacity of their likely source regions, that some type of recycling process appears necessary. In an effort to address this problem, a variety of potential recycling mechanisms have been proposed [e.g., *Masursky et al.*, 1977; *Carr*, 1984; *Jakosky and Carr*, 1985; *Clow*, 1987; *Gulick and Baker*, 1990; *Baker et al.*, 1991; *Plescia and Crisp*, 1991; *Moore et al.*, 1991]. Although several of these schemes appear viable, virtually all require either a coincidence of environmental conditions, or a combination of physical properties, that is needlessly complex or whose occurrence is poorly constrained.

An assumption common to each of the above scenarios, is that the reservoirs of groundwater that were tapped in the formation of the valley networks and outflow channels were limited in capacity and isolated with respect to other reservoirs of groundwater present on the planet. However, as discussed in section 3.2, investigations of the kilometer-scale permeability of the Earth's crust suggest that virtually all terrestrial groundwater systems share some degree of hydraulic interconnection. Clearly, if this is true of the Earth, with an inferred mean crustal permeability of 10^{-2} darcies [*Brace*, 1980, 1984], then the case for hydraulic continuity on Mars, where some have argued for large-scale permeabilities as much as 10^5 times higher [*Carr*, 1979; *MacKinnon and Tanaka*, 1989], should be significantly stronger. The importance of this argument to the recharge of the valley networks and outflow channels is that, rather than drawing on small, isolated, and rapidly depleted local sources of groundwater, these features may have tapped an enormously larger and self-replenishing global reservoir, whereby any water that was discharged to the surface was eventually balanced by the introduction of an equivalent amount back into the aquifer through the process basal melting.

Yet, because neither the likely extent of hydraulic continuity within the crust nor the potential role of basal melting are widely recognized, most investigators have attempted to address the problem of local groundwater depletion by invoking local mechanisms of resupply. The common problem with such mechanisms is that once groundwater has been discharged to the surface, it is unable to infiltrate back through the frozen crust to replenish the system from which it was initially withdrawn. In support of this conclusion recall that under current climatic conditions, the thickness of the cryosphere, even at the equator, is likely to exceed 2 km (section 2.2). Further, a necessary prerequisite for the widespread occurrence of groundwater is that the thermodynamic sink represented by the cryosphere must already be saturated with ice. Thus, the cryosphere acts as an impermeable self-sealing barrier that effectively precludes the local resupply of subpermafrost groundwater either by the infiltration of water discharged by catastrophic floods, or by atmospheric precipitation on some highland source region. Note that the problem of local infiltration and subsurface replenishment is not significantly improved even if the cryosphere is initially dry, for as water attempts to infiltrate the cold, dry crust, it will quickly freeze, creating a seal that prevents any further infiltration from the ponded water above.

Indeed, virtually the only way a subpermafrost groundwater system can be directly replenished, is if the intervening cryosphere is somehow thawed throughout. This is essentially the explanation advocated by *Baker et al.* [1991] to account for both the episodic recharge of the Chryse outflow channels and the development of recent (Amazonian age) valley networks on the flanks of several large volcanoes. *Baker et al.* [1991] have proposed that an episode of intense volcanic activity, centered on Tharsis, may have triggered a massive regional melting of ground ice that ultimately resulted in the catastrophic release of as much as 6.5×10^7 km^3 of groundwater onto the surface. They argue that this massive discharge inundated the northern plains, covering approximately 10–30% of the planet with a standing body of water 10^2–10^3 m deep. In support of this conclusion, *Baker et al.* [1991] cite the enormous discharge rates inferred from the dimensions of the Chryse outflow channels, as well as geomorphic evidence of ancient shorelines discovered by *Parker et al.* [1989] throughout the northern plains.

Perhaps the most controversial element of the *Baker et al.* [1991] model is the need for a late, transient greenhouse climate to thaw the cryosphere at the time of the Chryse flooding. *Baker et al.* [1991] require this geologically short but extreme change in climate because they believe it to be the only way that the large volumes of water discharged by the outflow channels and younger valley networks could have been reassimilated into the crust. This problem is viewed as critical not only because of the present absence of this water on the surface, but because the magnitude of erosion associated with the channels implies a sustained or episodic discharge that *Baker et al.* [1991] believe can only be explained if the source regions where somehow replenished. As noted by *Carr* [1991], however, there is little geologic evidence to support such a dramatic and recent episode of global warming.

In light of the above, is there any compelling need to invoke a different climate to account for the origin of the valley networks (either old or new) or the repeated occurrence of catastrophic floods? As discussed in section 4.4.3, impact-generated hydrothermal systems, such as those proposed by *Newsom* [1980] and *Brakenridge et al.* [1985], appear perfectly capable of generating the valley networks found in the cratered highlands even under current climatic conditions. The small number of more recent networks, found on the flanks of Alba Patera and several other large volcanoes, can be similarly explained as the result of local hydrothermal activity [*Gulick and Baker*, 1990]. In neither instance is it necessary to invoke a change in climate nor, given a hydraulic link to a global aquifer, any additional mechanism of local resupply.

A similar conclusion is reached regarding the repeated occurrence of catastrophic floods. As discussed by *Carr* [1979], one consequence of the tectonic uplift of Tharsis is that it may have placed the frozen crust in the lower elevations around Chryse Planitia under a substantial hydraulic head, leading to its eventual failure and the catastrophic release of groundwater onto the surface. However, as the discharge continued, the local hydraulic head eventually declined to the point where the water-saturated crust was able to refreeze at the point of breakout, ultimately reestablishing the original ground ice thickness. The water released by such events may have formed temporary lakes or seas that eventually froze and sublimed away, with the resulting vapor ultimately cold-trapped at the poles. Such a process may well explain the origin of the large polar ice sheets inferred by both *Allen* [1979*a*] and *Baker et al.* [1991]. The identification of possible eskers near the south polar cap [*Carr et al.*, 1980; *Howard*, 1981; *Kargel and Strom*, 1992] is also consistent with this interpretation and with the subsequent reassimilation of the water into the crust through the process of basal melting.

However, basal melting is not necessarily restricted to just the poles. As discussed by *Clifford* [1987*b*], wherever the deposition and long-term retention of material occurs at the surface, the added insulation will result in the upward displacement of the melting isotherm at the base of the cryosphere until thermal equilibrium is reestablished. Thus, if the frozen lakes or seas that were formed by the discharge of the outflow channels persisted for more than 10^5–10^6 years, the local groundwater system may have been indirectly replenished by the onset of melting at the base of the cryosphere. It is likely, however, that this replenishment was only temporary. For with the eventual sublimation of the frozen lakes or seas on the surface, the melting isotherm should have returned to its original location, creating a cold-trap at the base of the cryosphere for any vapor or liquid supplied by the groundwater below (section 4.4.1). In this way, any water that was temporarily liberated from the cryosphere by basal melting, was eventually reassimilated into the frozen crust.

Note that nothing in this proposed cycle is precluded by the current climate. Indeed, given the continued uplift of Tharsis and the probable occurrence of other crustal disturbances (such as earthquakes, impacts, and volcanic eruptions), failures of the cryosphere's hydraulic seal were undoubtedly common. This suggests that the cycling of water by catastrophic floods, surface deposition, basal melting, and groundwater recharge, may have been repeated many times throughout geologic history, without the need to invoke any special conditions regarding either the geology or climate of Mars.

7.2. *The Polar Mass Balance and High Obliquities*

It is generally accepted that the Martian polar layered deposits owe their origin and apparent youthfulness to the annual deposition of dust and H_2O and that the magnitude of this deposition has been modulated by quasiperiodic variations in insolation due to changes in the planet's orbital elements and obliquity [*Cutts et al.*, 1979; *Pollack et al.*, 1979; *Toon et al.*, 1980]. On the basis of their evident thickness and the scarcity of craters with diameters larger than 300 m, *Plaut et al.* [1988] estimate that the present deposits accumulated at the rate of ~10 km/b.y. over a time span of ~10^8 years. However, studies by *Fanale et al.* [1982, 1986] suggest that conditions conducive to polar deposition are not unique to the present climate but are characteristic of the planet over a broad range of likely obliquities and orbital variations. Therefore, because the polar regions represent the planet's dominant thermodynamic sink for H_2O, any crustal water released to the atmosphere should ultimately be cold trapped at the poles.

Considering only those sources of water for which there is both unambiguous evidence and a reliable estimate of their minimum volumetric contribution (i.e., volcanism and catastrophic floods), we find that the minimum inventory of H_2O that should have accumulated at the poles over geologic time is equivalent to a global layer ~65 m deep (Table 6), a volume roughly 2–5 times greater than that observed in the residual caps. Given more reasonable estimates of channel discharge, as well as the volumes of water contributed by the valley networks, impacts, and the sublimation of equatorial ground ice, the disparity between the expected and observed polar inventories increases by over an order of magnitude. Although the water lost by atmospheric escape (~60 m, *Jakosky* [1990]) and oxidation of the regolith (~27 m, *Owen et al.* [1988]) may explain some of this discrepancy, these loss mechanisms fall considerably short of resolving the imbalance for any reasonable estimate of total crustal discharge and expected polar inventory (Table 6). Given this situation, and the fact that the polar regions are the planet's dominant sink for H_2O, how does one account for both the youthfulness of the present deposits and the apparent deficit of older material at the poles?

Clearly one possibility is that the estimated volume of water supplied to the poles by various crustal sources is wrong, and that all of the water ever released to the atmosphere is now stored in the polar ice. In that event, the apparent youthfulness of the current deposits might be explained by the simple recycling of old polar laminae into new [*Toon et al.*, 1980]. This possibility is raised by current models of the evolution of the polar troughs [*Howard*, 1978; *Howard et al.*, 1982]. These features, which form the conspicuous spiral patterns visible in the remnant caps, are thought to originate near the edge of the deposits and then migrate, through the preferential sublimation of ice from their equatorward facing slopes, toward the pole. Dust, liberated from the ice, may then be scavenged by the polar winds and redistributed over the planet, while the sublimed ice may simply be recycled by cold trapping on the poleward facing slopes and on the flats that separate the troughs. By these processes, *Toon et al.* [1980] suggest that the polar deposits have reached a state of equilibrium whereby ancient (~10^9 year old) polar material is continually reworked, maintaining a comparatively youthful surficial appearance in spite of its great age.

Although it is possible that the volume of water supplied to the poles by various crustal sources is significantly less than current estimates, such a conclusion is inconsistent with both our present understanding of the processes that have affected the evolution of the surface (sections 4.1 and 4.2) and with the growing evidence that Mars is water rich [e.g., *Carr*, 1986, 1987; *Squyres*, 1989]. The case for the local recycling of old polar laminae is also at odds with the observations of *Howard et al.* [1982], whose detailed examination of the polar stratigraphy has revealed that the erosion of equatorward facing scarps has not kept pace with layer deposition, an observation that requires a net long-term accumulation of material in the polar terrains.

Another potential solution to the mass balance problem is suggested by recent theoretical studies which indicate that the obliquity of Mars is chaotic and may reach peak values in excess of 50° [*Bills*, 1990; *Ward and Rudy*, 1991; *Touma and Wisdom*, 1993; *Laskar and Robutel*, 1993]. Under such conditions, periods of intense polar erosion may alternate with periods of accumulation, redistributing the polar dust and H_2O over much of the planet. This possibility was first considered by *Jakosky and Carr* [1985] in connection with the origin of the valley networks. Their work was based on the then accepted belief that, prior to the formation of Tharsis, Mars had experienced obliquities as high as 45° [*Ward et al.*, 1979], values that significantly exceeded those that were thought to characterize the planet after the development of Tharsis (~11° - 38° [*Ward*, 1979]).

Although the length of time Mars spends near its maximum obliquity during a given cycle is brief (~10^4 years), the resulting increase in peak and mean annual insolation at polar latitudes could affect the polar mass balance in several important ways. For example, *Jakosky and Carr* [1985] have argued that, at an obliquity of 45°, summer polar temperatures may rise high enough to result in the sublimation of 20 cm of ice from the perennial caps. Therefore, over the 10^4 years that such obliquities persist, a total of as much as 2 km of ice might be removed from the caps. *Jakosky and Carr* [1985] suggest that both dynamical considerations and cold nighttime temperatures may conspire to limit the maximum distance that the resulting vapor is transported from the cap. This, they argue, could lead to the

precipitation of ice at low- and mid-latitudes, with surface accumulations of up to several tens of meters over the duration of the high obliquity portion of the cycle. The absorption of sunlight in the resulting snowpack, could then lead to transient summertime melting which they suggest may have contributed to the formation of the valley networks and the replenishment of equatorial reservoirs of H_2O.

While the calculations of *Jakosky and Carr* [1985] clearly demonstrate the potential for significant mass loss at times of high obliquity, there are at least two observations that appear to significantly constrain both the magnitude of polar erosion and the extent of equatorial deposition. Consider first the case for equatorial deposition and melting. A principle asset of the *Jakosky and Carr* [1985] model, in the context it was originally proposed, was that it provided a self-consistent explanation for both the geographic distribution of valley networks (which are concentrated at equatorial and temperate latitudes [*Carr and Clow*, 1981]) and their almost exclusive occurrence in terrains that predate the development of Tharsis [*Carr and Clow*, 1981; *Tanaka*, 1986]. This self-consistency breaks down, however, with the recognition that Mars has likely experienced high obliquities throughout its history, including the recent past [*Bills*, 1990; *Ward and Rudy*, 1991; *Touma and Wisdom*, 1993; *Laskar and Robutel*, 1993]. Although a few "young" valleys have been found on Alba Patera and several other large volcanoes [*Gulick and Baker*, 1990], their absence from any other terrains that post-date Tharsis strongly suggests an endogenic, rather than exogenic, origin. Thus, if melting and surface runoff has ever occurred in association with the development of equatorial snowpacks at high obliquity, its contribution to the formation of the valley networks and the replenishment of equatorial H_2O apparently ceased no later than the formation of Tharsis (~3.5-4 b.y.a. [*Wise et al.*, 1979]).

With regard to the magnitude of polar erosion, both the inferred 10^8-year age of the polar deposits [*Plaut et al.*, 1988] and the apparent frequency of high obliquity excursions [*Bills*, 1990; *Ward and Rudy*, 1991; *Touma and Wisdom*, 1993; *Laskar and Robutel*, 1993] appear to place a severe constraint on the magnitude of mass loss that the poles typically experience during such periods. For example, if the loss amounted to the ~10^2–10^3 m per high obliquity cycle originally suggested by *Jakosky and Carr* [1985], then the maximum "life cycle" of the deposits, from build-up to erosion, would necessarily be limited to just a few million years. Yet, if the inferred 10^8-year age of the deposits is correct, then they have not only survived a minimum of 10^3 obliquity cycles (many of which should have exceeded 45°), but have actually accumulated at the rate of ~10 km/b.y. [*Plaut et al.*, 1988]. This fact is consistent with previous theoretical studies indicating the existence of a long-term net depositional environment at the poles [*Fanale et al.*, 1982, 1986] and with the absence of observational evidence indicative of any massive, widespread erosion of the polar laminae [*Howard et al.*, 1982].

To summarize, it appears that any solution to the mass balance problem should (1) be consistent with theoretical models of the Martian climate, which indicate that a net depositional environment has existed at the poles throughout most of the planet's history [*Fanale et al.*, 1982, 1986], (2) be able to account for the observational evidence that the evolution of the polar terrains has indeed been dominated by depositional processes [*Howard et al.*, 1982], (3) be able to accommodate a rate of deposition, implied by the paucity of craters within the deposits, of from 10^{-5} to 10^{-4} m yr^{-1} [*Cutts et al.*, 1976; *Pollack et al.*, 1979; *Plaut et al.*, 1988], and (4) satisfy all of the previous conditions within the constraint imposed by the apparent deficit of older material that currently exists at the poles.

As discussed by *Clifford* [1987*b*], the process of basal melting appears to satisfy each of these requirements. Once the polar deposits have reached the required thickness for basal melting, they will have achieved a condition of relative equilibrium, whereby the accumulation of any H_2O at the ice cap's surface will eventually be offset by melting at its base. Indeed, a geothermal heat flux of 30 mW m^{-2} K^{-1} could easily keep pace with an H_2O deposition rate as high as ~3 x 10^{-3} m yr^{-1}. Therefore the occurrence of basal melting is consistent with both the prediction of climate models [*Fanale et al.*, 1982, 1986] and the observational evidence [*Howard et al.*, 1982], indicating that a long-term net depositional environment has existed at the poles.

8. Qualifications and Potential Tests

A model of any natural process is necessarily a compromise between the desire to consider all first-order effects, and the practical reality that it must be simple enough to be readily communicated and understood. Unfortunately, the inherent complexity of real world systems is often poorly represented when described in such general terms. With regard to the hydrologic and climatic behavior of water on Mars, the transport of H_2O through the atmosphere, over the surface, and beneath the ground, involves numerous individual processes, each of which may be significantly affected by natural variations in the local or global environment. Spatial variations, like local changes in the thermophysical properties of the crust, are perhaps the best understood and easiest to model. While characteristics like porosity, permeability and heat flow, may change appreciably from one location to another, this variation is likely to occur within a fairly well-defined range of limits based on our knowledge of the geology of the Earth and Moon, and what we have deduced about Mars from spacecraft investigations of its surface. Temporal changes are another matter. Some, like the decline in the planet's internal heat flow or the rise in solar luminosity, are evolutionary and, therefore, at least somewhat predictable. The occurrence of others, such as a major impact, the catastrophic discharge of an outflow channel, or the long-term chaotic evolution of the Martian obliquity and orbital elements, completely defy prediction, yet their impact on the local or global environment may, at times, completely overwhelm all other effects. It is the synergistic interaction of these various elements that has governed the hydrologic and climatic behavior of water on Mars.

Clearly, given this many free parameters, the number of possible permutations of events and conditions that may have affected the Martian climate is virtually endless. One example is the evidence for polar wandering presented by *Schultz and Lutz* [1988]. As has been stated many times in this analysis, given our present understanding of Martian climatic history, a net long-term loss of H_2O from the equatorial crust to the atmosphere appears irreversible. This conclusion assumes, however, that the geographic location of the planet's spin axis has remained fixed with time, an assumption that *Schultz and Lutz* [1988] have vigorously challenged. Perhaps the most persuasive evidence for polar wandering comes from the identification of several extensive antipodal layered deposits near the equator that possess a number of striking morphologic similarities to the polar layered terrains. To account for these features, *Schultz and Lutz* [1988] have proposed that over a time scale of several billion years, the crust of Mars has undergone a major reorientation in relation to

its spin axis. They attribute this movement to changes in the planet's moment of inertia caused by the formation of Tharsis. While the actual dynamics necessary to produce this shift are presently unclear, the slow migration of the geographic location of the poles provides a mechanism for moving the planet's cold trap and atmospherically replenishing subsurface H_2O on a global scale.

It is important to note, however, that while polar wandering [*Schultz and Lutz*, 1988], massive polar erosion at high obliquities [*Jakosky and Carr*, 1985], and recent transient global warming [*Baker et al.*, 1991], may all have occurred, none of these scenarios is required to explain any aspect of the hydrologic evolution of a water-rich Mars that cannot already be satisfactorily explained under the physical and climatic conditions we observe on the planet today. This conclusion is based on only two assumptions: (1) that the physical properties of the Martian crust, including porosity, permeability, and crustal thermal conductivity, are no different then those which characterize the Earth and Moon, and (2) that Mars possesses an inventory of water that exceeds the pore volume of the cryosphere by as little as a few percent. Given these conditions, basic physics dictates that the processes of surface deposition, basal melting, groundwater flow, and the thermal transport of H_2O, will thermodynamically and hydraulically link the atmospheric, surface, and subsurface reservoirs of water on Mars into a single self-compensating system.

Although unequivocal evidence of a planetary-scale groundwater system is currently lacking, its existence is consistent with the calculations presented in section 2 and with the geomorphic evidence that Mars possesses an inventory of water equivalent to a global ocean 0.5–1 km deep [*Carr*, 1987]. More direct evidence that such a system has existed throughout much of Martian geologic history is provided by the timing and thermodynamic implications of the outflow channels. As discussed in section 2.3, a prior condition for the existence of any large volume of groundwater is that the pore volume of the cold-trap represented by the cryosphere must first be saturated with ice. This conclusion follows from the fact that, given an available reservoir of water at depth, thermal processes will supply enough H_2O to saturate the cryosphere in less than 10^7 years (sections 4.4.1 and 4.5). Since the youngest outflow channels may be less than 1 billion years old [*Tanaka*, 1986; *Tanaka and Scott*, 1986; *Parker et al.*, 1989; *Mouginis-Mark*, 1990; *Rotto and Tanaka*, 1991; *Baker et al.*, 1992], this suggests that an inventory of water in excess of that stored in the cryosphere has persisted on Mars until very recent times, and may continue to persist to the present day.

While theoretical arguments for a planetary-scale groundwater system based on the thermodynamic significance of the outflow channels are interesting, they fall short of an actual proof. Unfortunately, at present, the channels are the best evidence that we have. However, as the exploration of Mars continues, there will be opportunities for more direct investigations of the subsurface that should resolve this issue conclusively. While prospects for a Mars Deep Drilling Project are likely to remain dim for the foreseeable future, at least two other geophysical methods, active seismic exploration [*Tittmann*, 1979; *Zykov et al.*, 1988] and electromagnetic sounding [*Rossiter et al.*, 1978; *Ehrenbard et al.*, 1983], could be used to detect and map the distribution of ground ice and groundwater beneath the planet's surface.

Assuming that such investigations are actually conducted, what observations would provide conclusive evidence that Mars possesses an interconnected groundwater system of global scale? First, the detection of groundwater at locations far removed from any obvious source of transient production, such as volcanoes or other active geothermal regions, would establish that Mars is both water-rich and that it possesses an inventory of H_2O that significantly exceeds the pore volume of the cryosphere. Second, should it be found that the absolute elevation of the water table is the same at widely separated locations (disregarding local differences caused by recent tectonic activity, anomalous geothermal heating, or prolonged deposition at the surface), it would strongly indicate that groundwater on Mars has hydrostatically adjusted on a global basis, a condition that can only be reached if the system is interconnected. If this last condition is actually observed, it will essentially confirm the single most important element of the model presented here, that Mars possesses an interconnected groundwater system of global extent. Since all the remaining elements of the model follow from this foundation, and from basic physics, the greatest remaining uncertainty will be the extent to which basal melting, groundwater flow, and the thermal transport of H_2O in the crust, have competed with, or complemented, other processes in the transport of water above, across, or beneath the Martian surface.

9. Conclusions

The analysis presented here leads to the following conclusions:

1. If the inventory of H_2O on Mars exceeds by more than a few percent the quantity required to saturate the pore volume of the cryosphere, then a subpermafrost groundwater system of global extent will necessarily result.

2. Under the climatic conditions that have prevailed throughout most of Martian geologic history, the inherent instability of equatorial ground ice has lead to a net atmospheric transport of H_2O from the hot equatorial region to the colder poles. Theoretical arguments and various lines of morphologic evidence suggest that this poleward flux of H_2O has been augmented by additional releases of water resulting from impacts, catastrophic floods, and volcanism.

3. Based on the conditions postulated in conclusion 1, the deposition and retention of material at the poles (or any other location) will eventually result in basal melting. The downward percolation of meltwater into the underlying global aquifer will then result in the rise of the local water table in the form of a groundwater mound.

4. Given a geologically reasonable value of large-scale permeability (i.e., $\geq 10^{-2}$ darcies), the gradient in hydraulic head created by the development of groundwater mounds at both poles could drive the equatorward flow of a significant volume of groundwater ($\geq 10^8$ km^3 H_2O) over the course of the planet's history.

5. At equatorial and temperate latitudes, the presence of a geothermal gradient will result in a net discharge of the groundwater system as vapor is thermally pumped from the warmer (higher vapor pressure) depths to the colder (lower vapor pressure) near-surface crust. By this process a gradient as small as 15 K km^{-1} could drive the vertical transport of 1 km of water to the freezing front at the base of the cryosphere every 10^6–10^7 years, or the equivalent of a 10^2–10^3 km of water over the 4.5 billion year history of the planet. In this manner, much of the ground ice that has been lost from the crust may ultimately be replenished.

While particular aspects of the model presented in this paper may be debated (e.g., the actual porosity and permeability of the crust, the magnitude of polar deposition, etc.), the occurrence of subsurface transport on Mars is essentially contingent on a single

factor: does the present planetary inventory of H_2O exceed, by more than a few percent, the quantity of water required to saturate the pore volume of the cryosphere? If so, then basic physics suggests that the hydrologic model described here will naturally evolve. Given a geologically reasonable description of the crust, the quantity of H_2O transported through the subsurface may then play an important role in the geomorphic evolution of the Martian surface and the long-term cycling of H_2O between the atmosphere, polar caps, and near-surface crust.

Acknowledgements. The first draft of this paper was written in 1980. Since that time, both the paper and the ideas presented in it, have had a long and tortuous evolution. Both have benefited from the input I've received from many friends and colleagues. I would especially like to thank Bruce Jakosky, Fraser Fanale, Michael Carr, Daniel Hillel, George McGill, Bill Irvine, Peter Schloerb, Bruce Bills, Mark Cintala, Deborah Domingue, Jim Zimbelman, Scott Murchie, Karen Miller and Jose Valdez, for having reviewed earlier drafts of this paper and provided many helpful suggestions for its improvement. I would also like to thank Pete Schultz, Matt Golembek, Lisa Rossbacher, Steven Squyres, Mike Malin, Ruslan Kuzmin, Alan Howard, Laurie Johansen, Peter Mouginis-Mark, Nadine Barlow, Bob Miller, and Ken Tanaka, for having indulged me in many extended discussions about water on Mars. My thanks also to Amanda Kubala and Brian Fessler, who through the years have provided invaluable programming and technical assistance, and to Fran Waranius and Stephen Tellier, who located copies of countless, but much needed, references. I am especially grateful and indebted to the following people: to Bob Huguenin, who provided much of the initial encouragement, freedom, and financial support that allowed me to begin this research; to Kevin Burke and David Black, who have generously continued that support while I've been at LPI; to my friend Jonathan Eberhart, who helped a very frightened graduate student make it through his first professional talk; and, most of all, to my wife Julie and daughter Miranda, without whose love and support I would have given this up long ago. This research was supported by the Lunar and Planetary Institute, which is operated by the University Space Research Association under contract No. NASW-4574 with the National Aeronautics and Space Administration, and by a grant from NASA's Planetary Geology and Geophysics Program. LPI Contribution No. 807.

NOTATION

a	radius of basal melting/recharge area, m.
C_{ps}	heat capacity of water, 2092 J kg^{-1} K^{-1}.
C_{pw}	heat capacity of steam, 4186 J kg^{-1} K^{-1}.
ρC_p	volumetric heat capacity of impact melt, 4.2×10^6 J m^{-3} K^{-1}.
D_{AB}	bulk molecular diffusion coefficient of H_2O in CO_2, cm^2 s^{-1}.
D_c	transition diameter between simple and complex crater morphology, ~6 km on Mars.
D_{eff}	effective diffusion coefficient of H_2O in CO_2, cm^2 s^{-1}.
D_f	final crater diameter, m.
D_{KA}	Knudsen diffusion coefficient of H_2O, cm^2 s^{-1}.
D_{tc}	diameter of transient crater cavity, m.
E_k	projectile kinetic energy, J.
E_s	seismic energy, J.
g	mean Martian acceleration of gravity, 3.71 m s^{-2}.
h	height above local datum, m.
h_i	initial height of water table above local datum, m.
h_m	central height of groundwater mound above local datum, m.
$\bar{h}$	$= .5\ (h + h_i)$, weighted mean depth of saturation, m.
H	polar deposit thickness required for basal melting, m.
k	crustal permeability, m^2.
k_f	frozen permeability, m^2.
K_{Mars}	porosity decay constant, 2820 m.
L_f	latent heat of fusion of H_2O, 3.35×10^5 J kg^{-1}.
L_v	latent heat of vaporization of H_2O, 2.3×10^6 J kg^{-1}.
Δm_{steam}	steam mass transported by hydrothermal convection, kg m^{-2}.
M	Gutenberg-Richter magnitude of seismic event.
M_A	molecular weight of H_2O, 0.018 kg mol^{-1}.
P	total gas pressure, dynes cm^{-2}.
P_{H_2O}	vapor pressure of H_2O, dynes cm^{-2}.
q_l	thermally induced liquid flux, m s^{-1} (per unit area).
q_v	thermally induced vapor flux, m s^{-1} (per unit area).
Q_d	$= 2\pi a h\ v$, radial discharge through aquifer, m^3 s^{-1}.
Q_f	frictional heat due to glacial sliding, W m^{-2}.
Q_g	geothermal heat flux, W m^{-2}.
Q_r	$= \pi\ a^2\ w$, aquifer recharge volume, m^3 s^{-1}.
ΔQ_{melt}	heat content of impact melt, J m^{-2}.
r	radius, m.
R	universal gas constant, 8.314 J mol^{-1} K^{-1}.
R_v	water vapor gas constant, 461.9 J kg^{-1} K^{-1}.
S	heat generation per unit volume of planet, W m^{-3}.
t	time, s.
T	temperature, K.
T_i	initial impact melt temperature, 1473 K.
T_f	final impact melt temperature, K.
T_{mp}	melting point temperature, K.
T_{ms}	mean annual surface temperature, K.
ΔT_{steam}	temperature interval over which steam is heated, K.
ΔT_{water}	temperature interval over which water is heated, K.
u_o	$= a^2 v\varepsilon / 4kg\ \bar{h}\ t$.
U	projectile impact velocity, m s^{-1}.
v	aquifer specific discharge, m s^{-1}.
V_b	basal sliding velocity, m s^{-1}.
V_m	impact melt volume, km^3.
V_{tc}	maximum volume of transient crater cavity, m^3.
w	aquifer recharge rate, m s^{-1}.
$W(u_o)$	well function for a nonleaky aquifer.
z	depth, m.
Δz	thickness, m.
Z	$= h^2 - h_i^2$, m^2.
α	$(= \kappa/\rho c)$, thermal diffusivity, m^2 s^{-1}.
β	empirical dimensionless factor [*Cary*, 1966], 1.83 ± 0.79.
ε	effective porosity.
κ	thermal conductivity, W [illegible] K^{-1}.
$\Phi(z)$	crustal porosity at a depth [illegible] 1.00 = 100%.
λ	collisional mean free path of an H_2O molecule in the Martian atmosphere, ~10 μm.
ν	kinematic viscosity, m^2 s^{-1}.
ρ	density, kg m^{-3}.
τ_b	basal shear stress, Pa.
ψ	soil water potential, Pa.

REFERENCES

Allen, C. C., Volcano-ice interactions on Mars, *J. Geophys. Res.*, *84*, 8048–8059, 1979*a*.

Allen, C. C., Areal distribution of Martian rampart craters, *Icarus*, *39*, 111–123, 1979*b*.

Ambroggi, R. P., Water under the Sahara, *Sci. Am.*, *214*, 21–29, 1966.

Anderson, D. M., and A. R. Tice, The unfrozen interfacial phase in frozen soil water systems, in *Ecological Studies. Analysis and Synthesis*, vol. 4, edited by A. Hadas, D. Swartzendruber, P. E. Rijtema, M. Fuchs, and B. Yaron, pp. 107–124, Springer-Verlag, New York, 1973.

Anderson, D. M., E. S. Gaffney, and P. F. Low, Frost phenomena on Mars, *Science*, *155*, 314–322, 1967.

Anderson, M. P., Field studies in groundwater hydrology—A new era, *Rev. Geophys.*, *25*, 141–147, 1987.

Arvidson, R. E., K. A. Goettel, and C. M. Hohenberg, A post-Viking view of Martian geologic evolution, *Rev. Geophys*, *18*, 565–603, 1980.

Arvidson, R. E., J. L. Gooding, and H. J. Moore, The Martian surface as imaged, sampled, and analyzed by the Viking Landers, *Rev. Geophys.*, *27*, 39–69, 1989.

Athy, L. F., Density, porosity, and compaction of sedimentary rocks, *Bull. Am. Assoc. Petrol. Geol.*, *14*, 1–24, 1930.

Baker, V. R., *The Channels of Mars*, 198 pp., University of Texas Press, Austin, 1982.

Baker, V. R., and J. B. Partridge, Small Martian valleys: Pristine and degraded morphology, *J. Geophys. Res.*, *91*, 3561–3572, 1986.

Baker, V. R., R. G. Strom, V. C. Gulick, J. S. Kargel, G. Komatsu, and V. S. Kale, Ancient oceans, ice sheets and the hydrologic cycle on Mars, *Nature*, *352*, 589–594, 1991.

Baker, V. R., M. H. Carr, V. C. Gulick, C. R. Williams, and M. S. Marley, Channels and valley networks, in *Mars*, edited by H. H. Kieffer, B. M. Jakosky, C. W. Snyder, and M. S. Mathews, pp. 493–522, University of Arizona Press, Tucson, 1992.

Banin, A., and D. M. Anderson, Effects of salt concentration changes during freezing on the unfrozen water content of porous materials, *Water Resour. Res.*, *10*, 124–128, 1974.

Barlow, N. G., Constraints on early events in Martian history as derived from the cratering record, *J. Geophys. Res.*, *95*, 14,191–14,201, 1990.

Barlow, N. G., and T. L. Bradley, Martian impact craters: Correlations of ejecta and interior morphologies with diameter, latitude, and terrain, *Icarus*, *87*, 156–179, 1990.

Bath, M., Earthquake energy and magnitude, *Phys. Chem. Earth*, *7*, 115, 1966.

Bentley, H. W., F. M. Phillips, S. N. Davis, M. A. Habermehl, P. L. Airey, G. E. Calf, D. Elmore, H. E. Grove, and T. Torgersen, Chlorine 36 dating of very old groundwater, 1, The Great Artesian Basin, Australia, *Water Resour. Res.*, *22*, 1991–2001, 1986.

Bills, B. G., The rigid body obliquity history of Mars, *J. Geophys. Res.*, *95*, 14,137–14,153, 1990.

Binder, A. B., and M. A. Lange, On the thermal history, thermal state, and related tectonism of a moon of fission origin, *J. Geophys. Res.*, *85*, 3194–3208, 1980.

Birch, F., Flow of heat in the Front Range, Colorado, *Geol. Soc. Am. Bull.*, *61*, 567–630, 1950.

Birch, F., The velocity of compressional waves in rocks to 10 kilobars, Part 2, *J. Geophys. Res.*, *66*, 2199–2224, 1961.

Blasius, K. R., and J. A. Cutts, Global patterns of crater ejecta morphology on Mars, *Bull. Am. Astron. Soc.*, *13*, 709, 1981.

Blasius, K. R., J. A. Cutts, B. H. Lewis, and A. V. Vetrone, Three simple classes of Martian crater ejecta, I, Global relationships of class abundance to latitude and terrain, *NASA Tech. Memo., TM 84211*, 93–95, 1981.

Booth, M. C., and H. H. Kieffer, Carbonate formation in Marslike environments, *J. Geophys. Res.*, *83*, 1809–1815, 1978.

Bouyoucos, G. J., Effect of water vapor and capillary moisture in soils, *J. Agric. Res.*, *5*, 141–172, 1915.

Brace, W. F., Resitivity of saturated crustal rocks to 40 km based on laboratory measurements, in *The Structure and Physical Properties of the Earth's Crust*, *Geophys. Monogr. Ser.*, vol. 13, *edited* by J. G. Heacock, AGU, pp. 243–255, Washington, D.C., 1971.

Brace W. F., Permeability of crystalline and argillaceous rocks, *Int. J. Rock Mech. Min. Sci. Geomech. Abstr.*, *17*, 241–251, 1980.

Brace, W. F., Permeability of crystalline rocks: New in situ measurements, *J. Geophys. Res.*, *89*, 4327–4330, 1984.

Brace, W. F., and D. L. Kohlstedt, Limits on lithospheric stress imposed by laboratory experiments, *J. Geophys. Res.*, *85*, 6248–6252, 1980.

Brakenridge, G. R., The origin of fluvial valleys and early geologic history, Aeolis Quadrangle, Mars, *J. Geophys. Res.*, *95*, 17,289–17,308, 1990.

Brakenridge, G. R., H. E. Newsom, and V. R. Baker, Ancient hot springs on Mars: Origins and paleoenvironmental significance of small Martian valleys, *Geology*, *13*, 859–862, 1985.

Brass, G. W., Stability of brines on Mars, *Icarus*, *42*, 20–28, 1980.

Bullard, E. C., Heat flow in South Africa, *R. Soc. London Proc. A*, *173*, 474–502, 1939.

Burdon, D. J., Flow of fossil groundwater, *Q. J. Eng. Geol.*, *10*, 97–124, 1977.

Byerlee, J. D., and W. F. Brace, Stick-slip, stable sliding, and earthquakes: Effect of rock type, pressure, strain rate, and stiffness, *J. Geophys. Res.*, *73*, 6031–6037, 1968.

Carr, M. H., Formation of Martian flood features by release of water from confined aquifers, *J. Geophys. Res.*, *84*, 2995–3007, 1979.

Carr, M. H., *The Surface of Mars*, 232 pp., Yale University Press, New Haven, Conn., 1981.

Carr, M. H., The stability of streams and lakes on Mars, *Icarus*, *56*, 476–495, 1983.

Carr, M. H., Formation of Martian valley networks as a consequence of large impacts, *Lunar Planet. Sci. Conf.*, *XV*, 131–132, 1984.

Carr, M. H., Mars: A water-rich planet?, *Icarus*, *68*, 187–216, 1986.

Carr, M. H., Water on Mars, *Nature*, *326*, 30–35, 1987.

Carr, M. H., The ancient ocean hypothesis: A critique, *Bull. Am. Astron. Soc.*, *23*, 1206, 1991.

Carr, M. H., and G. G. Schaber, Martian permafrost features, *J. Geophys. Res.*, *82*, 4039–4055, 1977.

Carr, M. H., L. S. Crumpler, J. A. Cutts, R. Greeley, J. E. Guest, and H. Masursky, Martian impact craters and the emplacement of ejecta by surface flow, *J. Geophys. Res.*, *82*, 4055–4065, 1977.

Carr, M. H., W. A. Baum, K. R. Blasius, G. A. Briggs, J. A. Cutts, T. C. Duxbury, R. Greeley, J. Guest, H. Masursky, B. A. Smith, L. A. Soderblom, J. Veverka, and J. B. Wellman, Viking Orbiter views of Mars, *NASA Spec. Publ*, *SP-441*, Washington, D.C., 182 pp., 1980.

Cary, J. W., Onsager's relation and the non-isothermal diffusion of water vapor, *J. Phys. Chem*, *67*, 126–129, 1963.

Cary, J. W., Soil moisture transport due to thermal gradients: Practical aspects, *Soil Sci. Soc. Am. Proc.*, *30*, 428–433, 1966.

Castany, G., Hydrogeology of deep aquifers: The hydrogeologic basin as the basis of groundwater management, *Episodes*,. *3*, 18–22, 1981.

Cathles, L. M., Scales and effects of fluid flow in the upper crust, *Science*, *248*, 323–329, 1990.

Chylek, P., and G. W. Grams, Scattering by nonspherical particles and the optical properties of Martian dust, *Icarus*, *36*, 198–203, 1978.

Clark, B. C., Implications of abundant hygroscopic minerals in the Martian regolith, *Icarus*, *34*, 645–665, 1978.

Clark, B. C., and D. C. Van Hart, The salts of Mars, *Icarus*, *45*, 370–378, 1981.

Clark, B. C., A. K. Baird, H. J. Rose, P. Toulmin, K. Keil, A. J. Castro, W. C. Kelliher, C. D. Rowe, and P. H. Evans, Inorganic analysis of Martian surface samples at the Viking landing sites, *Science*, *194*, 1283–1288, 1976.

Clark, S. P., Thermal conductivity, in *Handbook of Physical Constants*, Geological Society of America, New Haven, Conn., 1966.

Clifford, S. M., Mars: Ground ice replenishment from a subpermafrost groundwater system, in: *Proc. 3rd Colloq. Planet. Water*, pp. 68–75, State University of New York at Buffalo, 1980*a*.

Clifford, S. M., Mars: Polar cap basal melting as a recharge mechanism for a global groundwater system, *Lunar Planet. Sci. Conf.*, *XI*, 165–167, 1980*b*.

Clifford, S. M., A pore volume estimate of the Martian megaregolith based on a lunar analog, Papers presented to the Third Int. Colloq. on Mars, *LPI Contrib. 441*, pp. 46–48, Lunar and Planetary Inst., Houston, Tex., 1981*a*.

Clifford, S. M., A model for the climatic behavior of water on Mars, Papers presented to the Third Int. Colloq. on Mars, *LPI Contrib. 441*, pp. 44–45, Lunar and Planetary Inst., Houston, Tex., 1981*b*.

Clifford, S. M., Mechanisms for the vertical transport of H_2O in the Martian regolith, Papers presented to the Conf. on Planet. Volatiles, *LPI Contrib. 488*, pp. 23–24, Lunar and Planetary Inst., Houston, Tex., 1982.

Clifford, S. M., Ground ice in the equatorial region of Mars: A fossil remnant of an ancient climate or a replenished steady-state inventory?, *Proc. Fourth Int. Conf. on Permafrost*, pp. 163–168, National Academy Press, Washington, D.C., 1983.

Clifford, S. M., *A Model for the Climatic Behavior of Water on Mars*, Ph.D. thesis, University of Massachusetts, Amherst, 1984.

Clifford, S. M., Crustal pore volume, cryospheric depth, and the global occurrence of groundwater, *Symposium on Mars: Evolution of its Climate and Atmosphere*, LPI Tech Rept. 87-01, *edited* by V. Baker, M. Carr, F. Fanale, R. Greeley, R. Haberle, C. Leovy, and T. Maxwell, pp. 32–34, Lunar and Planetary Inst., Houston, Tex., 1987*a*.

Clifford, S. M., Polar basal melting on Mars, *J. Geophys. Res.*, *92*, 9135–9152, 1987*b*.

Clifford, S. M., and F. P. Fanale, The thermal conductivity of the Martian crust, *Lunar Planet. Sci. Conf.*, *XVI*, 144–145, 1985.

Clifford, S. M., and D. Hillel, The stability of ground ice in the equatorial region of Mars, *J. Geophys. Res.*, *88*, 2456–2474, 1983.

Clifford, S. M., and D. Hillel, Knudsen diffusion: The effect of small pore size and low gas pressure on gaseous transport in soil, *Soil Sci.*, *141*, 289–297, 1986.

Clifford, S. M., and L. A. Johansen, Splosh craters: Evidence for the replenishment of ground ice in the equatorial region of Mars, *Lunar Planet. Sci. Conf., XIII*, 121–122, 1982.

Clow, G. D., Generation of liquid water on Mars through the melting of a dusty snowpack, *Icarus*, *72*, 95–127, 1987.

Cooper, H. H., J. D. Bredehoeft, I. S. Papadopulos, and R. R. Bennet, The response of well-aquifer systems to seismic waves, in *The Great Alaska Earthquake of 1964*, pp. 122–132, National Academy of Sciences, Washington, D.C., 1968.

Costard, F. M., Asymmetric distribution of volatiles on Mars, *Lunar Planet. Sci. Conf., XX*, 187–188, 1989.

Crater Analysis Techniques Working Group, Standard techniques for presentation and analysis of crater size-frequency data, *NASA Tech. Memo., TM 79730*, 1978.

Crescenti, G. H., Analysis of permafrost depths on Mars, *NASA Tech. Memo., TM 86247*, 115–132, 1984.

Croft, S. K., The scaling of complex craters, *J. Geophys. Res.*, *90*, C828–C842, 1985.

Cutts, J. A., Nature and origin of layered deposits of the Martian polar regions, *J. Geophys. Res.*, *78*, 4231, 1973.

Cutts, J. A. and B. H. Lewis, Models of climate cycles recorded in Martian polar layered deposits, *Icarus*, *50*, 216–244, 1982.

Cutts, J. A., G. A. Briggs, M. H. Carr, R. Greeley and H. Masursky, North polar region of Mars: Imaging results from Viking 2, *Science*, *194*, 1329–1337, 1976.

Cutts, J. A., K. R. Blasius, and W. J. Roberts, Evolution of Martian polar landscapes: Interplay of long-term variations in perennial ice cover and dust storm intensity, *J. Geophys. Res.*, *84*, 2975–2993, 1979.

Davies, G. F., and R. E. Arvidson, Martian thermal history, core segregation, and tectonics, *Icarus*, *45*, 339–346, 1981.

Davis, S. N., Porosity and permeability of natural materials, in *Flow Through Porous Media, edited* by R. J. M. DeWiest, pp. 53–89, Academic, San Diego, Calif. 1969.

Davis, S. N., and R. J. M. De Wiest, *Hydrogeology*, 463 pp., John Wiley, New York, 1966.

de Marsily, G., E. Ledoux, A. Barbreau, and J. Margat, Nuclear waste disposal: Can the geologist guarantee isolation?, *Science*, *197*, 519–527, 1977.

Dence, M. R., R. A. F. Grieve, and P. B. Robertson, Terrestrial impact structures: Principal charateristics and energy considerations, in *Impact and explosion Cratering*, edited by D. J. Roddy, R. O. Pepin, and R. B. Merril, pp. 247–276, Pergamon, New York, 1977.

Dvorak, J. J. and R. J. Phillips, Lunar Bouguer gravity anomalies: Imbrian age craters, *Proc. Lunar Planet. Sci. Conf., 9th*, 3651–3668, 1978.

Dzurisin, D., and K. R. Blasius, Topography of the polar layered deposits of Mars, *J. Geophys. Res.*, *80*, 3286–3306, 1975.

Eakin, T. E., A regional interbasin groundwater system in the White River area, southeastern Nevada, *Water Resour. Res.*, *2*, 251–271, 1966.

Edlefsen, N. E., and A. B. C. Anderson, Thermodynamics of soil moisture, *Hilgardia*, 298 pp., 1943.

Edmunds, W. M., and E. P. Wright, Groundwater recharge and paleoclimate in the Sirte and Kufra Basins, Libya, *J. Hydrol.*, *40*, 215–241, 1979.

Ehrenbard, R. L., P. Hoekstra, and G. Rozenberg, Transient electromagnetic soundings for permafrost mapping, in *Proceedings of the Fourth International Conference on Permafrost*, pp. 272–277, National Academy Press, Washington, D.C., 1983.

Fanale, F. P., Martian volatiles: Their degassing history and geochemical fate, *Icarus*, *28*, 179–202, 1976.

Fanale, F. P., J. R. Salvail, W. B. Banerdt, and R. S. Saunders, Mars: The regolith-atmosphere-cap system and climate change, *Icarus*, *50*, 381–407, 1982.

Fanale, F. P., J. R. Salvail, A. P. Zent, and S. E. Postawko, Global distribution and migration of subsurface ice on Mars, *Icarus*, *67*, 1–18, 1986.

Farmer, C. B., and P. E. Doms, Global and seasonal variation of water vapor on Mars and the implications for permafrost, *J. Geophys. Res.*, *84*, 2881–2888, 1979.

Fetter, C. W. Jr., *Applied Hydrology*, 488 pp., Charles E. Merrill, Columbus, Ohio, 1980.

Flasar, M. F., and R. M. Goody, Diurnal behaviour of water on Mars, *Planet. Space Sci.*, *24*, 161–181, 1976.

Freeze, R. A. and J. A. Cherry, *Groundwater*, 604 pp., Prentice-Hall, Englewood Cliffs, New Jersey, 1979.

Freeze, R. A., and P. A. Witherspoon, Theoretical analysis of regional groundwater flow, 2, Effect of water-table configuration and subsurface permeability variation, *Water Resour. Res.*, *3*, 623–634, 1967.

Gabert, G. M., Groundwater-level fluctuations in Alberta, Canada, in *The Great Alaska Earthquake of 1964*, pp. 190–195, National Academy of Sciences, Washington, D.C., 1968.

Gault, D. E., J. E. Guest, J. B. Murray, D. Dzurisin, and M. C. Malin, Some comparisons of impact craters on Mercury and the Moon, *J. Geophys. Res.*, *80*, 2444–2460, 1975.

Gold, T., B. T. O'Leary, and M. Campbell, Some physical properties of Apollo 12 lunar samples, *Proc. Lunar Sci. Conf., 2nd*, *3*, 2173–2181, 1971.

Gooding, J. L., Chemical weathering on Mars: Thermodynamic stability of primary minerals (and their alteration products) from mafic igneous rocks, *Icarus*, *33*, 483–513, 1978.

Gough, D. I., Electromagnetic exploration for fluids in the Earth's crust, *Earth Sci. Rev.*, *32*, 3–18, 1992.

Grantz, A., G. Plafker, and R. Kachadoorian, Alaska's Good Friday earthquake, March 27, 1964: A preliminary geologic evaluation, *U. S. Geol. Surv. Circ.*, *491*, 35 pp., 1964.

Greeley, R., Release of juvenile water on Mars: Estimated amounts and timing associated with volcanism, *Science*, *236*, 1653–1654, 1987.

Greeley, R., and B. Schneid, Magma generation on Mars: Amounts, rates, and comparisons with Earth, Moon, and Venus, *Science*, *254*, 996–998, 1991.

Greeley, R., and P. D. Spudis, Volcanism on Mars, *Rev. Geophys.*, *19*, 13–41, 1981.

Grieve, R. A. F., and M. J. Cintala, An analysis of diferrential impact melt-crater scaling and implications for the terrestrial impact record, *Meteoritics*, *27*, 526–538, 1992.

Grieve, R. A. F., and J. B. Garvin, A geometric model for excavation and modification of terrestrial simple impact craters, *J. Geophys. Res.*, *89*, 11,561–11,572, 1984.

Gulick, V. C., Magmatic intrusions and hydrothermal systems on Mars, in *Workshop on the Martian Surface and Atmosphere Through Time*, pp. 50–51, Lunar and Planetary Institute, Houston, Tex., 1991.

Gulick, V. C., and V. R. Baker, Origin and evolution of valleys on Martian volcanoes, *J. Geophys. Res.*, *95*, 14,325–14,345, 1990.

Gurnis, M., Martian cratering revisited: Implications for early geologic evolution, *Icarus*, *48*, 62–75, 1981.

Habermehl, M. A., The Great Artesian Basin, Australia, *BMR J. Aust. Geol. Geophys.*, *5*, 9–38, 1980.

Haimson, B. C., and T. W. Doe, State of stress, permeability, and fractures in the Precambrian granite of northern Illinois, *J. Geophys. Res.*, *88*, 7355–7371, 1983.

Hantush, M. S., Hydraulics of wells, in *Advances in Hydroscience*, edited by V. T. Chow, Academic, San Diego, Calif., 1964.

Hantush, M. S., Growth and decay of groundwater-mounds in response to uniform percolation, *Water Resour. Res.*, *3*, 227–234, 1967.

Harrill, J. R., Great Basin aquifer systems, Nevada-Utah, An overview, in *Water Today and Tomorrow*,pp. 590–597, American Society of Civil Engineers, New York, 1984.

Hartmann, W. K., Ancient lunar mega-regolith and subsurface structure, *Icarus*, *18*, 634–636, 1973.

Hartmann, W. K., Relative crater production rates on planets, *Icarus*, *31*, 260–276, 1977.

Hartmann, W. K., Dropping stones in magma oceans: Effects of early lunar cratering, in *Proc. of the Conf. on the Lunar Highland Crust*, edited by J. J. Ppike and R. B. Merrill, pp. 155–171, Pergamon, New York, 1980.

Hesse, K. H., A. Hissene, O. Kheir, E. Schnäcker, M. Schneider, and U. Thorweihe, Hydrological investigations of the Nubian Aquifer system, Eastern Sahara, *Berlin. Geowiss. Abh., Reihe A*, *75*, 397–464, 1987.

Higashi, A., On the thermal conductivity of soil, with special reference to that of frozen soil, *Eos Trans. AGU*, *34*, 737–748, 1953.

Hobbs, P. V., *Ice Physics*, Oxford University Press, New York, 1974.

Hodges, C. A., and H. J. Moore, The subglacial birth of Olympus Mons and its aureoles, *J. Geophys. Res.*, *84*, 8061–8074, 1979.

Horai, K., and S. Baldridge, Thermal conductivity of nineteen igneous rocks, I, Application of the needle probe method to the measurement of the thermal conductivity of rock, *Phys. Earth Planet. Inter.*, *5*, 151–156, 1972.

Horai, K., and C. Simmons, Thermal conductivity of rock-forming minerals, *Earth Planet. Sci. Lett.*, *6*, 359–368, 1969.

Horner, V. M., and R. Greeley, Pedestal craters on Ganymede, *Icarus*, *51*, 549–562, 1982.

Howard, A. D., Origin of the stepped topography of the Martian poles, *Icarus*, *84*, 581–599, 1978.

Howard, A. D., Etched plains and braided ridges of the south polar region of Mars: Features produced by basal melting of ground ice?, *NASA Tech. Memo., TM 84211*, 286–288, 1981.

Howard, A. D., J. A. Cutts and K. L. Blasius, Stratigraphic relationships within Martian polar cap deposits, *Icarus*, *50*, 161–215, 1982.

Hubert, M. K., and W. W. Rubey, Role of fluid pressure in mechanics of overthrust faulting, *Bull. Geol. Soc. Am.*, *70*, 115, 1959.

Huguenin, R. L., Mars: Chemical weathering as a massive volatile sink, *Icarus*, *28*, 203–212, 1976.

Hunt, C. B., and T. W. Robinson, Possible interbasin circulation of ground water in the southern part of the Great Basin, *U. S. Geol. Surv Prof. Pap*, *400-B*, 273, 1960.

Hyndman, R. D., and M. J. Drury, The physical properties of oceanic basement rocks from deep drilling on the mid-Atlantic ridge, *J Geophys. Res.*, *81*, 4042–4052, 1976.

Hyndman, R. D., and D. W. Hyndman, Water saturation and high electrical conductivity in the lower continental crust, *Earth Planet. Sci. Lett.*, *4*, 427–432, 1968.

Issar, A., Fossil water under the Sinai-Negev peninsula, *Sci. Am.*, *253*, 104–110, 1985.

Jackson, R. D., D. A. Rose, and H. L. Penman, Circulation of water in soil under a temperature gradient, *Nature*, *205*, 314–316, 1965.

Jakosky, B. M., The seasonal cycle of water on Mars, *Space Sci. Rev.*, *41*, 131–200, 1985.

Jakosky, B. M., Mars atmospheric D/H: Consistent with polar volatile theory?, *J. Geophys. Res.*, *95*, 1475–1480, 1990.

Jakosky, B. M. and M. H. Carr, Possible precipitation of ice at low latitudes of Mars during periods of high obliquity, *Nature*, *315*, 559–561, 1985.

Jakosky, B. M., and P. R. Christensen, Global duricrust on Mars: Analysis of remote sensing data, *J. Geophys. Res.*, *91*, 3547–3560, 1986.

Johansen, L. A., Martian splosh cratering and its relation to water, in *Proc. Second Colloq. on Planet. Water and Polar Processes*, pp. 109–110, U.S. Army Cold Regions Research and Engineering Laboratory, Hanover, 1978.

Jury, W. A. and J. Letey, Jr., Water vapor movement in soil: Reconciliation of theory and experiment, *Soil Sci. Soc. Am. J.*, *43*, 823–827, 1979.

Kahn, R., The evolution of CO_2 on Mars, *Icarus*, *62*, 175–190, 1985.

Kargel, J. S. and R. G. Strom, Ancient glaciation on Mars, *Geology*, *20*, 3–7, 1992.

Kasting, J. F., Climatic effects of enhanced carbon dioxide levels in Mars' early atmosphere, MECA Symposium on Mars: Evolution of Its Climate and Atmosphere, *LPI Tech. Rep. 87-01*, pp. 64–66, Lunar and Planet. Inst., Houston, Tex., 1987.

Kasting, J. F., CO_2 condensation and the climate of early Mars, *Icarus*, *94*, 1–13, 1991.

Keihm, S. J., and M. G. Langseth, Lunar thermal regime to 300 km, *Proc. Lunar Sci. Conf.*, *8th*, 499–514, 1977.

Kerrich, R., T. E. La Tour, and L. Willmore, Fluid participation in deep fault zones: Evidence from geological, geochemical, and $^{18}O/^{16}O$ relations, *J. Geophys. Res.*, *89*, 4331–4343, 1984.

Kersten, M. S., Thermal properties of frozen ground, in: *Proc. Int. Conf. Permafrost*, pp. 301–305, National Academy of Sciences, Washington, D. C., 1963.

Kozlovsky, Y. A., Kola super-deep: Interim results and prospects, *Episodes*, 9–11, 1982.

Kozlovsky, Y. A., The world's deepest well, *Sci. Am.*, *251*, 98–104, 1984.

Kuzmin, R. O., *Cryolithosphere of Mars*, pp. 1–140, Izdatel'stvo Nauka, Moscow, 1983.

Kuzmin, R. O., N. N. Bobina, and E. V. Zabalueva, and V. P. Shashkina, Structure inhomogeneities of the Martian cryolithosphere, *Solar Syst. Res.*, *XXII*, 195–212, 1988.

Lachenbruch, A. H., Some estimates of the thermal effects of a heated pipeline in permafrost, *Geol. Surv. Circ. 632*, 1970.

Lachenbruch, A. H., J. H. Sass, B. V. Marshall, and T. H. Moses, Jr., Permafrost, heat flow, and the geothermal regime at Prudhoe Bay, Alaska, *J. Geophys. Res.*, *87*, 9301–9316, 1982.

Laskar, J., and P. Robutel, The chaotic obliquity of the planets, *Nature*, *361*, 608–612, 1993.

LeGrand, H., Evalutaion techniques of fractured-rock hydrology, *J. Hydrol.*, *43*, 333–346, 1979.

LeGrand, H. E., and V. T. Stringfield, Karst hydrology—A review, *J. Hydrol.*, 20, 97–120, 1973.

Leighton, R. B., and B. C. Murray, Behavior of CO_2 and other volatiles on Mars, *Science*, *153*, 136–144, 1966.

Lucchitta, B. K., Mars and Earth: Comparison of cold-climate features, *Icarus*, *45*, 264–303, 1981.

Lucchitta, B. K., Geomorphic evidence for ground ice on Mars, in *Ices in the Solar System*, edited by J. Klinger et al., pp. 583–604, Reidel, Hingham, Mass., 1985.

MacKinnon, D. J., and K. L. Tanaka, The impacted Martian crust: Structure, hydrology, and some geologic implications, *J. Geophys Res.*, *94*, 17,359–17,370, 1989.

Mair, J. A., and A. G. Green, High resolution seismic reflection profiles reveal fracture zones within a homogeneous, granite batholith, *Nature*, *294*, 439–442, 1981.

Malin, M. C., Salt weathering on Mars, *J. Geophys Res*, *79*, 3888–3894, 1974.

Margat, J., and K. F. Saad, Deep-lying aquifers: Water mines under the desert?, *Nature Resour.*, *20*, 7–13, 1984.

Marino, M. A., Artificial groundwater recharge: I. Circular recharging area, *J. Hydrol*, *25*, 201–208, 1975.

Masursky, H., J. M. Boyce, A. L. Dial, G. G. Schaber, and M. E. Strobell, Classification and time of formation of the Martian channels based on Viking data, *J Geophys Res.*, *82*, 4016–4038, 1977.

Maxwell, J. C., Influence of depth, temperature, and geologic age on porosity of quartzose sandstones, *Bull. Am. Assoc. Pet. Geol.*, *48*, 697–709, 1964.

McCaig, A. M., Deep fluid circulation in fault zones, *Geology*, *16*, 867–870, 1988.

McGill, G. E., Buried topography of Utopia, Mars: Persistence of a giant impact depression, *J Geophys Res*, *94*, 2753–2759, 1989.

Mellon, M. T., and B. M. Jakosky, Geographic variations in the thermal and diffusive stability of ground ice on Mars, *J. Geophys. Res*, *98*, 3345–3364, 1993.

Melosh, H. J., Cratering mechanics—Observational, experimental, and theoretical, *Annu. Rev. Earth Planet. Sci.*, *8*, 65–93, 1980.

Melosh, H. J., *Impact Cratering: A Geologic Process*, 245 pp., Oxford University Press, New York, 1989.

Mifflin M. D., and J. W. Hess, Regional carbonate flow systems in Nevada, *J. Hydrol.*, *43*, 217–237, 1979.

Miller, R. D., Freezing phenomena in soils, in *Applications of Soil Physics*, edited by D. Hillel, Academic, San Diego, Calif., 1980.

Miller, R. D., J. P. G. Loch, and E. Bresler, Transport of water and heat in a frozen permeameter, *Soil Sci. Soc. Am. Proc.*, *39*, 1029–1036, 1975.

Moore, J. F., D. R. Janke, G. D. Clow, W. L. Davis, R. M. Haberle, C. P. McKay, and C. R. Stoker, A regional example of a hydrologic cycle on Mars, *Bull Am. Astron. Soc.*, *23*, 1173, 1991.

Morris, E. C., Recent (?) surface alterations from subsurface sources in the Olympus Mons area, *NASA Tech. Memo.*, *TM 81776*, 162–163, 1980.

Mouginis-Mark, P. J., Martian fluidized crater morphology: Variations with crater size, latitude, altitude, and target material, *J. Geophys. Res.*, *84*, 8011–8022, 1979.

Mouginis-Mark, P. J., Water or ice in the Martian regolith?: Clues from rampart craters seen at very high resolution, *Icarus*, *71*, 268–286, 1987.

Mouginis-Mark, P. J., Recent water release in the Tharsis region of Mars, *Icarus*, *84*, 362–373, 1990.

Murray, B. C., L. A. Soderblom, J. A. Cutts, R. P. Sharp, D. J. Milton, and R. B. Leighton, Geological framework of the south polar region of Mars, *Icarus*, *17*, 328–345, 1972.

Murray, B. C., W. R. Ward and S. C. Yeung, Periodic insolation variations on Mars, *Science*, *180*, 638–640, 1973.

Mutch, T. A., R. E. Arvidson, J. W. Head, K. L. Jones, and R. S. Saunders, *The Geology of Mars*, 400 pp., Princeton University Press, Princeton, N.J., 1976.

Nekut, A., J. E. P. Connerney, and W. A. Kuches, Deep crustal electrical conductivity: Evidence for water in the lower crust, *Geophys. Res. Lett.*, *4*, 239–242, 1977.

Neukum, G., and D. U. Wise, Mars: A standard crater curve and possible new time scale, *Science*, *194*, 1381–1387, 1976.

Newsom, H. E., Hydrothermal alteration of impact melt sheets with implications for Mars, *Icarus*, *44*, 207–216, 1980.

Nye, J. F., Water flow in glaciers: Jökulhlaups, tunnels and veins, *J. Glaciol.*, *17*, 181–207, 1976.

O'Keefe, J. D., and T. J. Ahrens, Shock effects from a large impact on the Moon, *Proc. Lunar Sci. Conf.*, *6th*, 2831–2844, 1975.

O'Keefe, J. D., and T. J. Ahrens, Impact cratering: The effect of crustal strength and planetary gravity, *Rev. Geophys.*, *19*, 1–12, 1981.

Onorato, P. I. K., D. R. Uhlmann, and C. H. Simonds, The thermal history of the Manicougan impact melt sheet, Quebec, *J. Geophys. Res.*, *83*, 2789–2798, 1978.

Owen, R., J. P. Maillard, C. deBergh, and B. L. Lutz, Deuterium on Mars: The abundance of HDO and the value of D/H, *Science*, *240*, 1767–1770, 1988.

Paige, D. A., The thermal stability of near-surface ground ice on Mars, *Nature*, *356*, 43–45, 1992.

Pang, K., J. M. Ajello, C. W. Hord, and W. G. Egan, Complex refractive index of Martian dust: Mariner 9 ultraviolet observations, *Icarus*, *27*, 55–67, 1976.

Parker, T. J., R. S. Saunders, and D. M. Schneeberger, Transitional morphology in West Deuteronilus Mensae, Mars: Implication for modification of the lowland/upland boundary, *Icarus*, *82*, 111–145, 1989.

Paterson, W. S. B., *The Physics of Glaciers*, 380 pp., Pergamon, New York, 1981.

Penner, E., Thermal conductivity of frozen soils, *Can. J. Earth Sci.*, *7*, 982–987, 1970.

Pepin, R. O., Volatile inventory of the terrestrial planets, *Rev. Geophys.*, *25*, 293–296, 1987.

Perez-de-Tejada, H., Plasma flow in the Mars magnetosphere, *J. Geophys. Res.*, *92*, 4713–4718, 1987.

Pettijohn, F. J., *Sedimentary Rocks*, 3rd ed., Harper and Row, New York, 1975.

Philip, J. R., and D. A. de Vries, Moisture movement in porous materials under temperature gradients, *Eos Trans. AGU*, *38*, 222–228, 1957.

Phillips, R. J., R. E. Arvidson, J. M. Boyce, D. B. Campbell, J. E. Guest, G. G. Schaber, and L. A. Soderblom, Impact craters on Venus: Initial analysis from Magellan, *Science*, *252*, 288–297, 1991.

Pieri, D., *Geomorphology of Martian Valleys*, Ph.D. thesis, Cornell University, Ithaca, New York, 1979.

Pieri, D., Martian valley morphology, distribution, age and origin, *Science*, *210*, 895–897, 1980.

Pike, R. J., Formation of complex impact craters: Evidence from Mars and other planets, *Icarus*, *43*, 1–19, 1980.

Pittman, E. F., The Great Australian Artesian Basin and the source of its water, *Geol. Surv. New South Wales*, 1914.

Plaut, J. J., R. Kahn, E. A. Guiness, and R. E. Arvidson, Accumulation of sedimentary debris in the south polar region of Mars and implications for climate history, *Icarus*, *75*, 357–377, 1988.

Plescia, J. B., and J. Crisp, Recent Elysium volcanism: Effects on the Martian atmosphere, in *Workshop on the Martian Surface and Atmosphere Through Time*, pp. 102–103, Lunar and Planetary Inst., Houston, Tex., 1991.

Pollack, J. B., D. Colburn, F. M. Flasar, R. Kahn, C. E. Carlston, and D. Pidek, Properties and effects of dust particles suspended in the Martian atmosphere, *J. Geophys. Res.*, *84*, 2929–2945, 1979.

Pollack, J. B., J. F. Kasting, S. M. Richardson, and K. Poliakoff, The case for a wet, warm, climate on early Mars, *Icarus*, *71*, 203–224, 1987.

Postawko, S. E., and W. R. Kuhn, Effect of the greenhouse gases (CO_2, H_2O, S_2O) on the Martian paleoclimate, *J. Geophys. Res.*, *91*, D431–D438, 1986.

Puri, B. R., and K. Murari, Studies in surface area measurements of soils, 1, Comparison of different methods, *Soil Sci.*, *96*, 331–336, 1963.

Ratcliffe, E. H., The thermal conductivity of ice: New data on the temperature coefficient, *Philos. Mag.*, *1*, 1197–1203, 1962.

Rittenhouse, G., Pore-space reduction by solution and cementation, *Am. Assoc. Pet. Geol. Bull.*, *55*, 80–91, 1971.

Robertson, E. C., and D. L. Peck, Thermal conductivity of vesicular basalt from Hawaii, *J. Geophys. Res.*, *79*, 4875–4888, 1974.

Rossbacher, L. A., and S. Judson, Ground ice on Mars: Inventory, distribution, and resulting landforms, *Icarus*, *45*, 39–59, 1981.

Rossiter, J. R., D. W. Strangway, A. Koziar, J. Wong, and G. R. Olhoeft, Electromagnetic sounding of permafrost, N.W.T., Canada, in summer and winter, in *Proceedings of the Third International Conference on Permafrost*, pp. 568–573, National Research Council of Canada, Ottowa, 1978.

Rothfield, L. B., Gaseous counterdiffusion in catalyst pellets, *AIChE J.*, *9*, 19–24, 1963.

Rotto, L., and K. L. Tanaka, Chryse Planitia region, Mars: Channeling history, flood-volume estimates, and scenarios for bodies of water in the northern plains, in *Workshop on the Martian Surface and Atmosphere Through Time*, pp. 111–112, Lunar and Planetary Inst., Houston, Tex., 1991.

Sanger, F. J., Degree-days and heat conduction in soils, in *Proc., International Conference on Permafrost*, pp. 253–262, National Academy of Sciences, Washington, D. C., 1963.

Sass, J. H., Heat flow values from the Precambrian shield of Western Australia, *J. Geophys. Res.*, *69*, 299–308, 1964.

Sass, J. H., and R. J. Munroe, Basic heat-flow data for the United States, *U.S. Geol. Surv. Open File Rep.*, *74-9*, 456 pp., 1974.

Saunders, R. S. and L. A. Johansen, Latitudinal distribution of flow-ejecta morphology types on the ridged plains of Mars, in *Proc. 3rd Colloq. Planet. Water*, pp. 97–98, State University of New York at Buffalo, 1980.

Schmidt, R. M. and K. R. Housen, Some recent advances in the scaling of impact and explosion cratering, *Int. J. Impact Eng.*, *5*, 543–560, 1987.

Schmidtke, K. D., E. A. McBean, and J. F. Sykes, Stochastic estimation of states in unconfined aquifers subject to artificial recharge, *Water Resour. Res.*, *18*, 1519–1530, 1982.

Schmoker, J. W., and D. L. Gautier, Sandstone porosity as a function of thermal maturity, *Geology*, *16*, 1007–1010, 1988.

Schneider, M., Hydrogeologie des Nubischen Aquifersystem am Südrand des Dakhla-Beckens, Südägypten/Nordsudan, *Berlin. Geowiss. Abh., Reihe A*, *71*, 1–66, 1986.

Schubert, G. and T. Spohn, Thermal history of Mars and the sulfur content of its core, *J. Geophys. Res.*, *95*, 14,095–14,104, 1990.

Schultz, P. H., Atmospheric effects on ejecta emplacement, *J. Geophys. Res.*, *97*, 11,623–11,662, 1992.

Schultz, P. H. and D. E. Gault, Seismic effects from major basin formations on the Moon and Mercury, *Moon*, *12*, 159–177, 1975*a*.

Schultz, P. H., and D. E. Gault, Seismically induced modification of lunar surface features, *Proc. Lunar Sci. Conf.*, *6th*, 2845–2862, 1975*b*.

Schultz, P. H., and D. E. Gault, Atmospheric effects on Martian ejecta emplacement, *J. Geophys. Res.*, *84*, 7669–7687, 1979.

Schultz, P. H., and D. E. Gault, On the formation of contiguous ramparts around Martian impact craters, *Lunar Planet. Sci. Conf.*, *XV*, 732–733, 1984.

Schultz, P. H., and H. Glicken, Impact crater and basin control of igneous processes on Mars, *J. Geophys. Res.*, *84*, 8033–8047, 1979.

Schultz, P. H., and A. B. Lutz, Polar wandering on Mars, *Icarus*, *73*, 91–141, 1988.

Schultz, P. H., R. A. Schultz, and J. Rogers, The structure and evolution of ancient impact basins on Mars, *J. Geophys. Res.*, *87*, 9803–9820, 1982.

Schultz, R. A., and H. V. Frey, A new survey of multiring impact basins on Mars, *J. Geophys. Res.*, *95*, 14,175–14,189, 1990.

Sclater, J. G., C. Jaupart, and D. Galson, The heat flow through oceanic and continental crust and the heat loss of the Earth, *Rev. Geophys.*, *18*, 269–311, 1980.

Scott, D. S. and F. A. L. Dullien, Diffusion of ideal gasses in capillaries and porous solids, *AIChE J*, *8*, 113–117, 1962.

Seeburger, D. A. and M. D. Zoback, The distribution of natural fractures and joints at depth in crystalline rock, *J. Geophys. Res.*, *87*, 5517–5534, 1982.

Shankland, T. J., and M. E. Ander, Electrical conductivity, temperatures, and fluids in the lower crust, *J. Geophys. Res.*, *88*, 9475–9484, 1983.

Sharp, R. P., and M. C. Malin, Channels on Mars, *Geol. Soc. Am. Bull.*, *86*, 593–609, 1975.

Shata, A. A., Hydrogeology of the Great Nubian Sandstone basin, Egypt, *Q. J. Eng. Geol.*, *15*, 127–133, 1982.

Shoemaker, E. M., Impact mechanics at Meteor Crater, Arizona, in *The Moon, Meteorites, and Comets*, edited by B. M. Middlehurst and G. P. Kuiper, pp. 301–336, University of Chicago Press, Chicago, Ill., 1963.

Short, N. M., Anatomy of a meteorite impact crater: West Hawke Lake, Manitoba, Canada, *Geol. Soc. Am. Bull.*, *81*, 609–648, 1970.

Siegfried, R. W., G. Simmons, D. Richter, and F. Horz, Microfractures produced by a laboratory scale hypervelocity impact into granite, *Proc. Lunar Sci. Conf.*, *8th*, 1249–1270, 1977.

Siegfried, R. W., R. G. McQueen, and G. Simmons, Shock-induced microfractures in six terrestrial igneous rocks characterized with differential strain analysis, *J. Geophys. Res.*, *86*, 6205–6218, 1981.

Simmons, G., T. Todd, and H. Wang, The 25-km discontinuity: Implications for lunar history, *Science*, *182*, 158–161, 1973.

Slusarchuk, W. A., and G. H. Watson, Thermal conductivity of some ice-rich permafrost soils, *Can. Geotech. J.*, *12*, 413–424, 1975.

Smith, M. W., Observations of soil freezing and frost heaving at Inuvik, Northwest Territories, Canada, *Can. J. Earth Sci.*, *22*, 283–290, 1985.

Smith, M. W., and C. R. Burn, Outward flux of vapour from frozen soils at Mayo, Yukon, Canada: Results and interpretation, *Cold Regions Sci. Technol.*, *13*, 143–152, 1987.

Smoluchowski, R., Mars: Retention of ice, *Science*, *159*, 1348–1350, 1968.

Snow, D. T., Rock fracture spacing, openings, and porosities, *J. Soil Mech. Found. Div., Am. Soc. Civ. Eng.*, *94*, 73–91, 1968.

Soderblom, L. A., and D. B. Wenner, Possible fossil H_2O liquid-ice interface in the Martian crust, *Icarus*, *34*, 622–637, 1978.

Soderblom, L. A., M. C. Malin, J. A. Cutts, and B. C. Murray, Mariner 9 observations of the surface of Mars in the north polar region, *J. Geophys. Res.*, *78*, 4197, 1973.

Soderblom, L. A., C. D. Condit, R. A. West, B. M. Herman, and T. J. Kreidler, Martian planetwide crater distributions: Implications for geologic history and surface processes, *Icarus*, *22*, 239–263, 1974.

Solomon, S. C., and J. W. Head, Heterogeneities in the thickness of the elastic lithosphere of Mars: Constraints on heat flow and internal dynamics, *J. Geophys. Res.*, *95*, 11,073–11,083, 1990.

Squyres, S. W., The evolution of dust deposits in the Martian north polar region, *Icarus*, *40*, 244–261, 1979.

Squyres, S. W., Urey Prize Lecture: Water on Mars, *Icarus*, *79*, 229–288, 1989.

Squyres, S. W., and M. H. Carr, Geomorphic evidence for the distribution of ground ice on Mars, *Science*, *231*, 249–252, 1986.

Squyres, S. W., D. E. Wilhelms, and A. C. Moosman, Large-scale volcano-ground ice interactions on Mars, *Icarus*, *70*, 385–408, 1987.

Stevenson, D. J., T. Sphon, and G. Schubert, Magnetism and the thermal evolution of the terrestrial planets, *Icarus*, *54*, 466–489, 1983.

Streltsova, T. D., Hydrodynamics of groundwater flow in a fractured formation, *Water Resour. Res.*, *12*, 405–414, 1976.

Tanaka, K. L., The stratigraphy of Mars, *J. Geophys. Res.*, *91*, E139–E158, 1986.

Tanaka, K. L., and D. H. Scott, The youngest channel system on Mars, *Lunar Planet Sci. Conf., XVII*, 865–866, 1986.

Taylor, S. T., and J. W. Cary, Linear equations for the simultaneous flow of matter and energy in a continuous soil system, *Soil Sci. Soc. Am. Proc.*, 167–172, 1964.

Thomas, J. M. and J. L. Mason, Ground-water levels in the Great Basin region of Nevada, Utah, and adjacent states, *U. S. Geol. Surv. Hydrol. Invest. Atlas*, *HA-694-B*, 1986.

Thompson, A. B., and J. A. D. Connolly, Migration of metamorphic fluid: Some aspects of mass and heat transfer, *Earth Sci. Rev.*, *32*, 107–122, 1992.

Thompson, B. G., A. Nekut, and A. F. Kuckes, A deep crustal electrictromagnetic sounding in the Georgia Piedmont, *J. Geophys. Res.*, *88*, 9461–9473, 1983.

Thorweihe, U., Isotopic identification and mass balance of the Nubian Aquifer System in Egypt, *Berlin. Geowiss. Abh., Reihe A*, 72, 87–97, 1986.

Tittmann, B. R., Brief note for consideration of active seismic exploration on Mars, *J. Geophys. Res.*, *84*, 7940–7942, 1979.

Todd, D. K., *Groundwater Hydrol.*, 336 pp., John Wiley, New York, 1959.

Todd, T., D. A. Richter, G. Simmons, and H. Wang, Unique characterization of lunar samples by physical properties, *Proc. 4th Lunar Sci. Conf., Geochiem. Cosmochim. Acta, Suppl. 4*, *3*, 2639–2662, 1973.

Toksöz, M. N., Planetary seismology and interiors, *Rev. Geophys.*, *17*, 1641–1655, 1979.

Toksöz, M. N., and A. T. Hsui, Thermal history and evolution of Mars, *Icarus*, *34*, 537–547, 1978.

Toksöz, M. N., F. Press, A. Dainty, K. Anderson, G. Latham, E. Ewing, J. Dorman, D. Lammlein, G. Sutton, and F. Duennebier, Structure, composition, and properties of lunar crust, *Proc. 3rd Lunar Sci. Conf., Geochiem. Cosmochim. Acta, Suppl. 3*, *3*, 2527–2544, 1972.

Toksöz, M. N., A. M. Dainty, S. C. Solomon, and K. R. Anderson, Structure of the Moon, *Rev. Geophys.*, *12*, 539–567, 1974.

Toksöz, M. N., A. T. Hsui, and D. H. Johnson, Thermal evolution of the terrestrial planets, *Moon Planets*, *18*, 281–320, 1978.

Toon, O. B., J. B. Pollack, W. Ward, J. A. Burns, and K. Bilski, The astronomical theory of climatic change on Mars, *Icarus*, *44*, 552–607, 1980.

Toth, J., A theoretical analysis of groundwater flow in small drainage basins, *J. Geophys. Res.*, *68*, 4795–4811, 1963.

Toth, J., Gravity-induced cross-formational flow of formation fluids, Red Earth Region, Alberta, Canada: Analysis, patterns, and evolution, *Water Resour. Res.*, *14*, 805–843, 1978.

Toulmin, P., III, A. K. Baird, B. C. Clark, K. Keil, H. J. Rose, Jr., P. H. Evans, and W. C. Kelliher, Geochemical and mineralogical interpretation of the Viking inorganic chemical results, *J. Geophys. Res.*, *82*, 4625–4634, 1977.

Touma, J. and J. Wisdom, The chaotic obliquity of Mars, *Science*, *259*, 1294–1296, 1993.

Turcotte, D. L., F. A. Cook, and R. J. Willemann, Parameterized convection within the Moon and the terrestrial planets, *Proc. Lunar Planet. Sci. Conf. 10th*, 2375–2392, 1979.

Wallace, D., and C. Sagan, Evaporation of ice in planetary atmospheres: Ice-covered rivers on Mars, *Icarus*, *39*, 385–400, 1979.

Waller, R. M., Water-sediment ejections, in *The Great Alaska Earthquake of 1964*, pp. 97–116, National Academy of Sciences, Washington, D.C., 1968.

Waltz, J. P., Groundwater, in *Introduction to Physical Hydrol.*, chap. 6.1, edited by R. J. Chorley, pp. 122–130, Methuen, New York, 1969.

Ward, W. R., Climatic variations on Mars, 1, Astronomical theory of insolation, *J. Geophys. Res.*, *79*, 3375–3386, 1974.

Ward, W. R., Present obliquity oscillations of Mars: Fourth-order accuracy in orbital e and I, *J. Geophys. Res.*, *84*, 237–241, 1979.

Ward, W. R., and D. J. Rudy, Resonant obliquity of Mars?, *Icarus*, *94*, 160–164, 1991.

Ward, W. R., J. A. Burns, and O. B. Toon , 2, Past obliquity oscillations of Mars: Role of the Tharsis uplift, *J. Geophys. Res.*, *84*, 243–259, 1979.

Warren, P. H., and K. L. Rasmussen, Megaregolith, insulation, internal temperatures, and bulk uranium content of the Moon, *J. Geophys. Res.*, *92*, 3453–3465, 1987.

Watkins, H. and J. S. Lewis, Loss of volatiles from Mars as the result of energetic impacts, Workshop on Water on Mars, *LPI Tech. Rep. 85-03*, pp. 93–95, Lunar and Planetary Inst., Houston, Tex., 1985.

Weertman, J., Mechanisms for the formation of inner moraines found near the edge of cold ice caps and ice sheets, *J. Glaciol.*, *3*, 965–978, 1961.

White, D. E., Magmatic, connate, and metamorphic waters, *Bull. Geol. Soc. Am.*, *68*, 1659–1682, 1957.

Wilhelms, D. E. and R. J. Baldwin, The role of igneous sills in shaping the Martian uplands, *Proc. Lunar Planet. Sci. Conf., 19th*, 355–366, 1989.

Williams, P. J. and M. W. Smith, *The Frozen Earth*, 306 pp., Cambridge University Press, New York, 1989.

Winograd, I. J., Interbasin movement of ground water at the Nevada Test Site, Nevada, *U. S. Geol. Surv. Prof. Pap.*, *450-C*, 108–111, 1962.

Wise D. U., M. P. Golembeck, and G. E. McGill, Tharsis province of Mars: Geologic sequence, geometry, and a deformation mechanism, *Icarus*, *38*, 456–472, 1979.

Youngquist, G. R., Diffusion and flow of gases in porous solids, in: *Flow Through Porous Media*, pp. 58–69, American Chemical Society, Washington, D.C., 1970.

Zent, A. P., F. P. Fanale, J. R. Salvail, and S. E. Postawko, Distribution and state of H_2O in the high-latitude shallow subsurface of Mars, *Icarus*, *67*, 19–36, 1986.

Zykov, Yu. D., N. Yu. Rozhdestvensky, and O. P. Chervinskaya, The study of frozen soils by geophysical methods, in *Proceedings of the Fifth International Conference on Permafrost*, pp. 537–542, Tapir Publishers, Trondheim, Norway, 1988.

S. M. Clifford, Lunar and Planetary Institute, 3600 Bay Area Boulevard, Houston TX 77058.

(Received December 26, 1991;
revised January 20, 1993;
accepted January 22, 1993.)